University of Alberta
Department of Civil &
Environmental Engineering

Structural Engineering Report No. 226

Rehabilitation of Unreinforced Masonry Walls withExternally Applied Fiber Reinforced Polymers

by

M. L. Albert

J.J.R. Cheng

and

A.E. Elwi

October, 1998

Rehabilitation of Unreinforced Masonry Walls with Externally Applied Fiber Reinforced Polymers

by

Michael L. Alberta

J.J.R. Cheng

A.E. Elwi

Structural Engineering Report 226

Department of Civil and Environmental Engineering

University of Alberta
Edmonton, Alberta

October, 1998

Abstract

Many existing unreinforced masonry walls are in need of rehabilitation. To investigate the feasibility of using Fiber Reinforced Polymers (FRP) as a strengthening material for loads in the out-of-plane direction a testing program was conducted. Thirteen tests were performed on ten full scale walls. Both undamaged and slightly damaged walls were tested. The parameters investigated were type, amount, and layout of reinforcement, axial load effects, and cyclic behaviour. This thesis starts with a brief review of the existing rehabilitation methods available and explains why the use of FRP is a possible alternative. Results of material tests performed on the masonry and fiber materials are then presented. The test set-up, instrumentation, and general test procedure are described. The general behaviour of the specimens is discussed with emphasis on the load - deflection and strain characteristics. The modes of failure are identified and categorized. Finally, an analytical model is proposed to predict the load - deflection response of FRP reinforced masonry walls. Overall results show that externally applied FRP greatly increases the strength and ductility of ungrouted, unreinforced masonry walls.

Table of Contents

List of Tables

List of Figures

List of Abbreviations and Notation

Abbreviations

ASTM = American Standard for Testing of Materials
CSA = Canadian Standards Association
FRP = Fiber Reinforced Polymers
HSS = Hollow Structural Section
ICST = Imperial block, Carbon Sheet
LVDT = Linear Variable Differential Transformer
MCS = Metric block, Carbon Strap
MCST = Metric block, Carbon Sheet
MGST = Metric block, Glass Sheet
MU = Metric block, Unreinforced

Notations

a = Depth of compression zone within masonry section
A = End web width of masonry block, fiber reinforcement layout designation, joint location designation
A_e = Effective area of masonry section
A_R = Tensile cross sectional area of fiber reinforcement and epoxy matrix
b = total width of masonry compression zone
B = Center web width of masonry block, fiber reinforcement layout designation, joint location designation
c = Depth to the Neutral Axis from the extreme compression fiber
C = Width of masonry face shell, fiber reinforcement layout designation, joint location designation, vertical compressive force acting normal to the plane of sliding
C_M = Compressive force in the masonry section

d = Distance from the extreme compression fiber to the centroid of the tensile force in the fiber reinforcement

D = Width of an individual masonry block, fiber reinforcement layout designation

Δ_t = Transition mid-span deflection

Δ_{tp} = Predicted transition mid-span deflection

Δ_u = Failure mid-span deflection

Δ_{up} = Predicted value of the failure mid-span deflection

E = Fiber reinforcement layout designation

E_M = Modulus of elasticity of masonry in compression

E_R = Modulus of elasticity of fiber reinforcement in tension

ε_m = Masonry strain

ε_r = Fiber reinforcement strain

f'_m = Compressive strength of masonry

ϕ_m = Safety factor for masonry

H = Overall height of an individual masonry block

I_{approx} = Approximated global value of moment of inertia over the entire span

I_{cr} = Cracked transformed moment of inertia

I_o = Gross transformed moment of inertia

jd = Internal moment arm

L = Overall length of an individual masonry block, total span between reaction points

L_1 = distance from reaction support to load point (shear span region)

M = Internal moment

M_f = Factored moment

μ = Friction coefficient

n = Modular ratio = E_R/E_M

P = Total applied lateral load, axial compressive load used in the calculation of masonry shear resistance

P_t = Transition load

P_{tp} = Predicted value of the transition load

P_u = Failure load obtained from test results

P_{up} = Predicted value of failure load

Q = Variable assigned to the Ad^2 portion of a typical moment of inertia calculation

R^2 = An indication of the accuracy of a linear regression analysis

ρ = Fiber reinforcement ratio = A_R/bd

S_1 = Idealized slope of the first section of the load - deflection response

S_{1p} = Predicted slope of the first section

S_2 = Actual second section slope of the load - deflection response from regression analysis results

S_{2p} = Predicted second section slope

σ_m = Stress in the masonry section

t_{avg} = Average thickness of fiber reinforcment tension coupons

T_R = Tensile force in the fiber reinforcement

θ = Angle of fiber reinforcement from vertical

V_f = Factored shear

v_m = Masonry shear strength

V_r = Sliding shear resistance of unreinforced masonry

W = Overall width of an individual masonry block

x = Unknown variable used in various calculations

1. INTRODUCTION

1.1 Problem Statement

A large percentage of existing buildings in North America and around the world have been constructed with unreinforced masonry. The masonry elements in these buildings were designed to primarily resist gravity and wind loads with little or no consideration of the forces generated by a seismic event. Typical damage suffered by these buildings during an earthquake ranges from minor cracking to catastrophic collapse. The use of Fiber Reinforced Polymers (FRP) as a rehabilitation and strengthening material is a valid alternative to conventional rehabilitation methods. Appealing characteristics of fiber reinforcement are high strength to weight ratio, extremely small thickness, low strains at ultimate stresses, immunity to corrosion, and ease of application. Little information exists regarding the out-of-plane behaviour of unreinforced, ungrouted masonry walls retrofitted with FRP. The research presented in this paper is a beginning of a data pool for information regarding this subject.

1.2 Objectives and Scope

The broad objective of the research is to examine the out-of-plane flexural resistance of unreinforced masonry walls strengthened with externally applied FRP. Emphasis is placed on the load - deflection response of the specimens tested. A number of variables which may affect this behaviour are identified and investigated. Because little information exists on this subject, an attempt is made to explain the overall behaviour of the specimens including crack patterns, and the interaction between the FRP and the masonry.

To achieve these objectives, one unreinforced masonry wall and twelve walls reinforced with various types and patterns of FRP were tested as simply supported beams standing on end and subjected to two out-of-plane live loads.

This produced a constant moment region between the loading lines where the primary data were collected.

1.3 Thesis Organization

A review of the current literature is presented in Chapter 2. This chapter summarizes the various conventional rehabilitation and strengthening methods as well as the current use of FRP in concrete structures. Chapter 3 explains the experimental program and includes such items as the materials used, details of the test specimens, and the details of the testing program. Chapter 4 summarizes the primary results of the tests. The load - deflection and strain behaviour are included and the failure modes described. The influence of the variables investigated on the behaviour of the specimens is presented in Chapter 5. This chapter also presents an analytical model which predicts the load - deflection response. Finally, the summary and conclusions are contained in Chapter 6.

2. LITERATURE REVIEW

2.1 Introduction

A review of the literature was conducted with the objective of finding relevant articles with respect to the rehabilitation of unreinforced masonry using standard procedures and the use of FRP in the rehabilitation and strengthening of concrete structures. There is very little available information on the use of FRP as a strengthening material for unreinforced masonry in the out-of-plane direction. The information that is available focuses on in-plane strengthening aspects. The following sections briefly outline the available rehabilitation and strengthening techniques and summarizes the existing use of FRP in masonry and other concrete structural applications.

2.2 Conventional Rehabilitation Methods

There is a variety of existing rehabilitation methods for unreinforced masonry walls in use today. Several authors have discussed various aspects of the different methods (Hamid et al., 1994, Modena, 1994, Kingsley, 1995). The most commonly used methods can be fit into categories of surface treatment, injection grouting, jacketing, internal reinforcement, and mechanical fasteners. The choice of which method to use depends on the nature and level of damage to the structure as well as the desired appearance of the finished rehabilitation.

Surface treatment covers a wide range of different materials and procedures. Reinforced plaster, shotcrete, and ferrocement are the most common. Typically, a metal grid is anchored to the existing wall and an extra layer of a cementitious material is applied on top. Hutchinson et al. (1984) tested a variety of surface coatings and concluded that they are generally effective in restoring and improving the in-plane strength of a damaged masonry wall.

Injection grouting is commonly used to repair small cracks or to fill ungrouted cores. For cracks and small voids, a liquid based epoxy is usually

employed. For larger voids a sand-cement grout is used. Manzouri et al. (1996) tested four clay brick walls that had been repaired using injection grouting. Again, results show that at least the original strength of the wall before being damaged was restored.

Jacketing is sometimes referred to as a form of surface treatment and involves using cast in place concrete or external steel elements to construct a frame around the damaged wall.

For hollow walls introducing internal reinforcing bars is an option. A vertical line of cores would be physically opened and a steel bar placed inside. Grout would then be injected into the core around the reinforcement to provide bond to the existing masonry. For improved performance, prestressed tendons can be introduced to the structure in a similar manner (Lissel et al. 1998).

Finally, to provide better transfer of forces, mechanical anchors or ties can be introduced to provide continuity between the wall and surrounding structure.

The above techniques have several disadvantages. They are all labour intensive and in some cases involve the use of highly skilled labour. The procedures are generally disruptive to the normal operation of a building. Procedures such as surface treatments and jacketing can add as much as 150 mm thickness to the existing wall. This possibly requires upgrading of the foundations and may increase the inertial forces generated by a seismic event. Surface treatments also interfere significantly with the insulation properties of the wall and adversely affects moisture migration and vapour condensation on interior surfaces.

2.3 Existing Use of FRP

The use of FRP as a rehabilitation and strengthening material is gaining acceptance among contractors and engineers. To date, the use of the material has been limited and usually restricted to research projects or demonstration projects. Several authors have summarized the use of FRP in structures in North America and Europe (Meier et al., 1992, Seible, 1995, Meier, 1996, Seible and Karbhari, 1995). Some field applications include strengthening of the "Ibach" bridge in Lucerne, Switzerland using carbon fiber sheets and the wrapping of concrete columns on the Santa Monica freeway in California with the same material. Also, a concrete bridge located south of Edmonton, Alberta was strengthened for shear using carbon FRP sheets by Alexander and Cheng (1996).

Tests have been performed on reinforced concrete beams reinforced with carbon fiber plates and sheets under simple bending with two loads applied at approximately one third the distance of the span away from the reaction supports (Arduini et al., 1997, Meier and Kaiser, 1991). Results show an overall improved behaviour of the beams but the mode of failure of the specimens was changed to a more brittle behaviour. The problem of premature peeling off of the fiber sheets due to excessive cracking was identified. Shear strengthening of concrete girders using externally bonded FRP sheets was studied by Droumoussis and Cheng (1994), Alexander and Cheng (1997), and Deniaud and Cheng (1998). Increases of the shear strength and ductility of the strengthened concrete girders were observed.

With respect to masonry applications, Schwegler (1994) examined the in-plane strength of masonry shear walls reinforced with a variety of FRP in various orientations subjected to seismic loads. Ehsani et al. (1997) performed tests on the shear behaviour of FRP sheets on small clay brick specimens. Tests were conducted using small scale clay brick beams reinforced with FRP under out-of-plane bending (Ehsani, 1995). Results show that the strength of the fibers has a direct effect on the mode of failure of the specimens. Finally, a full scale five

story masonry building was tested under simulated earthquake loads (Weeks et al., 1994). The structure was repaired using a variety of the previously mentioned techniques. FRP overlays were used in the lower stories and results show that the overlays helped increase the ductility and provided confinement against crushing of the masonry in compression regions at the toe of the wall.

Small scale out-of-plane tests have been performed on clay brick specimens reinforced with epoxy bonded Carbon Fiber Reinforced Plastics (Triantafillou, 1998). The clay brick specimens had an overall length of 900 mm and were tested under two out-of-plane line loads. Each specimen failed by masonry crushing, indicating a flexure failure, and showed a significant improvement in strength and ductility when compared to similar unreinforced specimens.

Other information regarding the out-of-plane strength of masonry walls reinforced with FRP is limited. The tests that have been performed show that FRP is effective in increasing the strength and ductility of unreinforced masonry walls. Other than work conducted by the author, large scale tests similar to the one presented in this thesis have not been reported to date.

3. EXPERIMENTAL PROGRAM

3.1 Introduction

The experimental program consisted of ten masonry walls reinforced with externally applied fiber reinforced polymers and related material tests. The walls were loaded in the out-of-plane direction by two line loads with the loading points 1.2 m from the reaction supports creating a constant moment region 1.4 m long. The parameters investigated were the type of reinforcement (carbon strap, carbon sheet, and glass sheet), amount of reinforcement, layout of reinforcement, axial load effects, and cyclic behavior. This chapter presents the ancillary material tests as well as the test set-up and details of the full scale wall specimens.

3.2 Materials

There were two groups of materials tested, those related to the masonry and those related to the FRP reinforcement. A communication error resulted in two different dimensions of masonry block being used, metric and imperial. As a result, the tests were separated into two series. Therefore, all ancillary tests were performed also in two series. Series One used the metric dimension blocks and Series Two used the imperial dimension block. Ancillary tests were performed on individual masonry blocks, mortar cubes, and masonry prisms to determine the mechanical properties of the specimens. For the fiber reinforcement, a number of tension coupons were tested for the glass fiber, carbon strap, and carbon sheet.

3.2.1 Masonry

3.2.1.1 Individual Units

A total of 30 masonry units were tested to determine the compressive strength, 15 for each series, in accordance with CSA Standard A165.1-M94 (1994). Both series of blocks had a specified manufactured strength of 15 MPa and were supplied by Edcon from Edmonton. Table 3.1 summarizes the results of the tests. The dimensions used in the table and mentioned below are explained in Fig. 3.1. The compressive strength for the blocks in Series One were calculated based on the following average dimensions: A = 29.2 mm, B = 34.7 mm, C = 35.2 mm, L = 390.4 mm, H = 190 mm, and W = 190.1 mm. The average net area was 38603 mm^2. For Series Two the following were used: A = 32.6 mm, B = 38.8 mm, C = 38.7 mm, L = 395 mm, H = 193 mm, and W = 193 mm. The average net area was 42623 mm^2. The results show that the compressive strength of the blocks used in the construction of Series Two walls was 20% lower than Series One.

3.2.1.2 Mortar

Type S mortar, supplied by IXL from Edmonton, was used in both series. A total of 36 standard 50 mm mortar cubes were tested, 18 for each series, in accordance with CSA Standard A369.1-M94 (1994) and ASTM Standard C109 M-95 (1995). Random samples of mortar were taken at various times during the construction of the walls. As a general rule, three cubes were made from samples taken from the top, middle, and bottom of each tub of mortar used. Table 3.2 summarizes the results of the tests. Three of the mortar cubes in Series One were loaded improperly and the results discarded. The remaining results show that the compressive strength of the mortar used in the construction of Series Two walls was almost 20% greater than Series One.

3.2.1.3 Prisms

Ten masonry prisms were tested for compressive strength. The age of the prisms at the time of testing was well beyond 28 days. It was intended that five prisms be constructed for each series but prisms were not constructed at the same time as the Series One specimens. As a result, all ten prisms were constructed at the same time as the Series Two specimens. Left over metric dimension masonry blocks and the Series Two mortar were used to build five prisms in an effort to simulate the material properties of Series One specimens. The remaining five prisms were built with imperial block. All prisms were constructed and tested in accordance with CSA Standard A369.1-M90 (1990). The prisms were one and a half blocks wide (0.6 m), and five courses high (1.0 m). Running bond was used and the joints were finished (tooled) in the same way as the wall specimens. A 200 mm Demec gauge was used to obtain the masonry strains during testing. Figure 3.2 shows the details of the prisms and instrumentation. In the figure, dimensions shown in brackets indicate the dimensions of the prisms constructed with imperial masonry block. Because the masons did not use a leveling line some height variability between prisms existed.

Table 3.3 summarizes the results of the tests. The modulus of elasticity was calculated based on the average net compressive area of the prisms and the last recorded strain measured over the height of the prisms. Naturally, there was large variability in the calculated compressive strengths of the prisms. The fact that the prisms were poorly constructed amplified the natural variability expected with masonry. It is interesting to note that a different mason constructed the prisms from each series. The mason who constructed the Series Two prisms showed a higher level of consistency with respect to the leveling, mortar joint thickness, and vertical straightness of the prisms. Not surprisingly, the Series Two prism results had a much lower coefficient of variation as the Series One prisms. The higher quality of construction for the Series Two prisms also explains why the strength was higher than the Series

One prisms. The imperfections in the construction of the Series One prisms, specifically the increased thickness of the mortar joints, caused premature failure. There is an obvious difference in material stiffness between the masonry block and the mortar joint. Because of this difference, each material will behave differently under loading. When subjected to a compressive load, the mortar joint experiences a lateral compression force, which in turn causes the surrounding masonry block to experience a lateral tension force. Hatzinikolas, Longworth, and Warwaruk (1978) proved that by increasing the thickness of a masonry joint, the tension force experienced by the surrounding masonry block increases. The Series One prisms contained several mortar joints which were greater than the specified 10 mm. As explained above, this increase in mortar joint thickness caused premature splitting of the Series One prisms and reduced the ultimate compression load.

3.2.2 Fiber Reinforcement

All fiber types used contained unidirectional fibers. All tension coupons made with the various FRP types were in accordance with ASTM Standard D3039 M-95a (1995). A 5 mm electric strain gauge was placed in the center of the coupons and, where feasible, an extensometer was also attached. The thickness was measured in six locations along the test length of the coupons and averaged. This was done because the epoxy used to impregnate the fibers varied in thickness considerably. All coupons were allowed to cure for one week before testing. Table 3.4 shows the results of all of the FRP tension tests.

3.2.2.1 Glass Sheet

The glass sheet used was supplied by Fyfe LLC and had the brand name Tyfo S. The sheets were delivered in large rolls and had to be cut to size. Two coupons were constructed at the same time as the application of the glass fibers to Specimen MGST 5. Both glass fiber coupons failed near the grips.

Consequently, the ultimate stress and strain was not achieved. Figure 3.3 shows the stress-strain behavior of the glass fiber coupons. The apparent difference in the two curves is mainly a result of the variation in measured thickness. The nature of the material suggests the two curves should be identical. Because only two specimens were tested, no statistical information other than the average could be calculated in Table 3.4.

3.2.2.2 Carbon Strap

The carbon strap used was supplied by Sika Canada Inc. and had the brand name Carbodur. The strap came in 50 mm wide strips that had to be cut to length. Four coupons were constructed at the same time as the application of the strap to Specimen MCS 6. Figure 3.4 shows the stress-strain behavior for all of the carbon strap coupons. The carbon strap has a very consistent thickness and all four tests follow almost the same path. The failure in all of the coupons occurred near the center of the test region.

3.2.2.3 Carbon Sheet

The carbon sheet was supplied by Mitsubishi Chemicals and had the brand name Replark 20. The sheets came in 250 mm wide rolls. The carbon matrix itself is delicate and a white mesh placed on one side, underneath the protective paper backing, helped maintain the integrity of the fibers during installation. Six coupons were constructed. Two were made during the application of the fibers to Specimen MCST 4. The remaining four coupons were made during the application of the fibers to specimens ICST 8 and ICST 9. Two of these were two layers thick. These four coupons were built using epoxy from a previously unopened container. The rest were constructed from a previously opened epoxy container. Both containers of epoxy were the same brand from the same manufacturer. The stress-strain behavior of the carbon sheet coupons is shown in Fig. 3.5. All of the coupons failed near the center of the test region.

Again, the variability in measured thickness is mainly the reason behind the inconsistent curves. The modulus of elasticity reported in Table 3.4 is calculated from a regression line fit to the data in Fig. 3.5 after 4000 microstrain. The lowest R^2 value, which is an statistical value used to determine the accuracy of a regression line with 1.0 indicating a perfect match, achieved from the regression analysis was 0.9991. The 4000 microstrain condition was imposed because the mounting of the extensometer caused some initial bending in the thin fiber coupons and is not representative of the true stiffness of the material.

3.3 Test Specimens

3.3.1 Details

As mentioned earlier, the full scale test specimens were constructed in two series. Series One consisted of four walls built with standard 200 mm block. Specified dimensions for each specimen of Series One was 3.99 m high, 1.19 m wide, and 0.19 m in depth. Series Two consisted of six walls built with standard 8 inch block. This changed the actual dimensions of these specimens to 4.05 m high, 1.205 m wide, and 0.193 m in depth. Each specimen was 20 courses high with #9 gauge wire joint reinforcement every 3rd course. None of the cores were grouted. The walls were built on 200 mm wide, 1200 mm long, and 50 mm thick steel base plates. Running bond was used and the joints were finished flush with the outside of the block. All specimens were allowed to cure for at least 28 days before the FRP was applied.

3.3.2 Workmanship

All specimens were built by professional masons. A different crew was employed for each series. The quality of work of the walls from Series One was excellent. The mortar joints had a consistent thickness of 10 mm which resulted in every course in the four walls being at the same height. The finishing of the

mortar joints was exactly as specified. The quality of work of the walls from Series Two was average to poor. The mortar joints ranged in thickness from 5 mm to 20 mm resulting in high variability in the height of the courses in each specimen. As a result, each of these six walls had slightly different heights. Some of the mortar joints were tooled, some left unfinished, and some finished as specified. A few head joints (vertical joints) were not completely filled with mortar. In general, the variability in quality of construction did not noticeably affect the test results but it did make preparation of the walls for reinforcement application and positioning of the walls in the test frame more difficult.

3.3.3 Reinforcement Strategy

Series One involved seven tests on the four walls and focused on varying the type of reinforcement. One wall was first tested without reinforcement, then tested again as a partially cracked wall, and finally as a fully cracked wall. One was reinforced on one side and tested until fully cracked, then additional reinforcement was placed on the opposite side and the wall was tested again in a cyclic manner. The remaining specimens were tested as undamaged specimens. Series Two involved six tests on the six walls and focused on varying the layout and amount of carbon fiber sheet. Axial load effects were also investigated in this series. Fig. 3.6 shows the different layout patterns tested. Table 3.5 summarizes the factors investigated for each test.

Because metric blocks were used in the construction of the specimens in Series One the designation (M) is used to identify the tests. Similarly (I), for imperial, is used to identify the specimens from Series Two. Each test is designated by the series, (M) or (I), followed by the type of reinforcement used; (CS) for carbon strap, (CST) for carbon sheet, and (GST) for glass sheet, followed by the test number. An additional number preceded by a hyphen indicates the specimen is being used again for the current test. For example, MCST 7-4, indicates Series One (metric walls), carbon sheet, test 7, and it is using the same specimen from test 4.

3.3.4 Application of Reinforcement

Each material used has its own method of application. Before any reinforcement was applied the surface of the masonry wall had to be prepared. For all reinforcement types the area that was to receive the reinforcement applied to it was sanded to remove any loose particles and the joints were ground to remove any high spots. Any unfilled or partially filled joints were patched with a hand mixed cement and sand compound and allowed to cure for at least 24 hours. In the field, mortar would normally be used to level the joints. The filling of voids and sanding allows a consistent, flat surface for the reinforcement to bond with. Next, the fine dust was removed using compressed air. For the specimen reinforced with angled carbon fiber sheets, ICST 12, the reinforcement was wrapped around the edges of the wall to simulate continuous reinforcement. To allow for this the corners were rounded with a grinder. This reduces the possibility that the reinforcement will be cut prematurely by the sharp edge of the wall.

The application of the carbon strap was relatively simple. After the wall was prepared as described above, the strap was bonded to the wall using a two part epoxy system. The epoxy was provided by Sika Canada Inc. and was designated as Sikadur Type 20, normal modulus. The specified mixing ratio was 3:1 by weight for parts A and B. For one 3650 mm by 50 mm carbon strap 600 g of Epoxy A and 200 g of Epoxy B were used. The epoxy was applied to the wall using a putty knife. Care was taken to ensure the epoxy was spread evenly over the bonding area. Next, the carbon strap was positioned and pressed into place by hand. A 30 mm wide plastic roller was then used to firmly press the strap into place until epoxy stopped squeezing out from underneath the strap. The excess epoxy around the edges of the strap was trimmed off with the edge of the putty knife.

The application of the glass sheets differed from that of the carbon straps. First, a primer coat had to be applied to enhance the bonding ability of the epoxy. The primer used was supplied by Mitsubishi Chemicals and was called

Epotherm Primer. Two coats, separated by 24 hours between coats, were applied to the Series One walls. The blocks used in the Series One walls seemed to absorb the primer so it was decided that a second coat should be applied. The mixing ratio was 2:1 by weight for Primer A and Primer B. The target quantity for coating the bonding area was 0.25 kg per square meter. It is important to note that the reinforcement must be applied to the primer within 72 hours after drying. Waiting longer than 72 hours makes the primer smooth and glassy reducing its effectiveness. The glass fibers were applied by technicians from the supplier Fyfe LLC. First, the glass fiber sheets were soaked in the epoxy. Next, a coat of epoxy was applied to the wall using a plastic trowel. The reinforcement was then pressed into place by hand and later smoothed with the plastic trowel to remove any air bubbles. After 24 hours of drying, a second coat of epoxy was applied to the bonded sheets.

For the carbon fiber sheets, application was similar to the glass fiber sheets. The same primer was used as a base coat. Again, two coats were applied to Series One walls but only one coat was applied to Series Two walls. The blocks used in the construction of Series Two walls did not absorb the primer as much as the previous blocks. As a result, only one coat of primer was required. After drying of the primer, the carbon sheets were applied using Epotherm Resin supplied by Mitsubishi Materials. The mixing ratio was 2:1 by weight for Resin A and Resin B. Target quantity for coating was 0.3 kg per square meter. The resin was applied to the wall using a standard paint roller. The carbon fiber was applied to the resin with the white mesh facing away from the surface and pressed into place by hand. After about half an hour, the paper backing was removed from the sheet and another coat of resin was applied to the outer surface of the sheet, pressing firmly to remove any air bubbles. This second coat ensures full penetration of the resin throughout the fibers. For specimen ICST 8, where two layers were used, the second sheet was applied following the same guidelines as the first after waiting about half an hour for the resin to penetrate into the first sheet.

For all cases, the reinforcement was allowed to cure for at least one week before testing. Instrumentation was applied after three days of curing. Figure 3.7 shows all three types of fiber reinforcement used. Photograph (a) shows the glass fiber sheets during installation, (b) shows the carbon straps after installation, and (c) shows one strip of primer before carbon sheets were applied and one strip after the fibers have been applied.

3.4 Testing Program

3.4.1 Test Set-up

All specimens were loaded in the test frame pictured in Fig. 3.8. The walls were tested as a simply supported beam standing on end. A hydraulic jack supplied the load which was transferred to the wall using a distribution frame constructed for the test. The jack load was centered on the distribution frame which then separated the concentrated load into two line loads located at a height of 1.3 m and 2.7 m from the base of the wall. The line loads rested along the full width of the wall. Details of the distribution frame are shown in Fig. 3.9. The frame was constructed using a combination of various Hollow Structural Sections (HSS). The loading points consisted of a knife edge and roller combination to allow for slight rotation and vertical movement. The distance between the center of the loading points was 1.4 m. The lower boundary conditions consisted of a larger version of the knife edge and roller combination resting on two rollers. Details of the lower supports are shown in Fig. 3.10. Again, this allowed for some rotation and freedom in the horizontal direction. It should be noted that the combined knife edge and roller boundary condition is not a perfect system. Because the knife edge spans almost the full width of the wall there is a significant amount of friction generated. However, the supports still performed well by allowing movement in the specified directions. The top and bottom reaction supports consisted of a built-up HSS section which spanned the width of the wall. A series of loose hinges tied back with steel rods to the

loading frame allowed for rotation and translation of the ends while providing stability by maintaining a tensile load. Figure 3.11 shows a typical reaction boundary condition.

The tests involving axial load required modifications to the test frame. A combination knife edge and roller boundary condition was placed on top of the wall to allow the axial load to remain vertical at all times. Load rods were supported from the ends of the knife edge arrangement, continued down the sides of the wall through the strong floor, and attached to springs. When compressed by a hydraulic jack, the springs maintained a constant axial load for the duration of the test. Details of the axial load modifications are shown in Fig 3.12. Photographs of some of the set-up details are shown in Fig. 3.13. Photograph (a) shows the compressed springs used under the strong floor to maintain a constant axial load, (b) shows the upper axial load modifications and a typical reaction assembly, and (c) shows the overall set-up before a specimen has been placed into position.

3.4.2 Instrumentation

The instrumentation consisted of various load cells to measure the jack load and reaction loads, Linear Variable Differential Transformers (LVDT's) to measure deflections, and Demec and electric strain gauges to measure masonry and reinforcement strains.

A 10 kN load cell was originally used for the first two tests to measure the applied load from the jack. The small capacity load cell was used primarily for greater accuracy in measuring the low loads experienced in the test of specimen MU 1, the unreinforced masonry wall. During the second test the load cell reached its capacity and the test had to be stopped. For all subsequent tests a 100 kN capacity load cell was used to handle the higher loads from the fiber reinforced walls. The reaction load was measured at the four corners of the specimen using load cells constructed for a previous experimental program. The details of a typical reaction load cell is shown Fig. 3.11.

The deflection of the wall was measured using a series of 13 LVDT's placed at 400 mm intervals along the height of the wall and 200 mm intervals around loading points. Figure 3.14 shows the positions of the LVDT's along the centerline of the specimen. It should be noted that the change in height of the Series Two walls did not change the location of the LVDT's. In most cases, the positioning of an individual LVDT changed only by 10 or 20 mm. The deflection measurements were taken on the compression side to minimize fluctuations in the readings due to separation of the mortar joints on the tension face. Because the loading frame prevented measuring of the mid-span deflection on the compression face, it was measured on the tension face.

Masonry strains were measured using a 50 mm Demec gauge. One division on the gauge equaled 25 microstrain. On average, most readings were read with a margin of error of ± 50 microstrain. While the position of the Demecs varied from test to test, two common areas were looked at. Gauges were placed in the horizontal direction and vertical direction. The horizontal Demecs measured the strain distribution from the edge of the wall to the centerline. Symmetry was assumed and readings were only taken on one side of the wall. The vertical Demecs measured the strain distribution between the loading points in the constant moment region. Demecs were placed on the tension face primarily; however, some were placed on the compression face to allow the neutral axis of the wall to be located. Figure 3.15 shows the typical positioning of the Demec gauges.

FRP reinforcement strains were measured using 5 mm long strain gauges. During the first few tests, Demecs were placed over a strain gauge to check the accuracy of the reinforcement gauge. Again, the location of the reinforcement gauges varied from test to test but concentrated on the mortar joint strains along the height of the wall. Horizontal symmetry was assumed and typically only one strip of reinforcement was gauged completely. Figure 3.16 shows the typical location of reinforcement strain gauges.

3.4.3 Test Procedure

The specimens were lifted into the test frame by an overhead crane. A built-up HSS section was placed on the top of the wall and steel rods placed down the sides to the base plate of the wall. Then, turnbuckles were used to introduce some axial load into the wall. The axial load increased the stability during lifting and prevented the proliferation of cracks. After the wall was placed on the lower boundary supports, the turnbuckles were removed and the axial load released from the system. Because of the variability in construction of the specimens, alignment of each specimen was difficult. Minor adjustments to the loading and reaction points had to be made for each test. The load frame was designed to have the load points centered on the 7th and 14th courses of the wall. The loading boundary conditions designed to allow free movement of the load points were able to adjust for the differences in height of each wall. Figure 3.17 shows how the load points could be adjusted. This adjustment typically resulted in the load point moving off the designed position on the wall.

After the specimen was properly aligned, lateral load was applied at a rate of 0.87 mm per minute. Because of the large weight of the load distribution frame, it was necessary to support it from the strong floor using wooden stilts until there was enough applied load from the jack to hold the frame in place. This usually occurred around 2.5 kN. The test was controlled using an existing computer controlled data acquisition system and all electronic readings were recorded using this system. Electronic readings were taken at approximately one quarter kN intervals. Demecs were recorded at regular intervals up to around 20 kN of load or whenever the strains became very large. General observations such as crack patterns and crack widths were made throughout each test. For the tests involving axial load, the axial load was applied immediately after positioning of the wall and before any lateral load was applied.

The procedure for test MCST 7-4, involving cyclic loading, was different. Because of the way that test was arranged, it was not possible to load the specimen in the reverse direction. As a result, the specimen was never taken

past zero during the cycles of loading and unloading. In fact, because of the 2.5 kN load required to support the distribution frame, the load was never taken below this value during the cycles. The specimen was loaded using the jack load as a guide for the beginning of the cycles. Three cycles were performed at 5 kN and 10 kN each. After this point, the wall was loaded to twice the deflection obtained at the 10 kN level and three cycles performed. Then the wall was loaded to three times the deflection and three cycles performed. Using successive multiples of the deflection obtained at 10 kN of load as a reference, three cycles were performed at each deflection multiple until the wall failed.

In general, most of the tests were continued until catastrophic failure occurred; however, a few tests were halted before failure so that the specimens could be used for additional tests or were not continued for safety reasons.

Table 3.1

Individual Masonry Unit Compressive Strengths

	Series One		Series Two	
Specimen Number	**Max. Load (kN)**	**Strength (MPa)**	**Max. Load (kN)**	**Strength (MPa)**
1	750.7	19.6	697.9	16.3
2	950.8	24.8	628.2	14.7
3	755.9	19.7	675.1	15.8
4	686.9	17.9	716.8	17.2
5	813.3	21.1	843.3	19.9
6	746.8	19.4	883.7	20.6
7	723.3	18.7	555.2	13.1
8	828.3	21.5	578.0	13.6
9	762.4	19.7	622.3	14.6
10	873.2	22.6	590.7	13.8
11	769.6	19.8	914.9	21.5
12	666.0	17.3	735.4	17.3
13	566.3	14.6	548.7	12.7
14	893.1	23.0	586.4	13.8
15	750.7	19.3	585.2	13.6
	mean	19.9	mean	15.9
	std. dev.	2.48	std. dev.	2.85
	C.O.V.	0.12	C.O.V.	0.18

Table 3.2

Mortar Cube Compressive Strengths

	Series One		Series Two	
Specimen Number	**Max. Load (kN)**	**Strength (MPa)**	**Max. Load (kN)**	**Strength (MPa)**
1			38.2	15.3
2	discarded		36.6	14.6
3			30.6	12.2
4	30.2	12.1	33.0	13.2
5	29.0	11.6	37.0	14.8
6	28.8	11.5	36.5	14.6
7	28.4	11.4	38.4	15.4
8	29.9	12.0	36.2	14.5
9	30.2	12.1	35.0	14.0
10	32.2	12.9	34.5	13.8
11	31.5	12.6	31.0	12.4
12	33.4	13.4	30.0	12.0
13	30.0	12.0	36.5	14.6
14	34.5	13.8	39.5	15.8
15	29.0	11.6	39.8	15.9
16	27.0	10.8	43.0	17.2
17	26.3	10.5	41.0	16.4
18	39.7	15.9	42.5	17.0
	mean	12.3	mean	14.7
	std. dev.	1.34	std. dev.	1.54
	C.O.V.	0.11	C.O.V.	0.11

Table 3.3

Masonry Prisms Test Results

	Series One			Series Two		
Specimen Number	**Max. Load (kN)**	**Strength (MPa)**	**E_m (MPa)**	**Max. Load (kN)**	**Strength (MPa)**	**E_m (MPa)**
1	312.8	6.5	N/A	789.2	14.8	11053
2	350.6	7.3	10847	671.9	12.6	10099
3	288.0	6.0	7638	585.2	10.9	9347
4	493.9	10.3	8255	759.8	14.2	10327
5	304.3	6.3	9880	763.1	14.3	10420
	mean	7.3	9155	mean	13.4	10249
	std. dev.	1.76	1472	std. dev.	1.60	616
	C.O.V.	0.24	0.16	C.O.V.	0.12	0.06

Table 3.4

Fiber Reinforcement Tension Test Results

Fiber Type	Specimen Number	Thickness (mm)	Max. Stress (MPa)	Max. Strain ($x10^{-6}$)	E_R (MPa)
Glass	1	1.940	121	8103	14970
Sheet	2	1.670	90	4425	20570
	mean	1.805	106	6264	17770
	1	1.258	2589	14216	182118
Carbon	2	1.255	2802	15114	185383
Strap	3	1.287	2762	14729	187527
	4	1.272	2843	15310	185696
	mean	1.268	2749	14842	185181
	std. dev.				2250
	C.O.V.				0.012
Carbon	1	0.940	413	12699	35100
Sheet	2	0.870	391	12560	35800
one	3	0.615	771	14213	56000
layer	4	0.490	747	12607	62600
	mean	0.729	581	13020	47375
	std. dev.				9323
	C.O.V.				0.197
two	5	1.510	471	11313	43500
layers	6	1.510	474	10966	44200
	mean	1.510	473	11140	43850

Table 3.5

Summary of Parameters Investigated

Specimen	Number of Strips	Width Per Strip (mm)	Layout Designation*	Additional Parameters
MU 1	N/A	N/A	N/A	
MCS 2-1	2	50	A	
MCS 3-2	2	50	A	
MCST 4	2	250	B	
MGST 5	2	250	B	
MCS 6	4	50	C	
MCST 7-4	2	250	B	Cyclic test
ICST 8	2	250	B	Two layers per strip
ICST 9	2	250	B	10 kN axial load
ICST 10	2	125	D	
ICST 11	2	250	B	
ICST 12	10	125	E	37 degree angle
ICST 13	2	250	B	30 kN axial load

* Refer to Figure 3.6

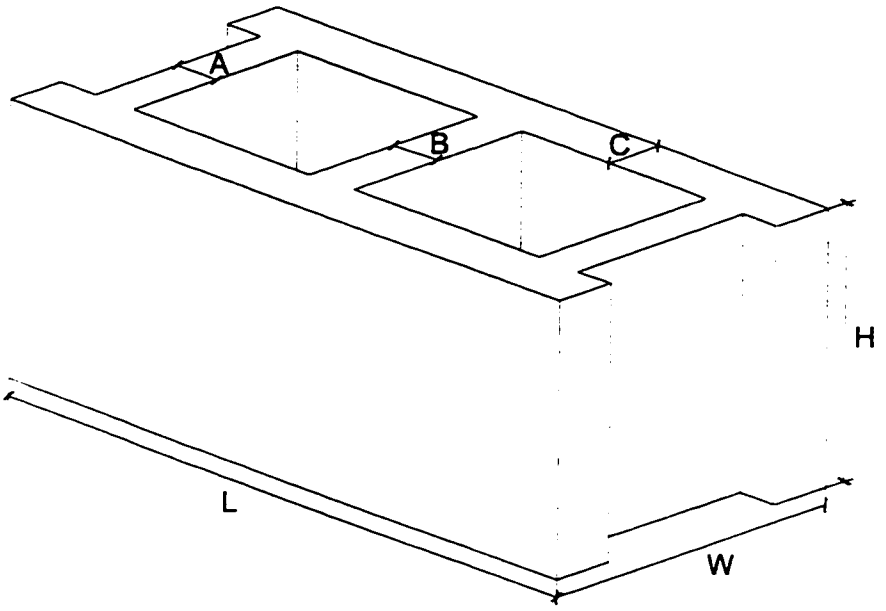

Figure 3.1 Simplified Dimensions of Masonry Unit

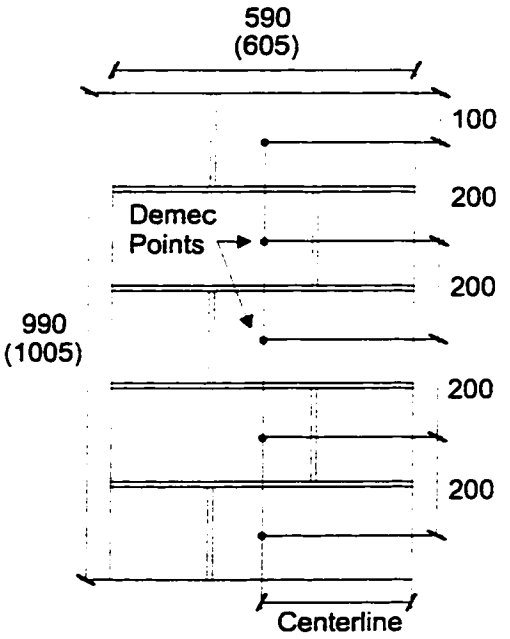

Figure 3.2 Masonry Prism Details

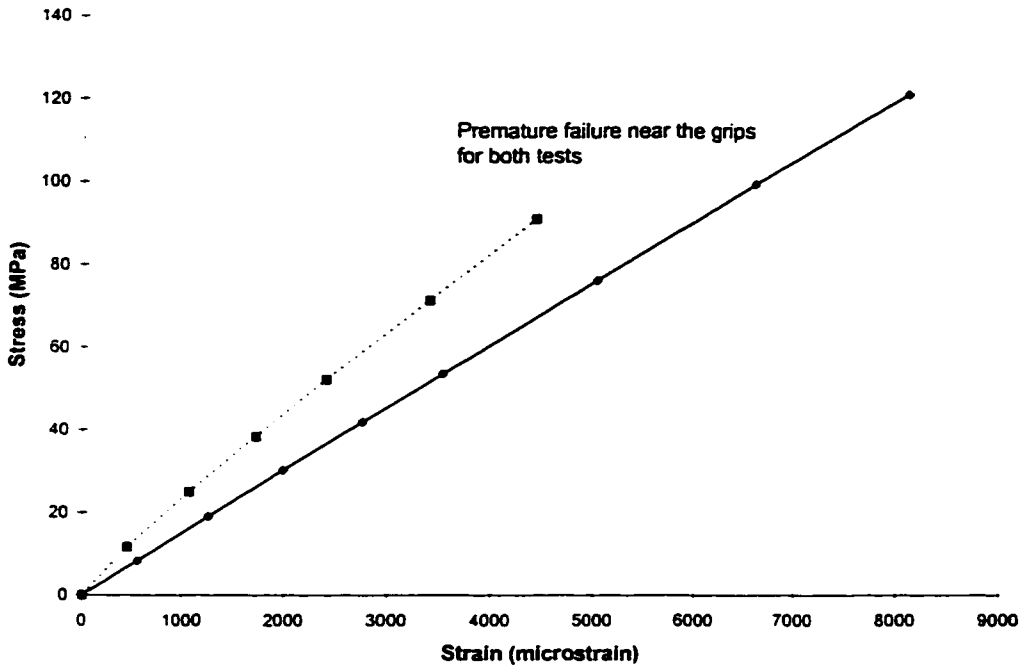

Figure 3.3 Glass Fiber Tension Test Behaviour

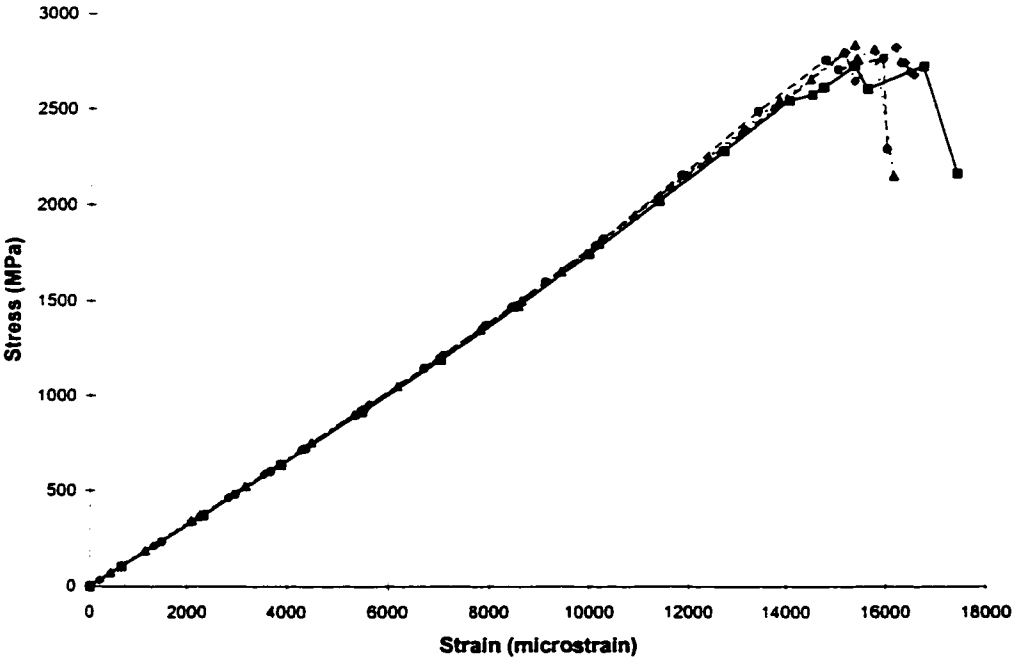

Figure 3.4 Carbon Strap Tension Test Behaviour

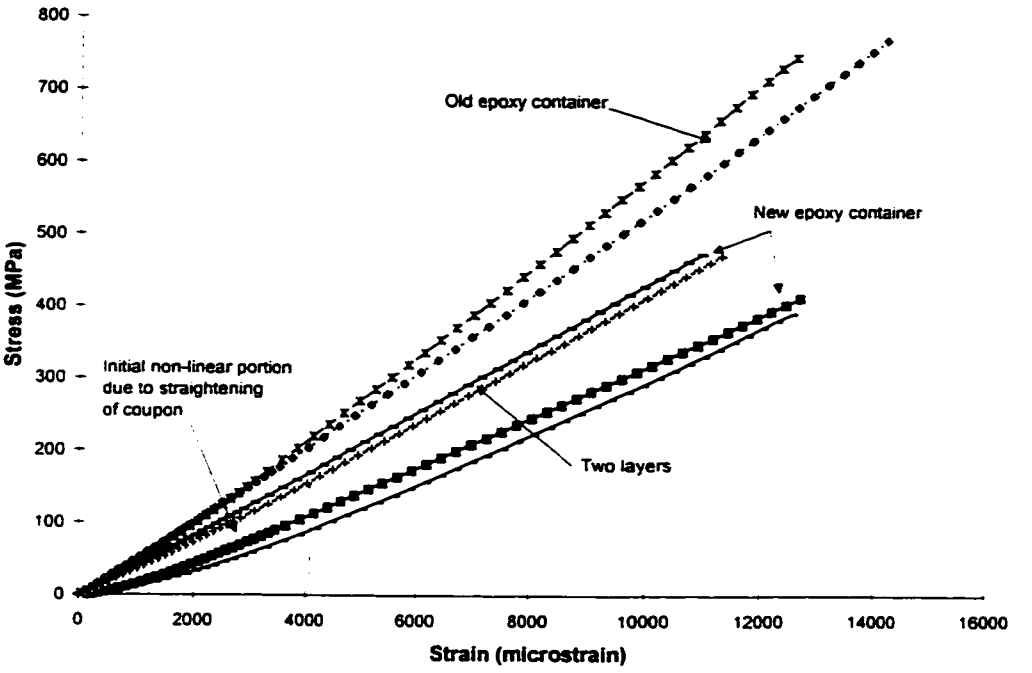

Figure 3.5 Carbon Sheet Tension Test Behaviour

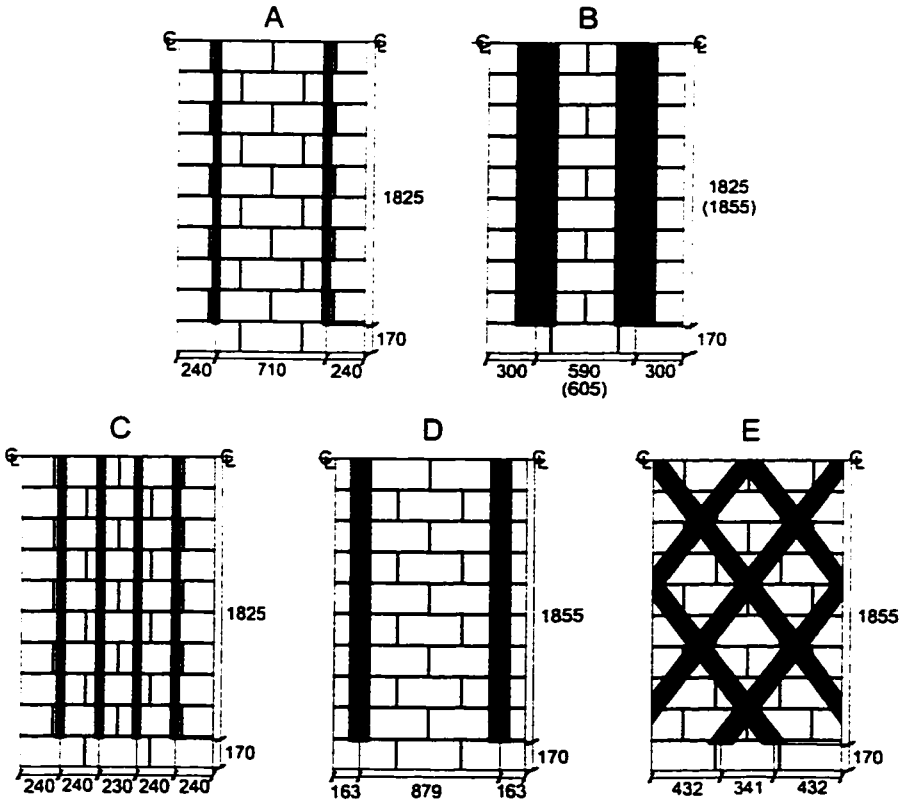

Figure 3.6 Fiber Reinforcement Layout Patterns

a. Glass Sheet

b. Carbon Strap

c. Carbon Sheet

Figure 3.7 Application of the Various Types of Fiber Reinforcement

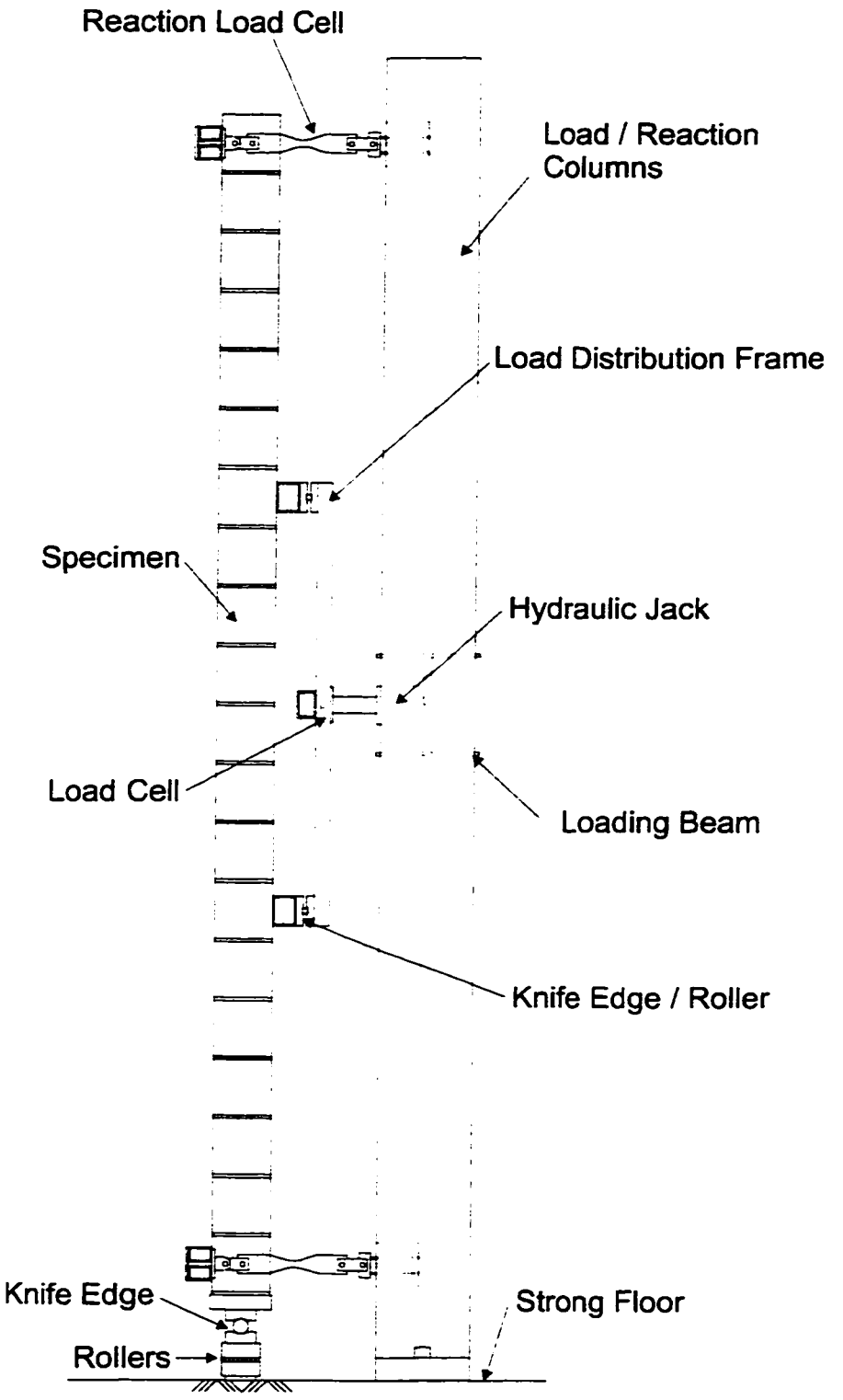

Figure 3.8 Test Set-up

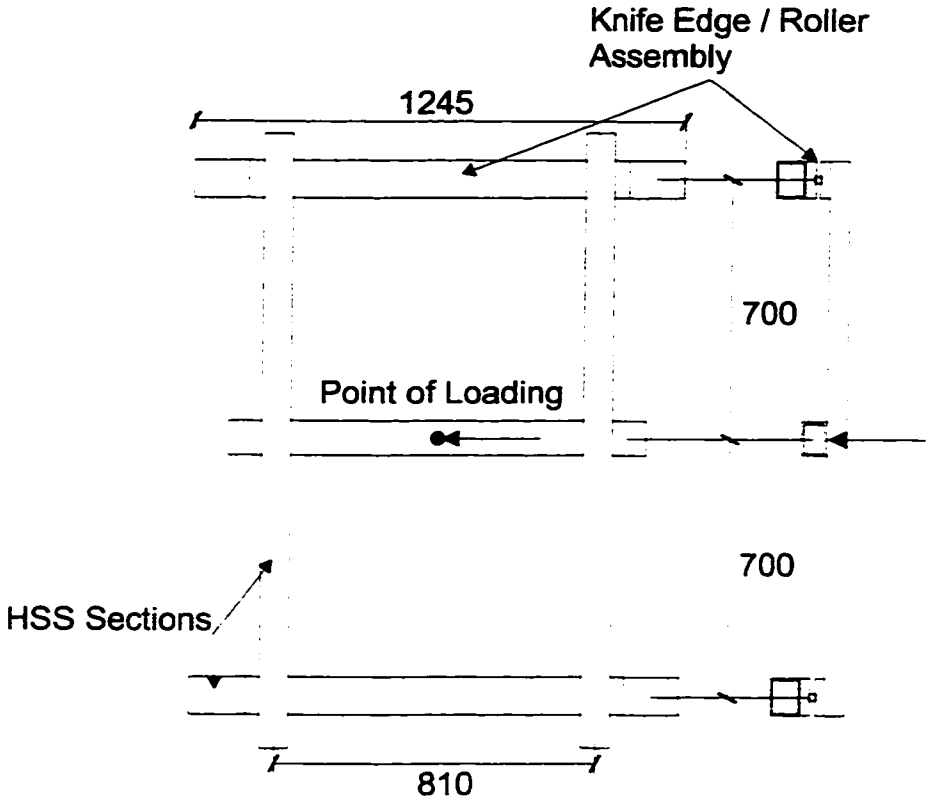

Figure 3.9 Load Distribution Frame Details

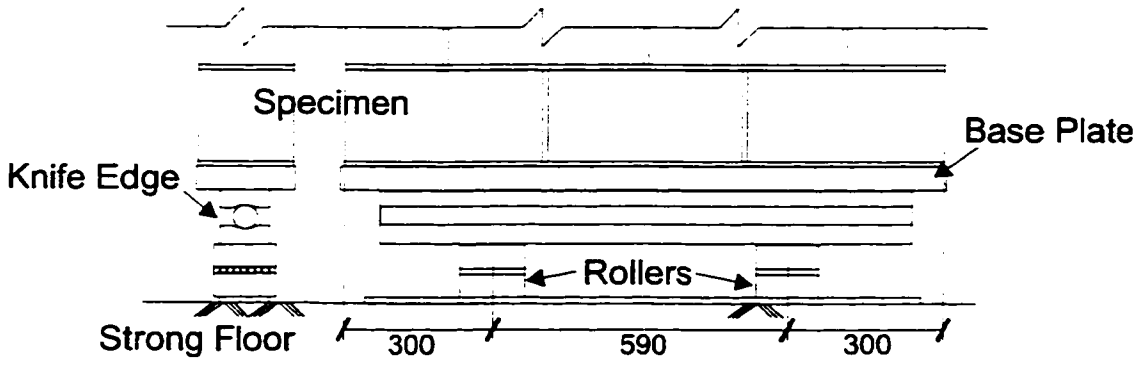

Figure 3.10 Lower Boundary Condition Details

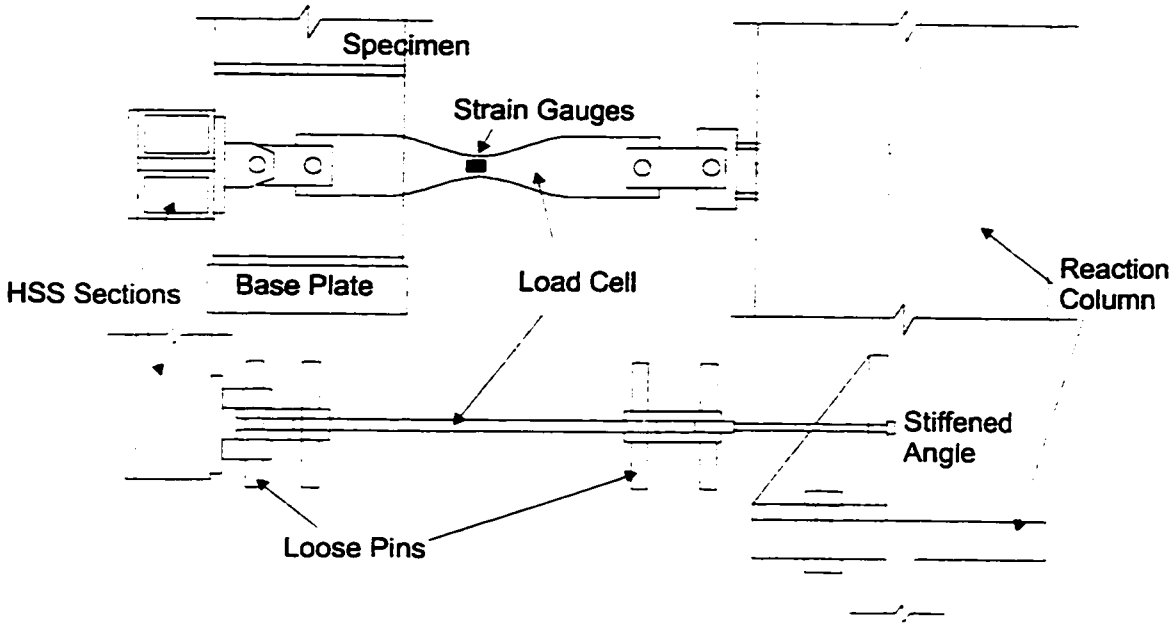

Figure 3.11 Reaction Assembly Details

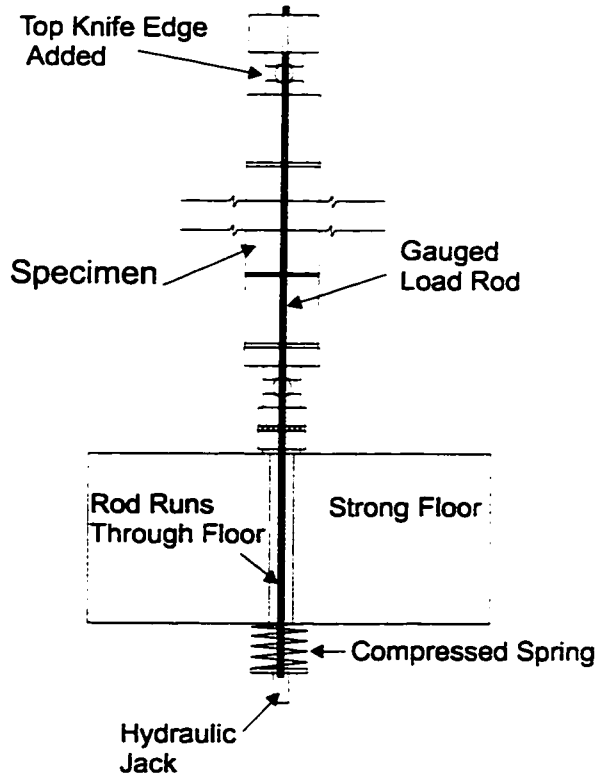

Figure 3.12 Axial Load Modifications

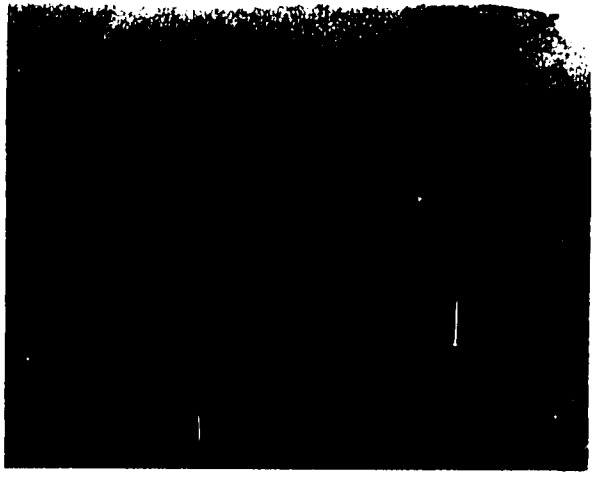

a. Axial Load Modifications

b. Upper Reaction Assembly and Axial Load Setup

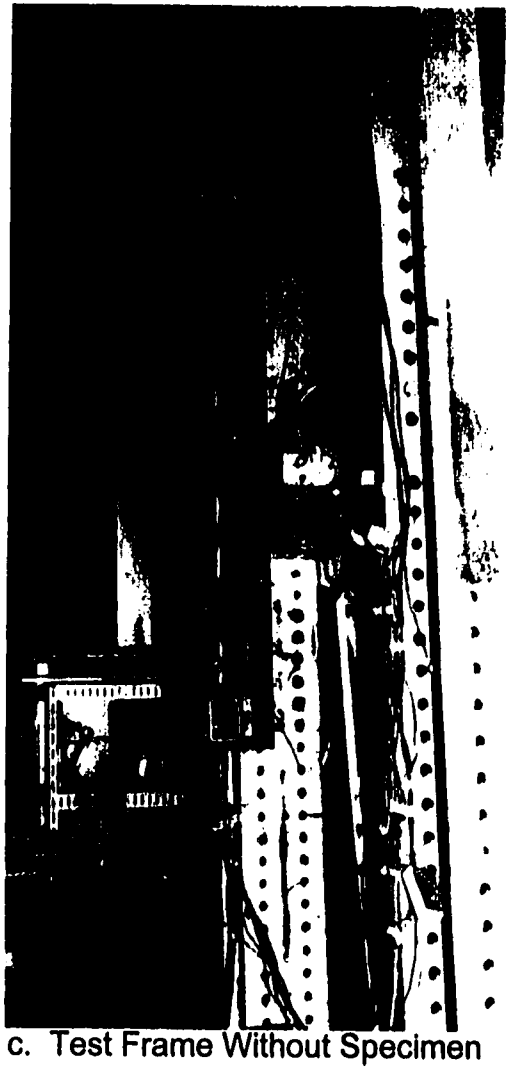

c. Test Frame Without Specimen

Figure 3.13 Various Set-up Details

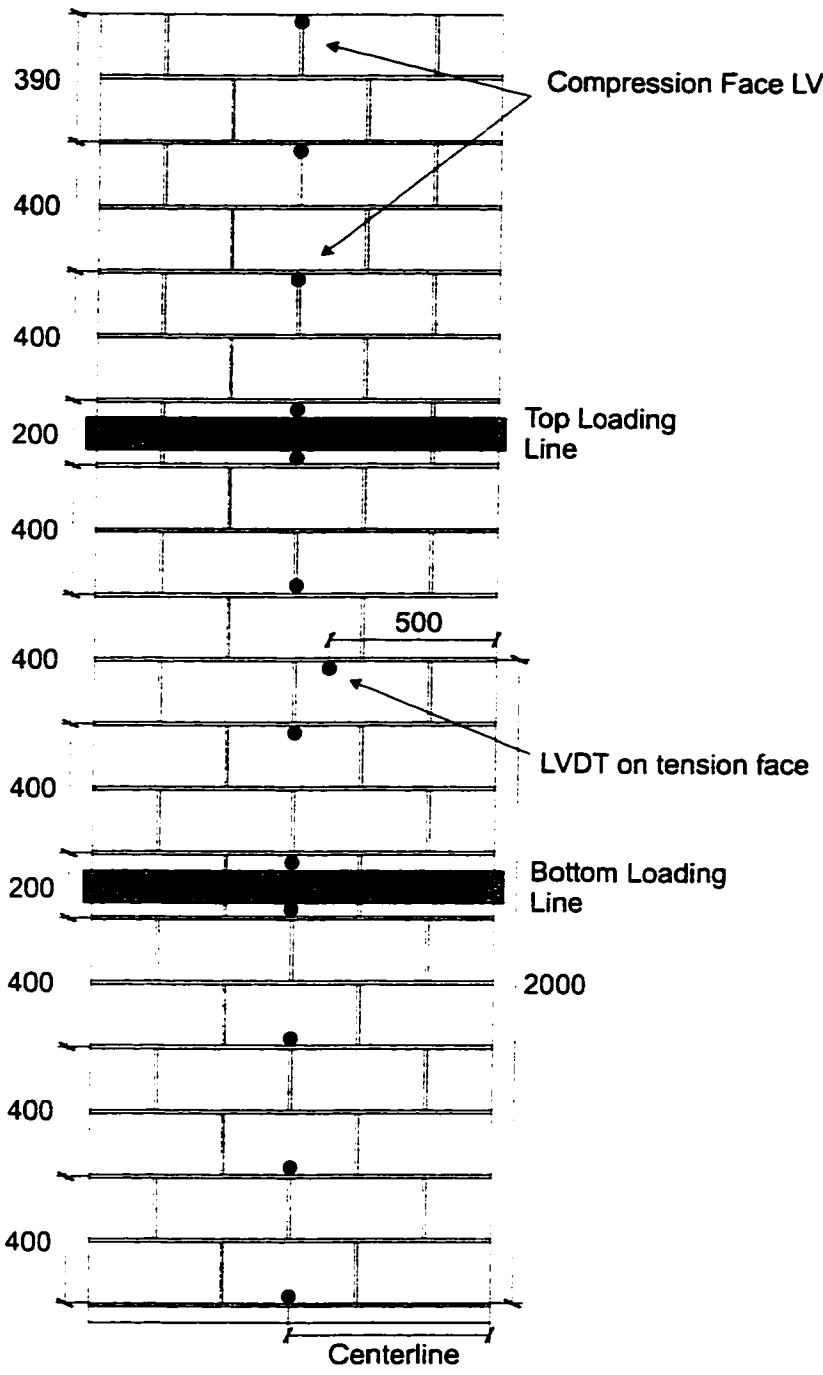

Figure 3.14 Deflection Measurement Positions

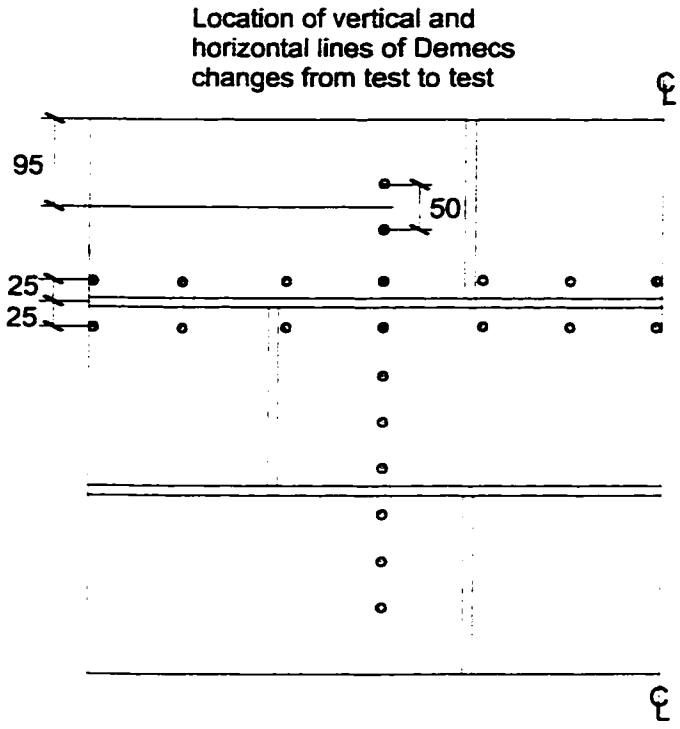

Figure 3.15 Typical Demec Gauge Positions

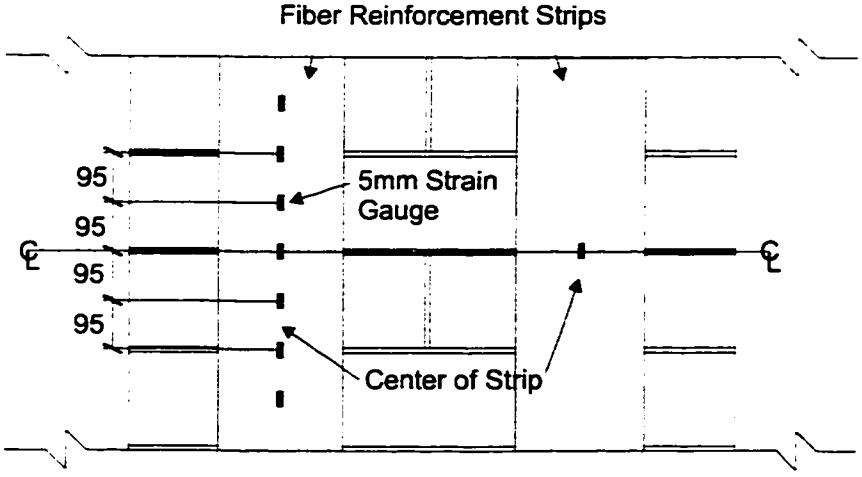

Figure 3.16 Typical Electric Strain Gauge Positions

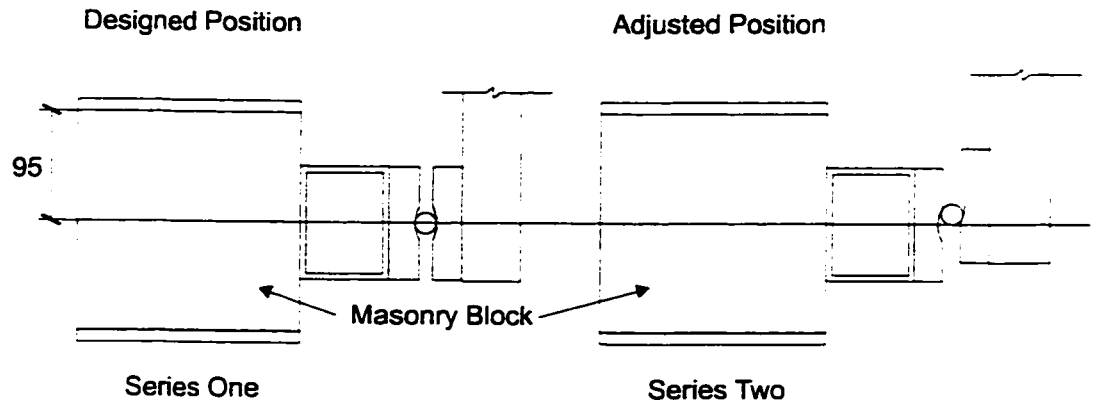

Figure 3.17 Positioning of Loading Points

4. TEST RESULTS

4.1 Introduction

This chapter examines the primary results obtained from the testing program. The major areas of interest are the load - deflection characteristics of the specimens, the tensile and compressive strain results, and the modes of failure. The overall general behaviour of a specimen during a typical test is also presented.

4.2 Load - Deflection Behaviour

The load vs. mid-span deflection response for specimen MU 1, the unreinforced wall, is shown in Fig. 4.1. The response is generally linear until one of the mortar joints separates and then it gradually loses its ability to carry the load. Figures 4.2 to 4.5 show the individual load - deflection responses as well as the combined responses for Series One and Series Two. Comparing the load vs. mid-span deflections for all 12 reinforced tests a definite behaviour pattern can be seen. The overall shape of the responses can be divided into two sections. The first section of the response is a gradual arc which continues until around 10 to 20 mm of mid-span deflection. This initial portion of the response is a result of the mortar joints losing their tensile capacity. As one joint debonds the load is transferred to the next joint until the wall is completely debonded in the constant moment region. Here, debonding refers to the mortar losing its bond to the adjacent masonry block. Only occasionally did a crack form within the mortar itself. Full debonding is defined by the crack or separation in the mortar joint reaching continuously from one edge of the wall to the other throughout the depth of the tension face shell. Chapter 5 will examine in detail the influence of material type and reinforcement ratio on the load - deflection behaviour.

The second portion of the response is identified approximately by a straight line. This part of the response represents the contribution of the reinforcement stiffness to the behaviour of the specimen. At this stage, all horizontal joints within the constant moment region are fully debonded. For the rest of the test the crack widths in the mortar joints simply increase as the wall experiences more deflection. Because the joints have already lost their ability to resist tensile forces and therefore, their ability to contribute to the wall stiffness, they no longer have an effect on the load - deflection behaviour of the wall. The straightness of this second portion is a result of the linear behaviour of the reinforcement material and is a good indication that the reinforcement alone controls the behaviour.

The difference in type of block used for construction, metric or imperial, appears to make a difference in the initial stiffness of the walls. Figure 4.6 shows the load - deflection curves for MCST 4, metric, and ICST 11, imperial. Both specimens are reinforced with the same type and amount of reinforcement, two 250 mm carbon fiber sheets. The wall built with imperial blocks appears to have a higher initial stiffness. This may be because the imperial blocks had a mass of 3.5 kg compared to 2.9 kg for the metric blocks. This translates into an increase in total mass of the wall by 36 kg over the metric dimension walls. While this value is not great, it, along with the increase in the moment of inertia of the imperial block, helps explain the difference in stiffness. It should be noted that masonry is a material that has a significant amount of "built-in" variability. While direct comparisons are made between the load - deflection curves it should be understood that exact values are subject to interpretation. However, the grouping of each series of tests suggests that a comparison of the overall behaviour can be made.

The above interpretation of the behaviour of the load - deflection curve is supported by the first three tests that were performed. Test MCS 2-1, two, 50 mm wide, carbon straps, is a re-test of MU 1, the unreinforced wall. The unreinforced wall cracked at a very low load and, since there was nothing to shift the load elsewhere, the single crack simply continued to enlarge. Only one joint

in the wall had fully debonded. No other joints had any visual cracks in them. Consequently, MCS 2-1 was a test of a relatively undamaged wall. Figure 4.7 shows the load - deflection curves for MCS 2-1 and MCS 3-2. The two section behaviour is visible, although somewhat reduced by the high stiffness of the reinforcement, in MCS 2-1 as the mortar joints debond. When the test was stopped, the majority of the joints in the constant moment region were fully cracked. A few joints still had not debonded across the full width of the specimen. MCS 3-2 was a re-test of MCS 2-1 and was essentially a test of a completely cracked wall. The load - deflection curve is relatively linear and shows that the tensile contribution from the masonry is completely missing. The reinforcement is forced to take all of the load.

4.3 Strain Behaviour

The strains recorded as described in Section 3.4.2 can be categorized into two main areas of interest, masonry strains and reinforcement strains. The next two sub-sections focus on general strain behaviour for a typical test.

4.3.1 Masonry Strains

As mentioned earlier, masonry strain measurements were situated in the horizontal and vertical directions. Horizontal strain readings were taken to identify the effect the reinforcement has on the strain pattern across the length of the wall. Vertical readings were taken between the load points to help identify any pattern in the masonry joint strains.

Figure 4.8 shows a typical vertical joint strain behaviour pattern recorded during test MCS 6, reinforced four 50 mm wide carbon straps. The strains were measured 300 mm from the North edge of the wall and 35 mm away from one of the strips of reinforcement. The figure shows that the joint strains are relatively uniform until a load of approximately 15 kN. This coincides with the change to the second portion of the load - deflection curve for this specimen. The strains

after this load become more erratic suggesting that each joint is now completely independent of its neighbour or fully separated.

The strains along the width of the wall can be separated further into block and joint strain behaviour. Block and joint strain refers to the location of the strain gauges, either centered within a block or over a joint. Some horizontal strain readings cross a strip of fiber reinforcement. While these strains are reinforcement strains, for the purpose of this section, they will be included under the categories of block and joint strain behaviour. Figures 4.9 and 4.10 show the typical block strain behaviour for a wall reinforced with carbon fiber sheet. Symmetry was assumed and readings were only taken up to the vertical center line of the wall. The Demec results shown are centered on the 6^{th} course at a height of 1.112 m from the base of the wall. This course is outside of the constant moment region, just below the lower load point. Figure 4.9 shows the results from test ICST 11, reinforced with two 250 mm wide carbon sheets. The figure shows that the strains are much higher on the reinforcement than in the block itself. The weak bond between the mortar and the block does not allow it to carry much tension. At a load of 5 kN the reinforcement is already picking up most of the load; however, some strain is transferred to the block directly next to the strip of reinforcement. Within the reinforcement itself the strains become higher as they approach the center of the strip. Figure 4.10 shows a similar trend for specimen ICST 10, reinforced with two 125 mm wide carbon sheets. Again there is a gradual increase in strain towards the reinforcement. In this case, the compression strains were recorded and a similar pattern is observed. While on the tension side the strains reduce to zero away from the reinforcement, the strains on the compression side gradually reduce to a constant level. The reason for the small jump in strain at 11 kN on the center line of the tension face is that a Demec point was situated over a vertical joint and the mortar had cracked between the gauge.

The typical joint strain behaviour is illustrated in Figures 4.11 to 4.14. All of the figures have the same basic trend but are situated at different joint heights. The tensile joint strain behaviour is essentially the opposite of the block

strain behaviour. The strain is high across the masonry joint and gradually reduces towards the reinforcement. The reinforcement restrains the joint from opening freely. Figures 4.11 and 4.12 are from specimen ICST 10 and illustrate how much the strains differ between locations. The joint strains in Fig. 4.11 were recorded at a height of 1.01 m, outside of the constant moment region. The joint strains in Fig. 4.12 were recorded at a height of 1.619 m, well within the constant moment region. The strain patters are similar; however, the strains recorded in the constant moment region are much higher. In both cases, the compression strains directly behind the reinforced area are constant, if not a little bit lower, than the surrounding strain in the masonry joint. This is more evident in Fig. 4.13. Figures 4.13 and 4.14 are both for specimen ICST 11 at a joint height of 1.619 m. They show the compression and tension behaviour of the joint respectively. They were kept separate so the scale could be left unaltered and the full effect of the strain behaviour could be more clearly seen.

The last item to be discussed is the load - masonry strain behaviour of the specimens. A typical load - masonry strain response is shown in Fig. 4.15. This figure shows the behaviour for joint tension strains only. Many of the readings taken for the block strains were too erratic to make an effective plot. The curve looks very much like a load - deflection response. The initial response is non-linear becoming linear after about 15 kN of load has been applied which corresponds with the change in slope of the load - deflection curve for specimen ICST 11.

4.3.2 Reinforcement Strains

The reinforcement strains can be categorized in much the same way as the masonry strains with one exception, since the reinforcement was oriented primarily in the vertical direction only vertical strains were recorded.

The strains along the height of the reinforcement were recorded for many of the tests and the results are all very similar. Sixteen joint strain gauges and ten block strain gauges were placed on specimen ICST 11 in an attempt to

obtain the full behaviour over the height for a typical specimen. Figure 4.16 shows the results of the block and joint strains superimposed over each other. During the beginning of the test the block strains in the constant moment region are uniform and later become more erratic but still remaining within about 1000 microstrain of each other. Similarly the joint strains start off uniform and become more erratic as the load increases. In both cases the strains alternate back and forth and for analysis purposes can reasonably be estimated by taking the average within the constant moment region. Figures 4.17 and 4.18 compare compression and tension reinforcement strains for specimen MCST 7-4. As will be explained in Chapter 5, MCST 7-4 had carbon fiber reinforcement on the compression face as well as the tension face, thus strain readings were available for the compression face. In general, the compression strains are more uniform than the individual tension strains across the joint.

Figure 4.19 shows a typical load - strain plot for both joint and block strains located within the constant moment region for specimen ICST 11. Again there is a distinct difference between the joint and block strains. The block strains are linear up to a load of approximately 14 to 15 kN. Subsequently the strains increase rapidly with very little increase in load until they stabilize and again assume a linear form. This initial change in slope of the curve again corresponds with the change in slope of the load - deflection curve for specimen ICST 11. The sudden increase in strain can be attributed to the reinforcement requiring a longer development length as the horizontal joints become fully cracked. The joint strains follow approximately the same initial slope as the block strains but then suddenly change slope around 5 kN. This indicates the point at which the joint in that particular location has begun to debond. The remainder of the curve has a relatively linear behaviour. Figure 4.20 compares the same tensile block and joint strain behaviour with its corresponding compression strains for specimen MCST 7-4. The compression strains are much more consistent and are not subject to the sudden variations that the tensile strains experience.

4.4 Failure Modes

Out of the thirteen specimens tested three general modes of failure were observed. For the purposes of this section, failure is defined as the point when the specimen can no longer accommodate an increase in load. The three modes of failure are: mortar debonding or sliding shear, flexure - shear, and rupture of the fiber reinforcement.

Mortar debonding, or sliding shear, involves the debonding of the mortar from the adjacent masonry block. This accounts for the failure of two specimens, MU 1, the unreinforced wall, and MCS 3-2, reinforced with two 50 mm wide carbon straps. The unreinforced wall lost its ability to carry load when the mortar separated from the block at the 13^{th} joint from the base of the wall. Figure 4.21 shows the separated joint. This occurred at a very low load, approximately 1 kN, and a mid-span deflection of only 0.7 mm. For specimen MCS 3-2 the 1^{st} joint from the base of the wall slipped in the horizontal direction. Figure 4.22 illustrates this mode of failure. The damage to the wall above the failed joint was caused by the impact of the wall against the stop bar used to prevent the wall from slipping out of the test frame and was not caused by the mentioned failure. This mode of failure occurred because the reinforcement did not have sufficient bonded area to restrain the shear forces. The figure shows how the joint simply pulled the bottom of the reinforcement off the wall. This was determined to be an undesirable mode of failure and for future tests carbon fiber patches were placed over the lower and upper reaction joints to provide enough shear resistance. Figure 4.23 illustrates this precaution.

The second, and most common, mode of failure was flexure-shear. Because the shear span to specimen depth ratio is high, pure shear was not expected to be an issue. However, the reinforced specimens experienced enough deflection to induce a flexural crack in the end blocks, usually between the 5^{th} and 7^{th} courses inclusive. Once this flexure crack had progressed perpendicular from the mortar joint about 15 mm in length, a shear crack would begin to propagate towards the compression face of the specimen. This

progression of the flexure-shear failure is illustrated in Fig. 4.24. The resulting failure is shown in Fig. 4.25. Six specimens failed in this manner. An additional specimen was unloaded before the shear cracks induced failure.

The final mode of failure was rupture of the fiber reinforcement, a form of flexure failure. Two specimens, ICST 10, reinforced with two 125 mm carbon sheets, and ICST 12, reinforced with ten 125 mm angled carbon sheets, failed in this manner. In both cases the reinforcement ruptured along one or two of the horizontal joints in the constant moment region. Flexure-shear cracks did not develop. Figures 4.26 and 4.27 show the failed joint for specimens ICST 10 and ICST 12 respectively. In Fig. 4.26 it can be clearly seen that the masonry is firmly bonded to the failed strip of reinforcement. Also, a crack pattern can be seen around the reinforcement. This will be explained further in the next section. Specimen ICST 12 failed at the joint which had the least surface area of reinforcement crossing it. The width of the separation in the joint, although somewhat amplified by the final failure, is evidently quite large.

Table 4.1 summarizes the failure modes for each specimen tested along with the corresponding failure load and mid-span deflection. In all of the reinforced specimens failure occurred without significant warning. The stress-strain behaviour of the materials used as reinforcement lacks any form of yielding typically associated with standard steel reinforcement. Because of this all of the failure modes can be classified as brittle.

4.5 General Behaviour of Wall

For all previous discussions symmetry of the specimen was assumed. Comparisons of the loads in the four reaction load cells showed that all of the tests were loaded uniformly. Mid-span reinforcement strains also confirm that the strains in each strip, in the cases where there were two strips of reinforcement, experienced approximately the same strains. These points, along with the following deflection plots, suggest that the assumption of symmetry is valid.

The deflection of the wall along the height was plotted for each specimen. Figure 4.28 shows the results of specimen MU 1, the unreinforced wall. A typical plot of the deflection along the height for the reinforced walls is shown in Fig. 4.29. Both figures show a consistent curvature. Although the figures show a deflection at the top of the wall this value should read zero. The deflection recorded is because the LVDT's are located only 1 m away from the wall. As the wall experiences curvature, the point where the LVDT is attached to the wall deflects vertically slightly. This causes the LVDT cable to lengthen producing a false horizontal deflection reading. This explanation is illustrated in Fig. 4.30. The majority of the curvature occurs between the load points in the constant moment region. In Fig. 4.28. the joint at which failure occurred is clearly shown as the location with the largest deflection.

Each reinforced specimen followed a series of steps before failure occurred. The first event that happens is the progressive separation of the horizontal mortar joints in the constant moment region. Once every joint has fully separated diagonal cracks begin to appear in random locations. The cracks begin at the edge of the reinforcement strips and angle up or down to the nearest horizontal joint. The difference in strain between the reinforcement and the adjacent joint, as shown in the section on strain behaviour, explains the formation of these diagonal cracks. In the tests which experienced mid-span deflections over 70 mm, the reinforcement would begin to pull the face of the masonry block away from the wall. This occurred when diagonal cracks had fully formed around a joint location. Next, horizontal flexure cracks would form in random locations. The cracks would typically start from the center of a block at the edge of the reinforcement strip and progress outwards towards the edge of the wall or towards the center of the wall. In some cases the flexure cracks spanned completely between the strips of reinforcement. Not all joints and blocks experienced these diagonal cracks and flexure cracks. Finally, if flexure failure had not occurred, flexure-shear cracks would form on the edge blocks of the wall. These cracks formed between the 5^{th} and 7^{th} courses from the base of the wall, just below the lower load point, as well as between the 14^{th} and 16^{th}

courses, just above the upper load point. One of these cracks would then progress until failure. The progression of the crack patterns is illustrated in Fig. 4.31. Photographs of the crack patterns are shown in Fig. 4.32 It is very difficult to see the debonded joints because the crack widths are less than 0.5 mm at the level of lateral load shown in the photographs. The other cracks have been highlighted with a black felt marker.

Table 4.1

Summary of Results

Specimen	Max. Load (kN)	Mid-Span Defl. (mm)	Mode of Failure	Location of Failure (from base of wall)
MU 1	1.0	0.7	mortar separation	13th joint
MCS 2-1	12.0	14	N/A	N/A
MCS 3-2	21.8	31	mortar slip	1st joint
MCST 4	28.9	58	N/A	N/A
MGST 5	36.0	70	flexure-shear	5th course
MCS 6	46.4	42	flexure-shear	6th course
MCST 7-4	32.7	78	flexure-shear	6th course
ICST 8	50.2	63	flexure-shear	7th course
ICST 9	33.0	71	N/A	N/A
ICST 10	20.9	82	rupture of fibers	11th and 12th joint
ICST 11	41.7	91	flexure-shear	7th course
ICST 12	22.7	62	rupture of fibers	12th joint
ICST 13	37.7	88	flexure-shear	6th course

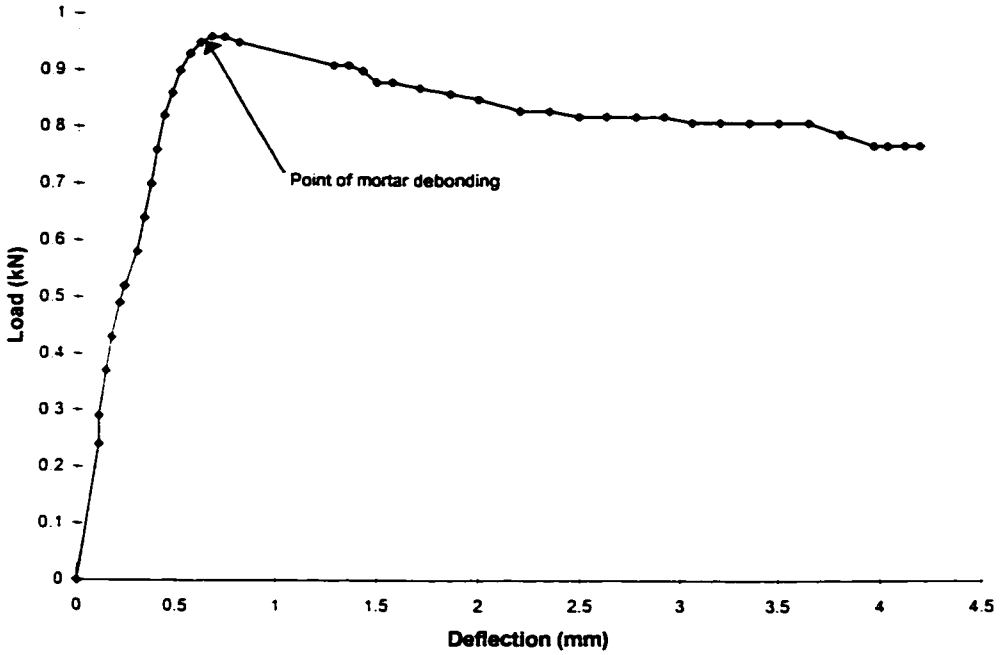

Figure 4.1 Load - Mid-span Deflection Response for Unreinforced Wall

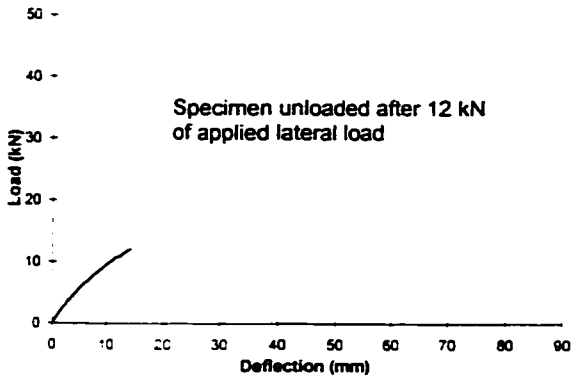

MCS 2-1
Two, 50 mm wide carbon straps

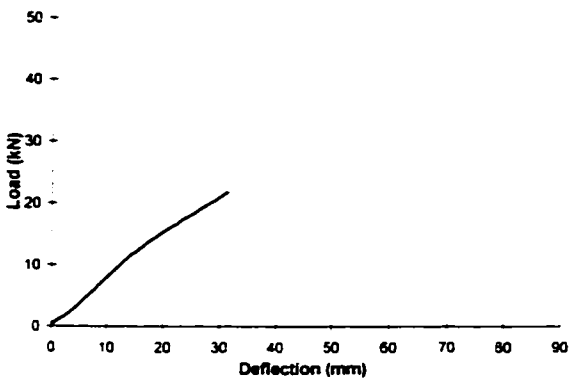

MCS 3-2
Two, 50 mm wide carbon straps

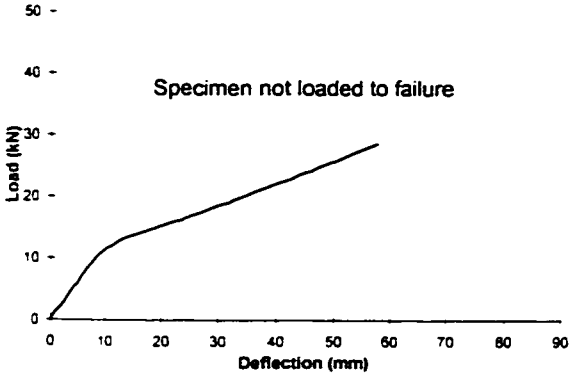

MCST 4
Two, 250 mm wide carbon sheets

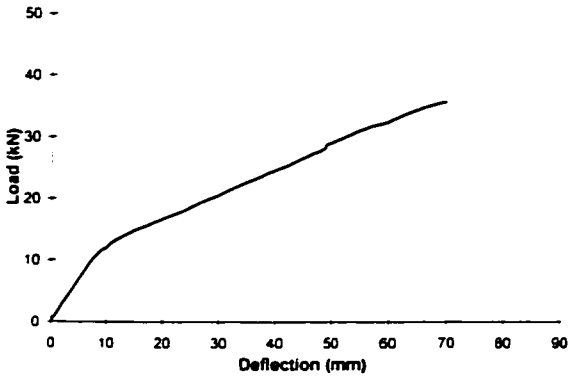

MGST 5
Two, 250 mm wide glass sheets

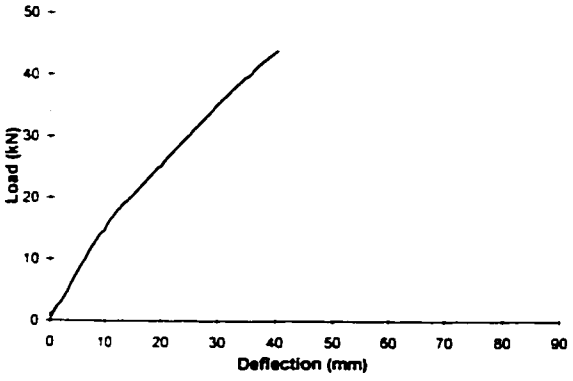

MCS 6
Four, 50 mm wide carbon straps

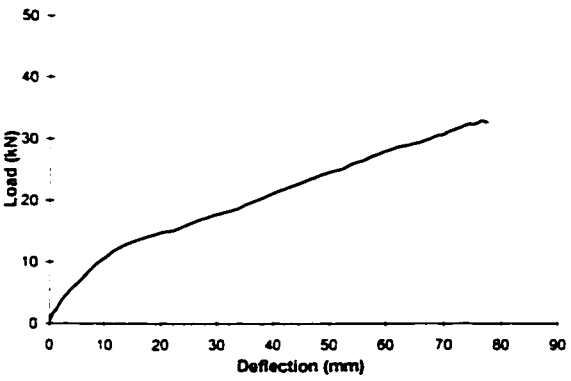

MCST 7-4
Two, 250 mm wide carbon sheets
cyclic loading

Figure 4.2 Series One Individual Load - Mid-span Deflection Responses

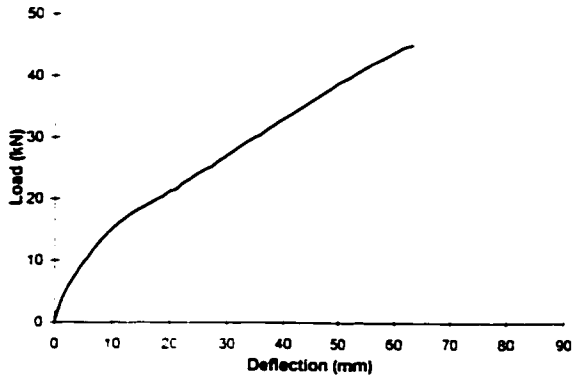

ICST 8
Two, 250 mm wide carbon sheets
two layers per sheet

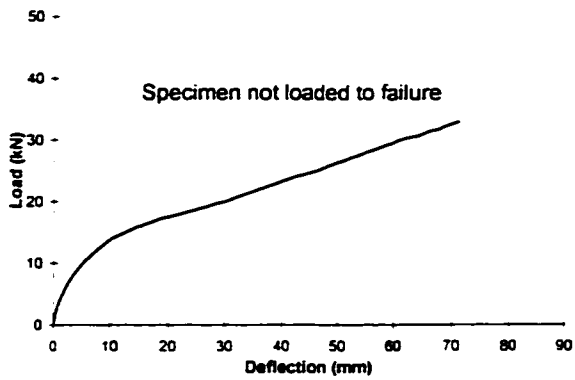

ICST 9
Two, 250 mm wide carbon sheets
10 kN applied axial load

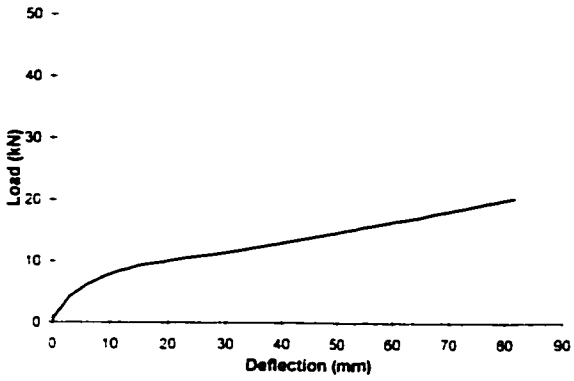

ICST 10
Two, 125 mm wide carbon sheets

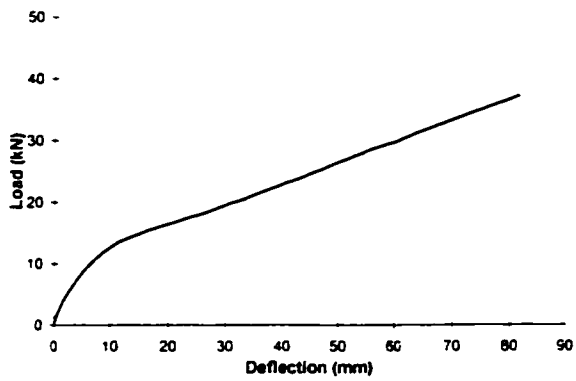

ICST 11
Two, 250 mm wide carbon sheets

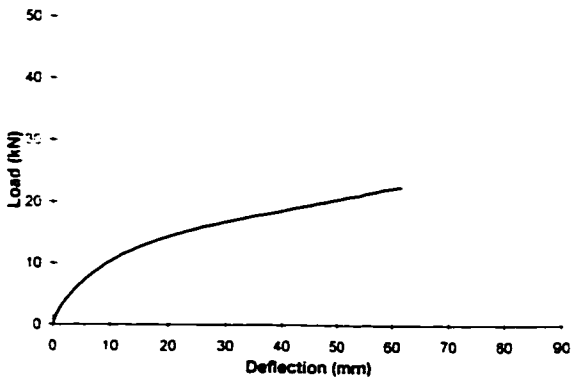

ICST 12
Ten, 125 mm wide carbon sheets
angled at 37° from vertical

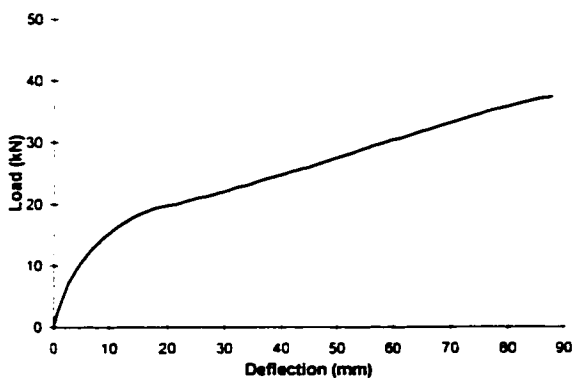

ICST 13
Two, 250 mm wide carbon sheets
30 kN applied axial load

Figure 4.3 Series Two Individual Load - Mid-span Deflection Responses

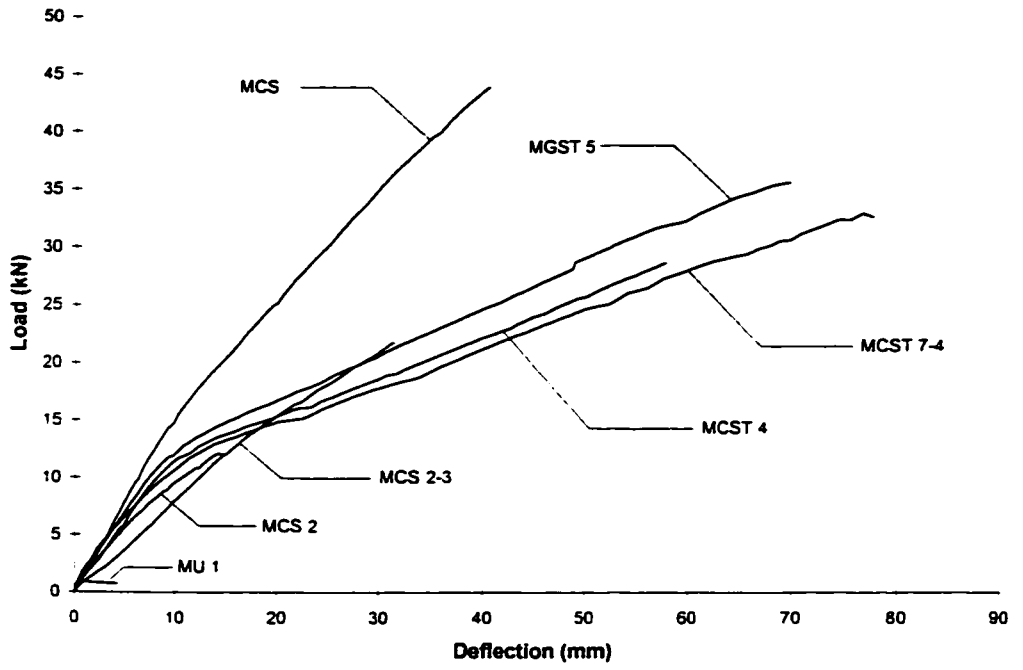

Figure 4.4 Comparison of Series One Load - Deflection Responses

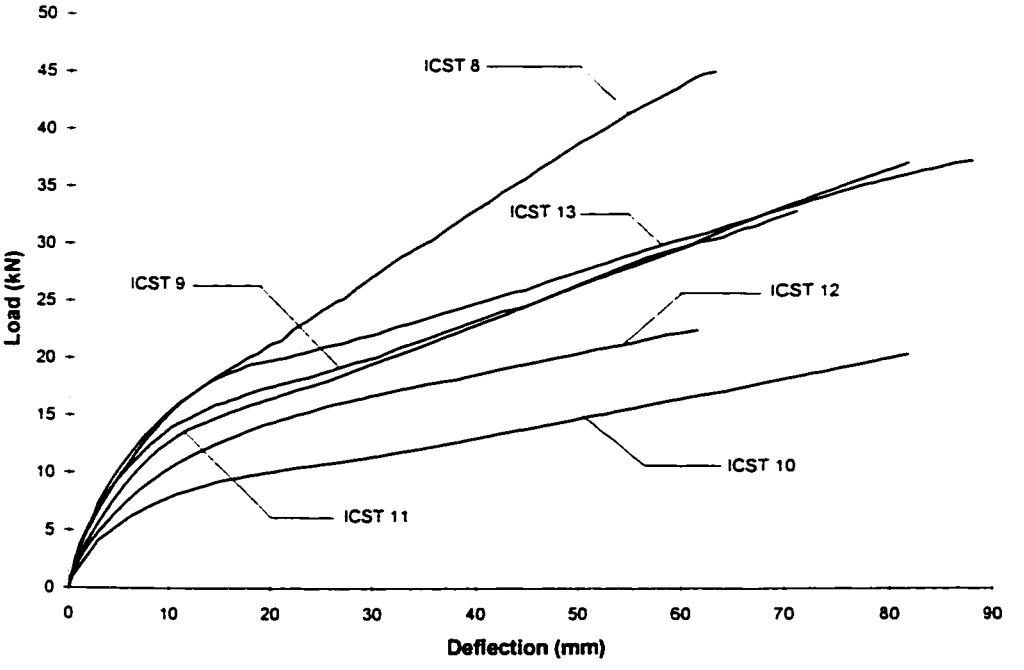

Figure 4.5 Comparison of Series Two Load - Deflection Responses

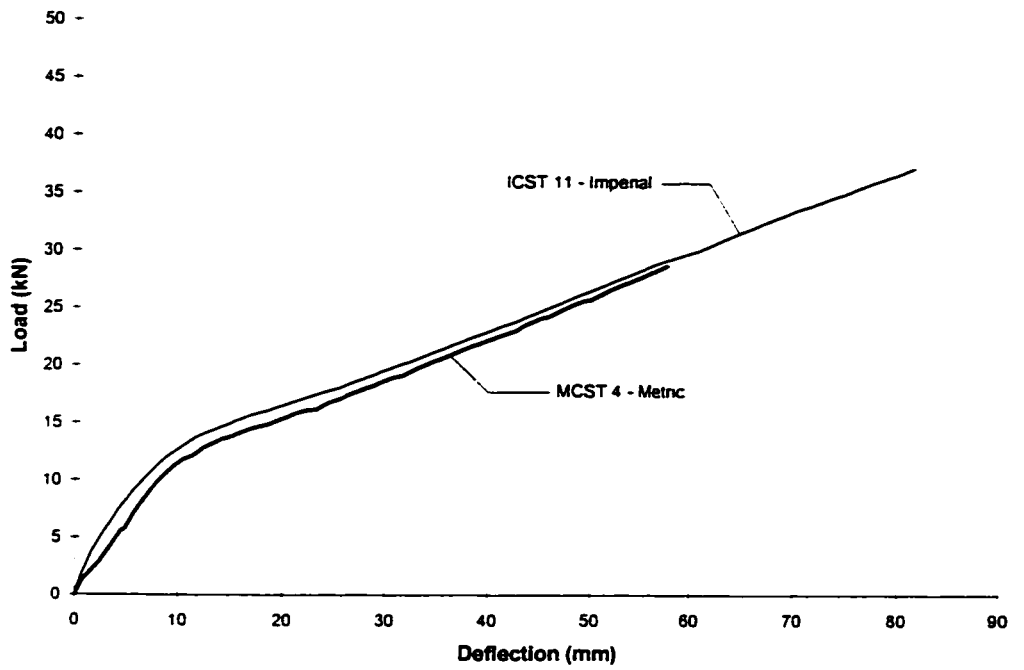

Figure 4.6 Difference Between Metric and Imperial Dimension Block

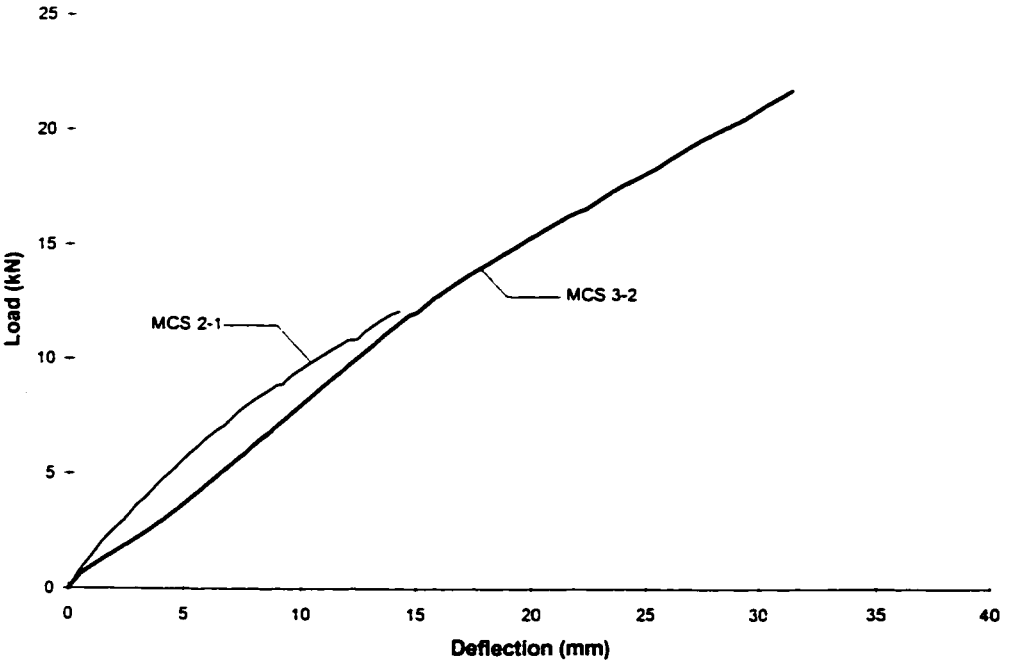

Figure 4.7 Comparison of Undamaged and Damaged Wall

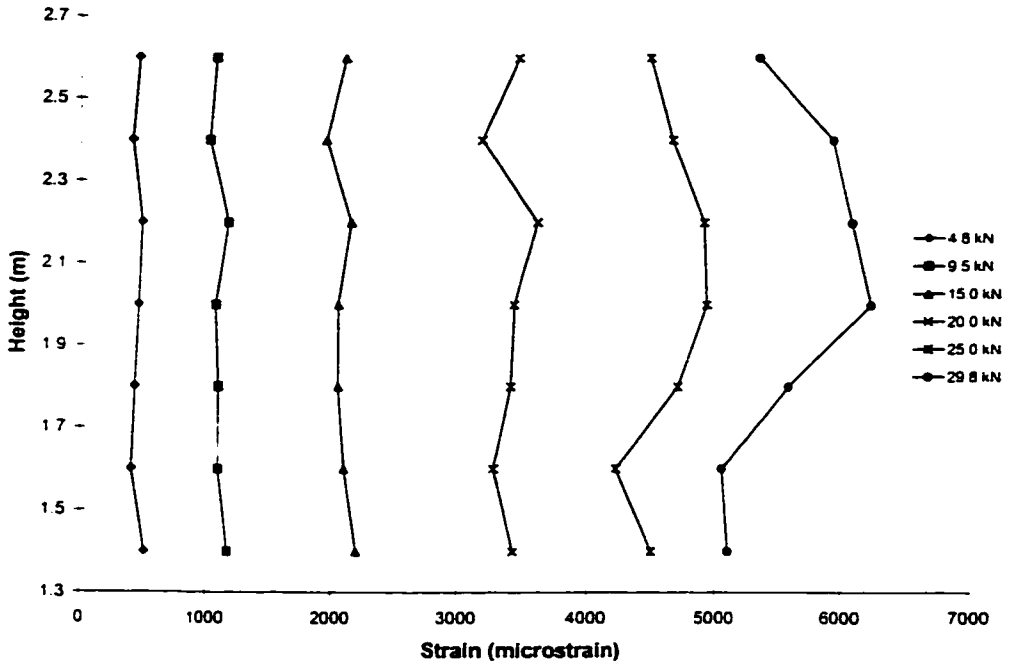

Figure 4.8 Typical Joint Strains Along the Height

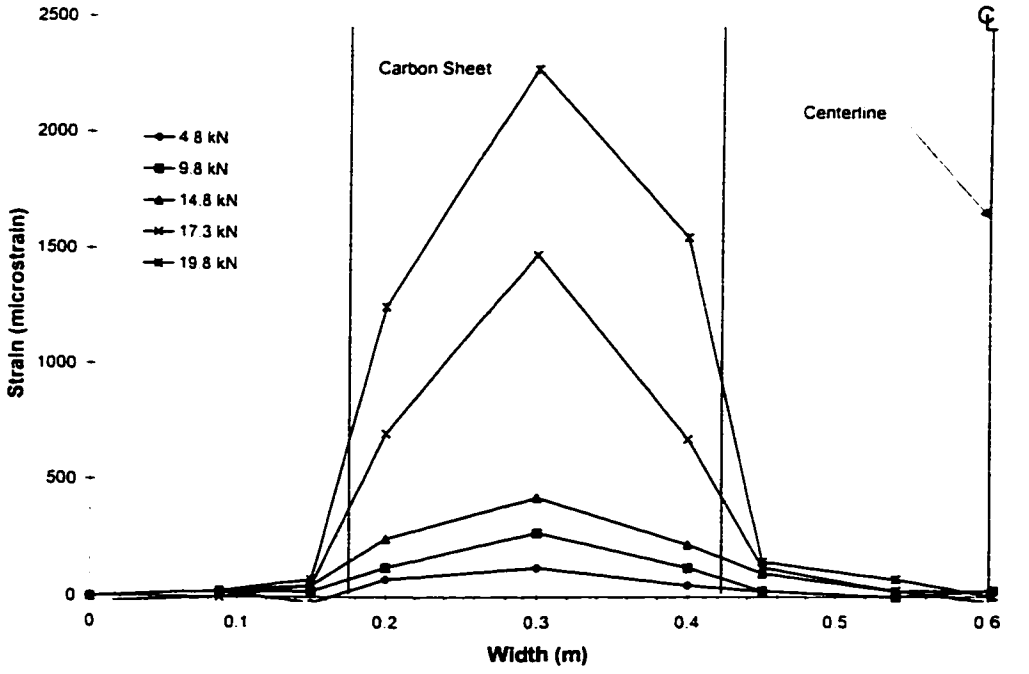

Figure 4.9 Block Strains Along the Width - Specimen ICST 11

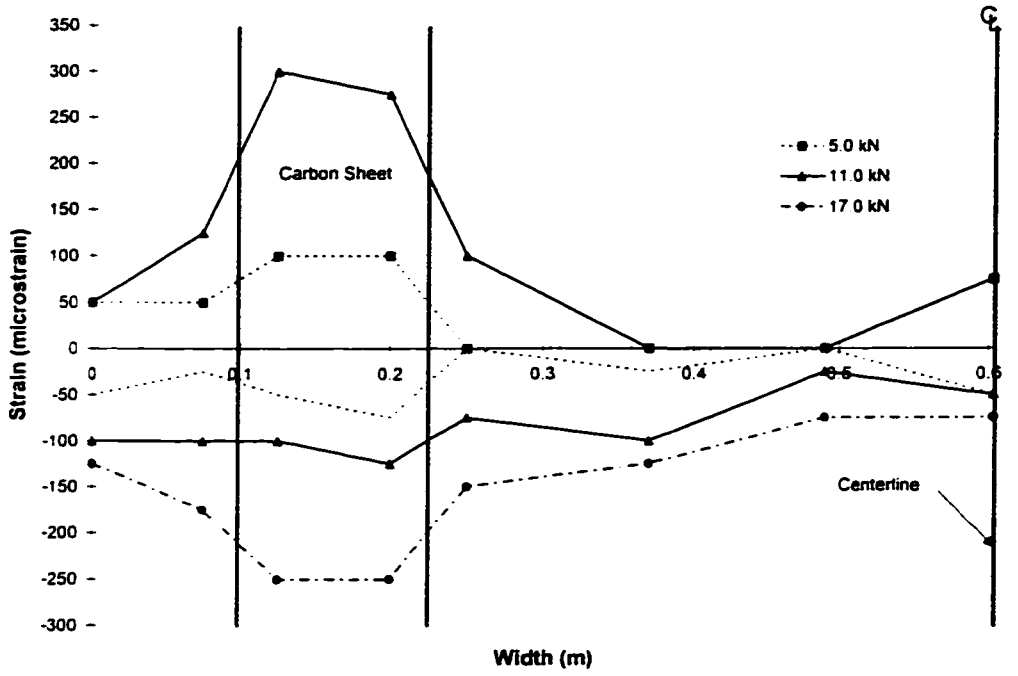

Figure 4.10 Block Strains Along the Width - Specimen ICST 10

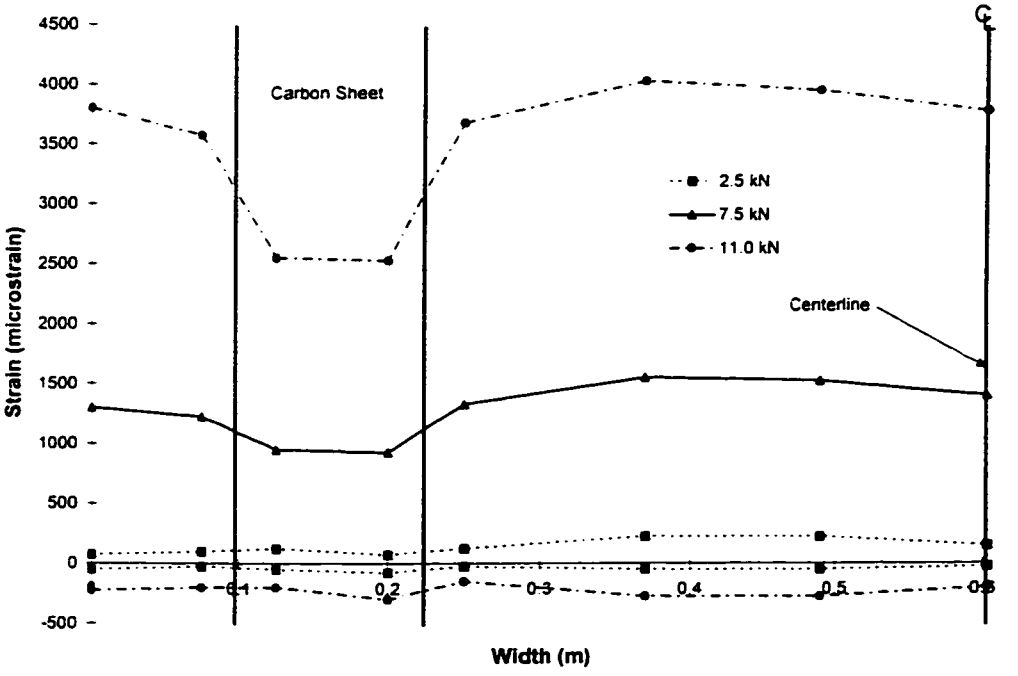

Figure 4.11 Joint Strain Behaviour at Height = 1.01 m - Specimen ICST 10

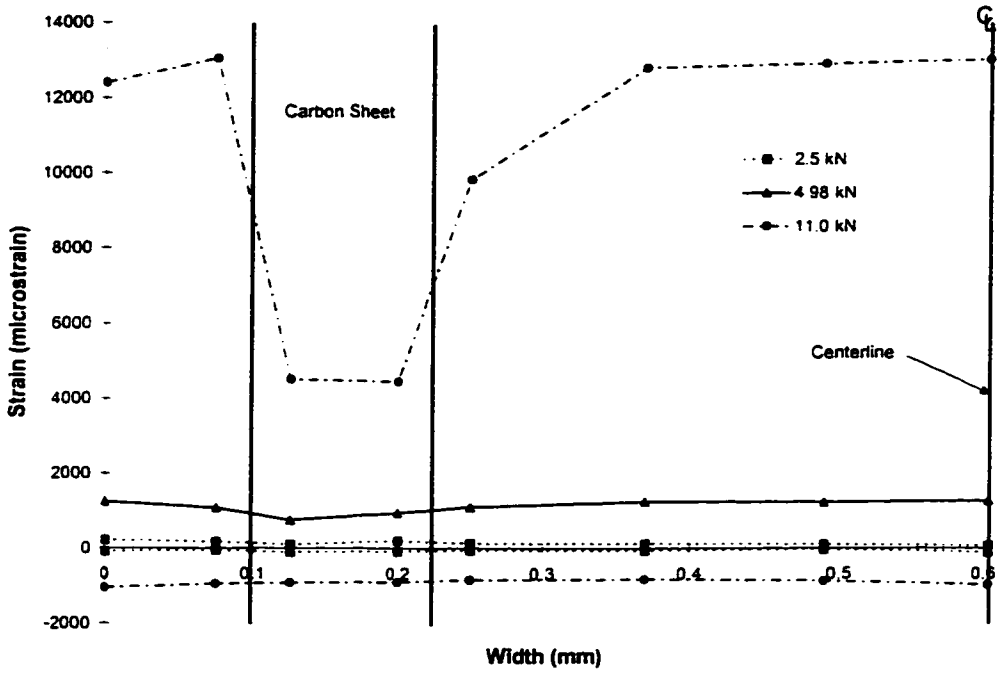

Figure 4.12 Joint Strain Behaviour at Height = 1.619 m - Specimen ICST 10

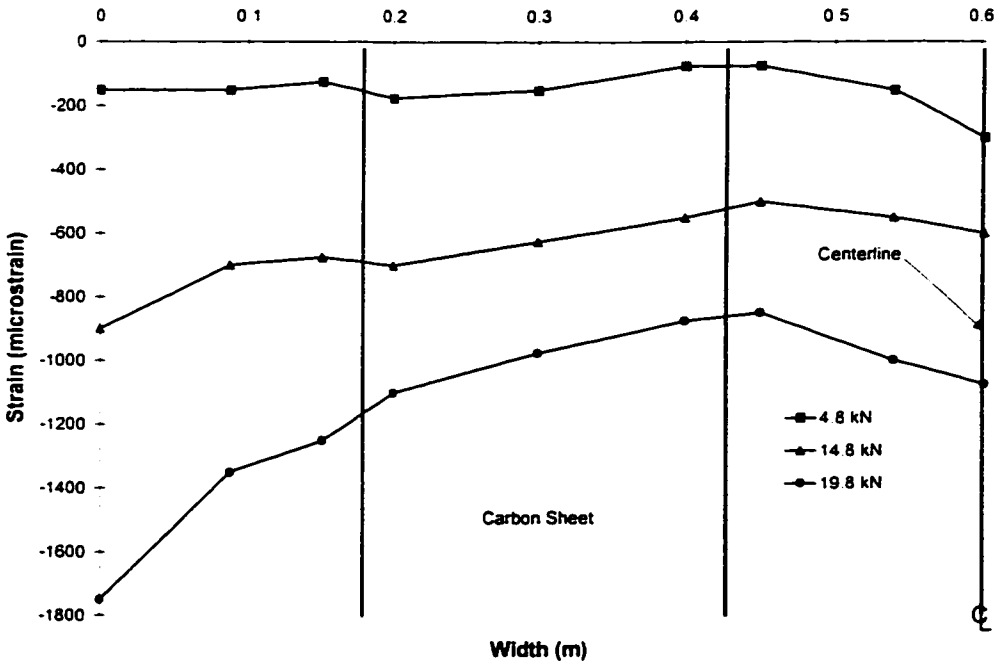

Figure 4.13 Compression Joint Strains at Height = 1.619 m - Specimen ICST 11

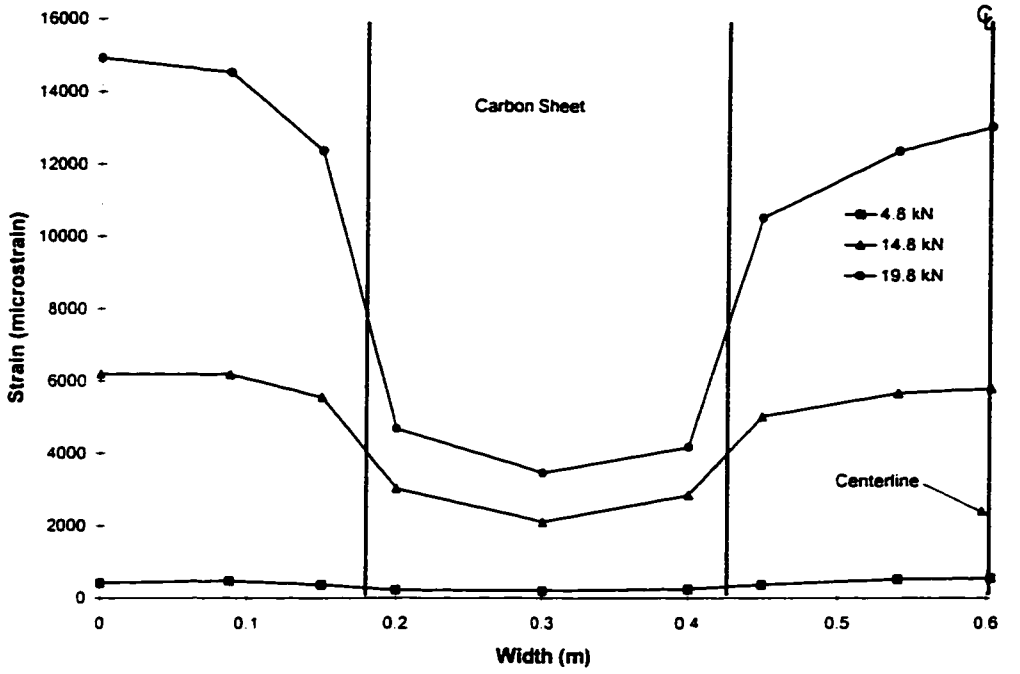

Figure 4.14 Tension Joint Strain at Height = 1.619 m - Specimen ICST 11

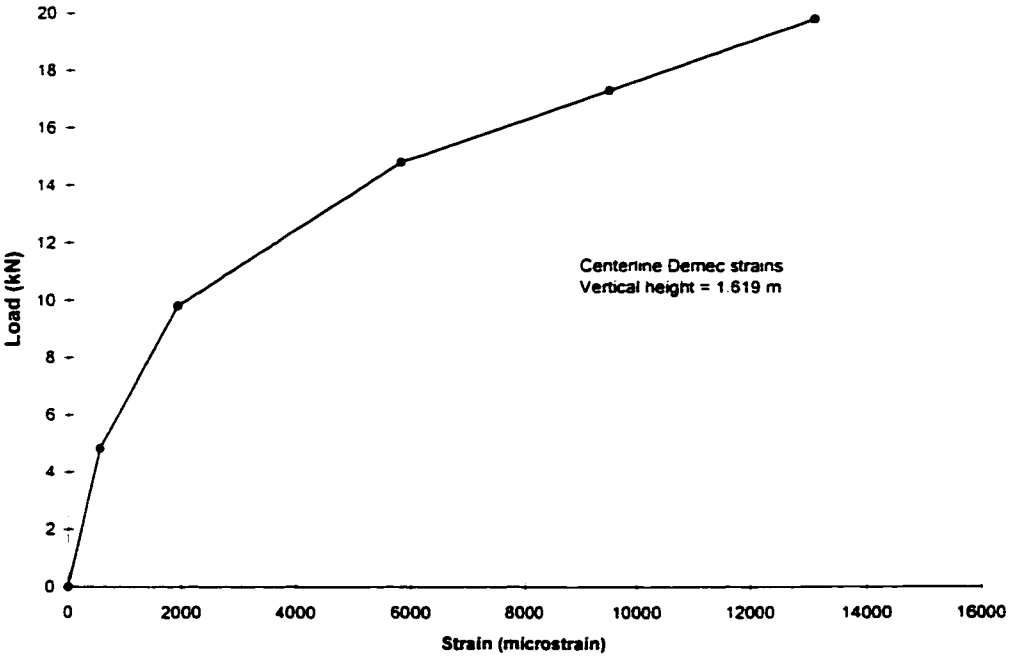

Figure 4.15 Load - Masonry Joint Tension Strain Behaviour

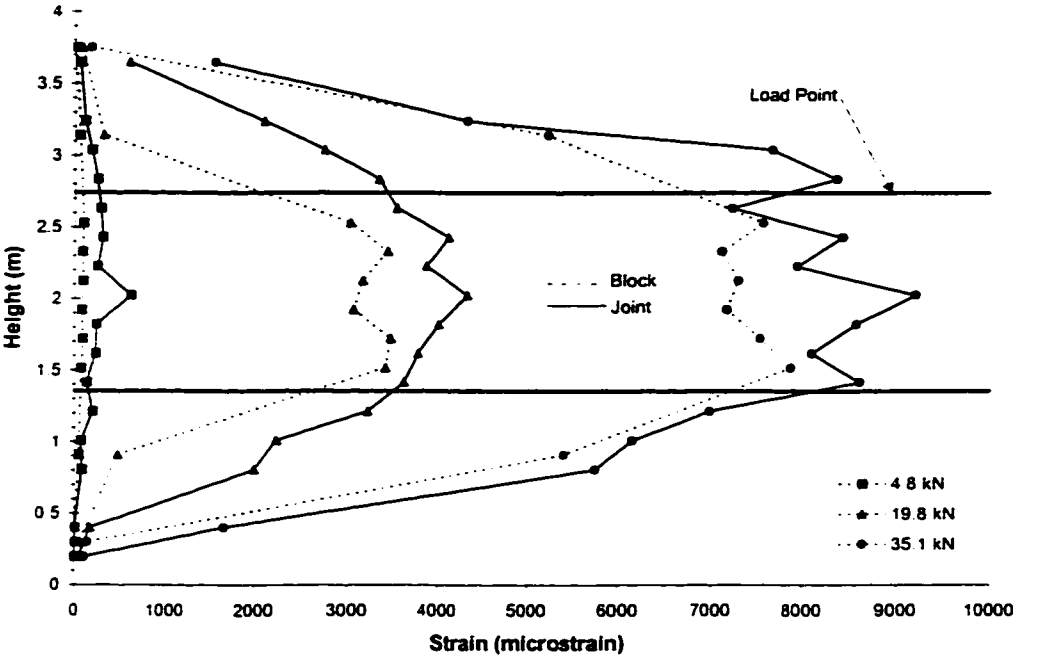

Figure 4.16 Block and Joint Reinforcement Strain Pattern

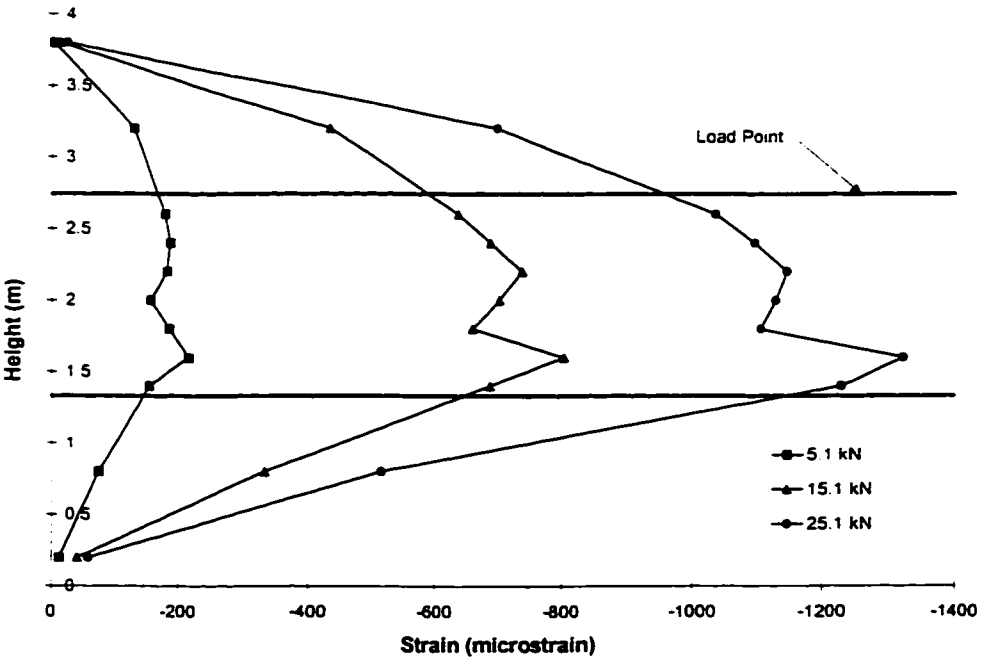

Figure 4.17 Compression Joint Strain Pattern - Specimen MCST 7-4

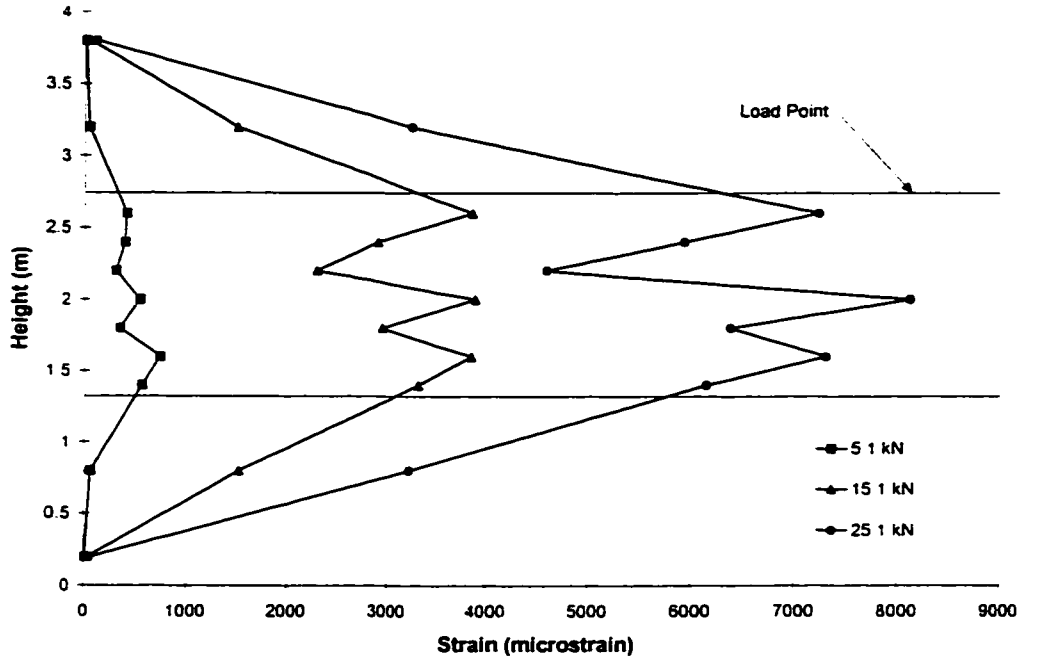

Figure 4.18 Tension Joint Strain Pattern - Specimen MCST 7-4

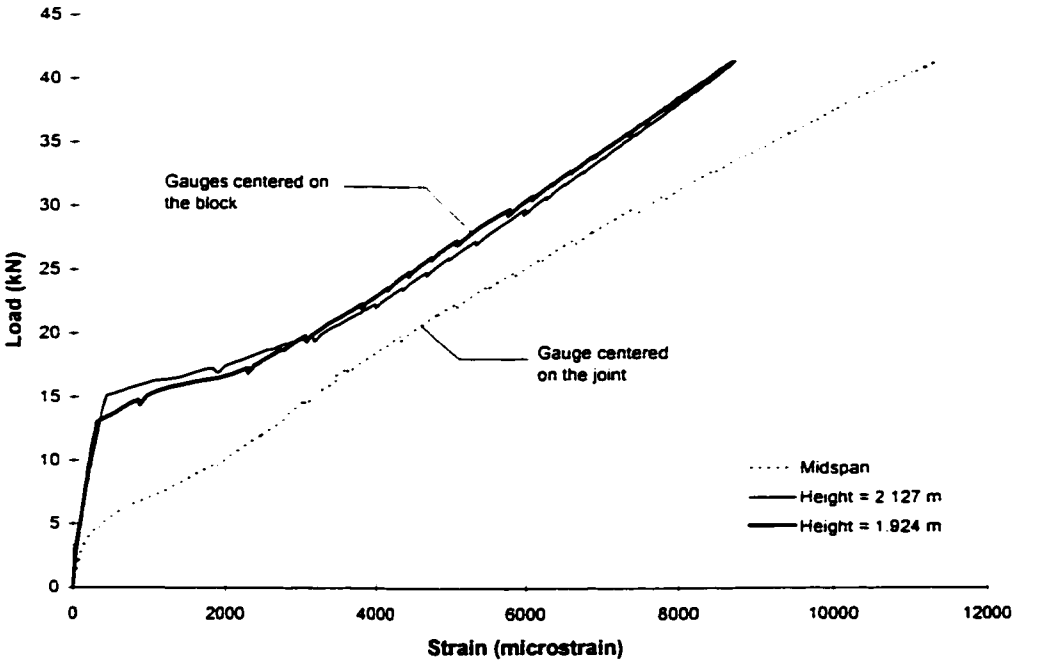

Figure 4.19 Fiber Reinforcement Load - Strain Behaviour

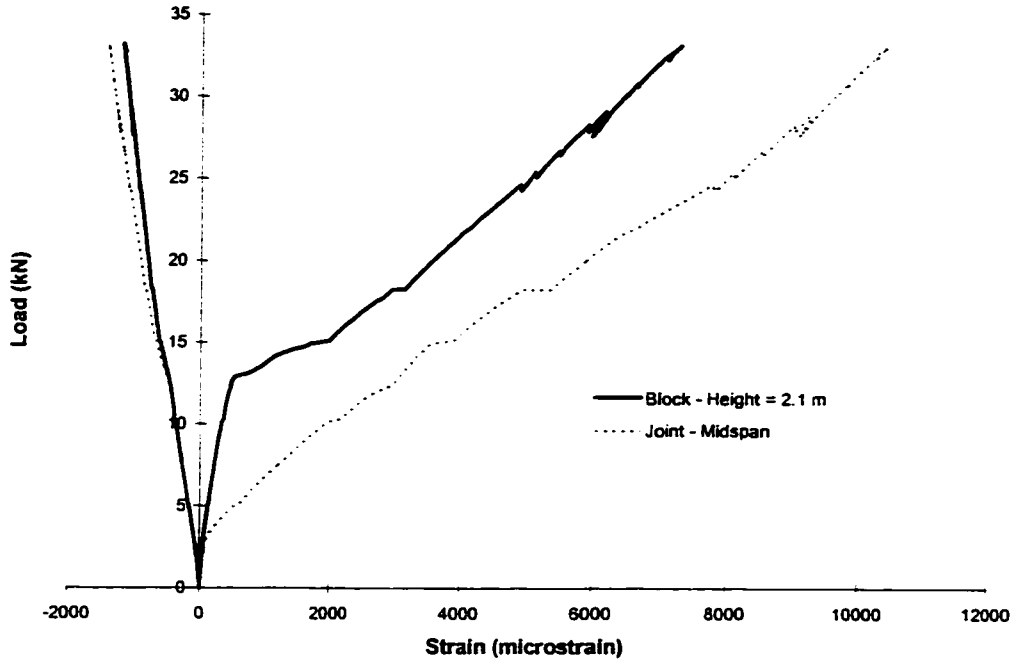

Figure 4.20 Compression and Tension Load - Strain Behaviour

Figure 4.21 Mortar Debonding Failure for Unreinforced Wall Specimen

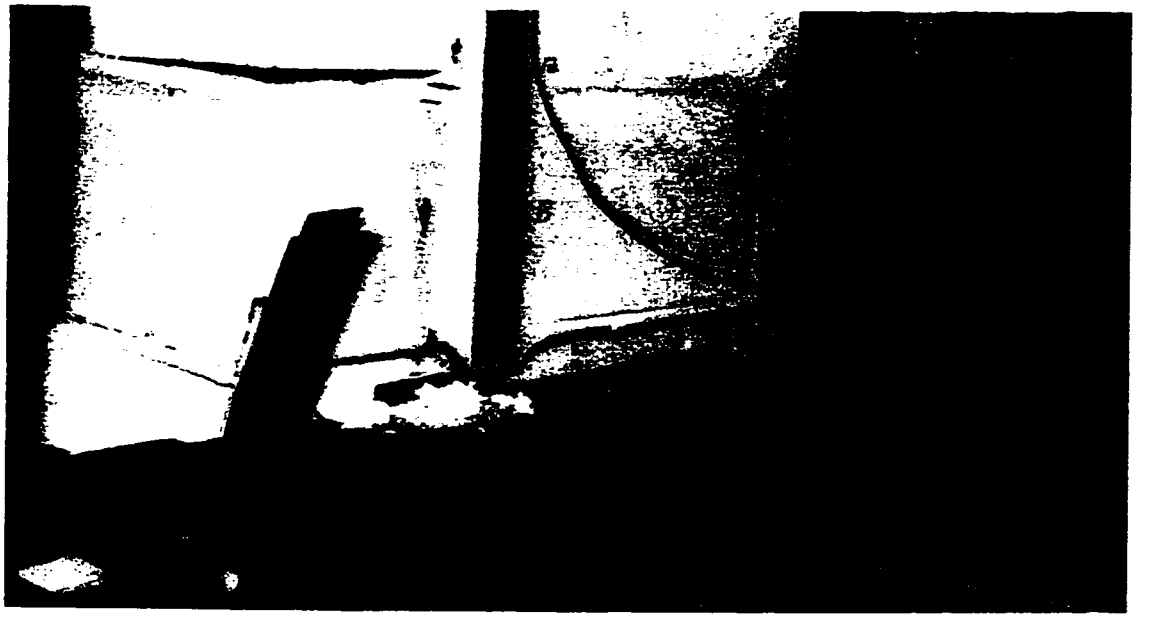

Figure 4.22 Sliding Shear at the Base of the Wall

Figure 4.23 Carbon Fiber Patches to Prevent Sliding Shear

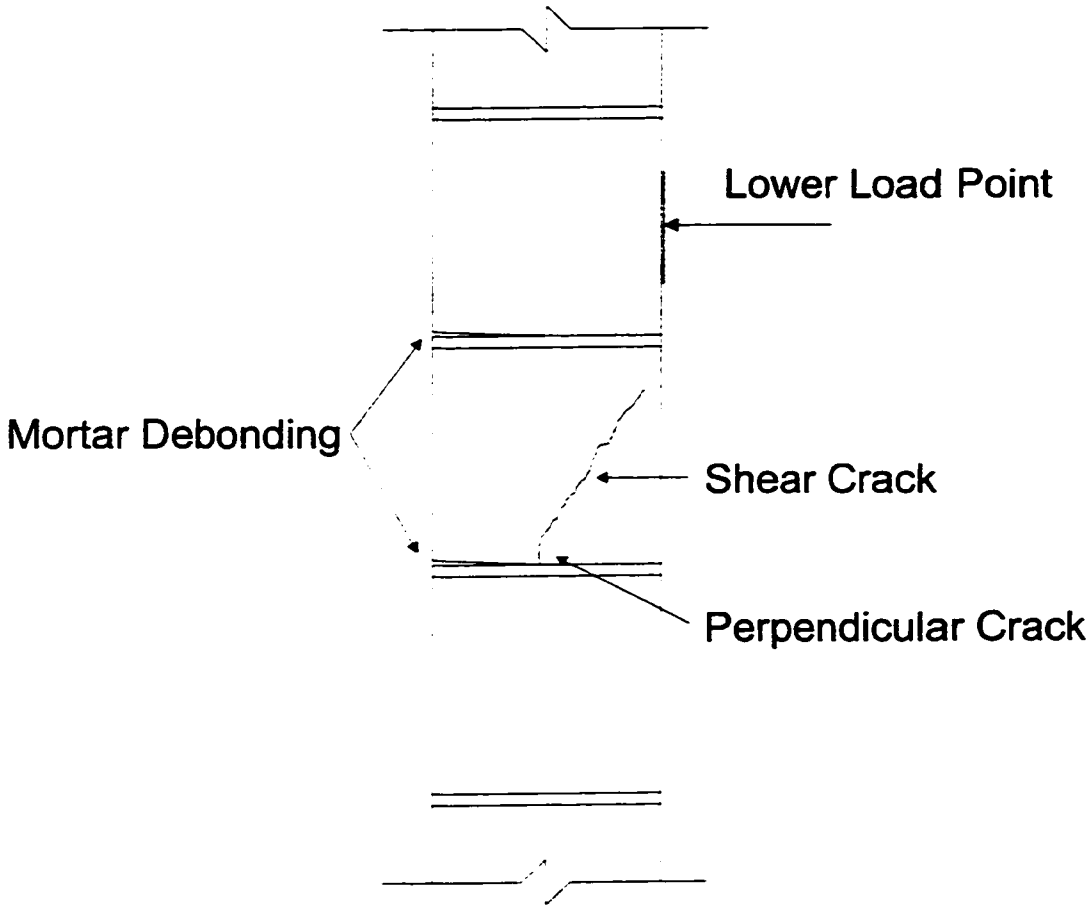

Figure 4.24 Progression of Flexure-Shear Failure

Figure 4.25 Flexure-Shear Failure Mode

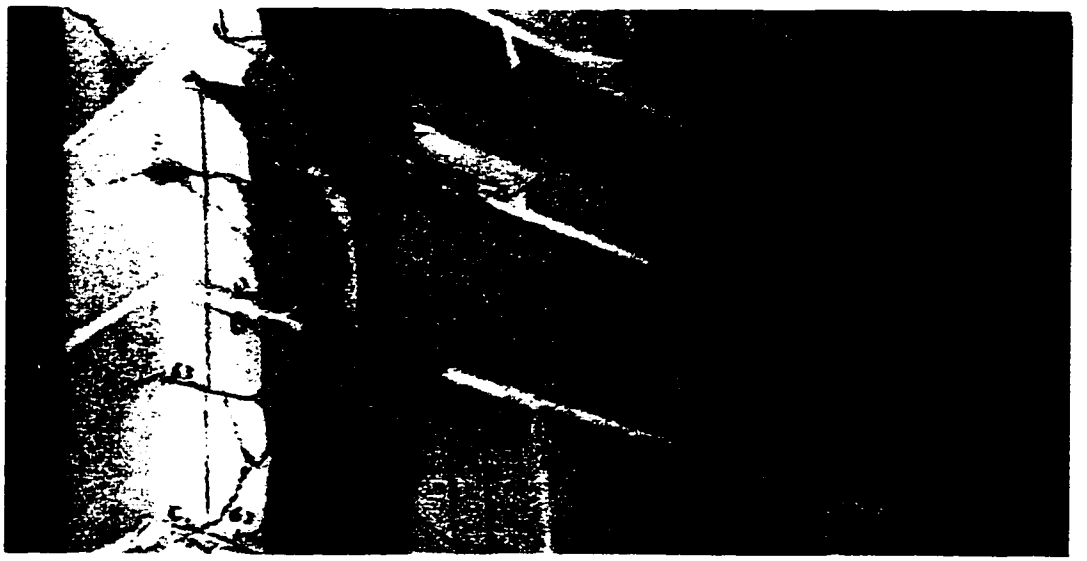

Figure 4.26 Rupture of Reinforcement - Specimen ICST 10

Figure 4.27 Rupture of Reinforcement - Specimen ICST 12

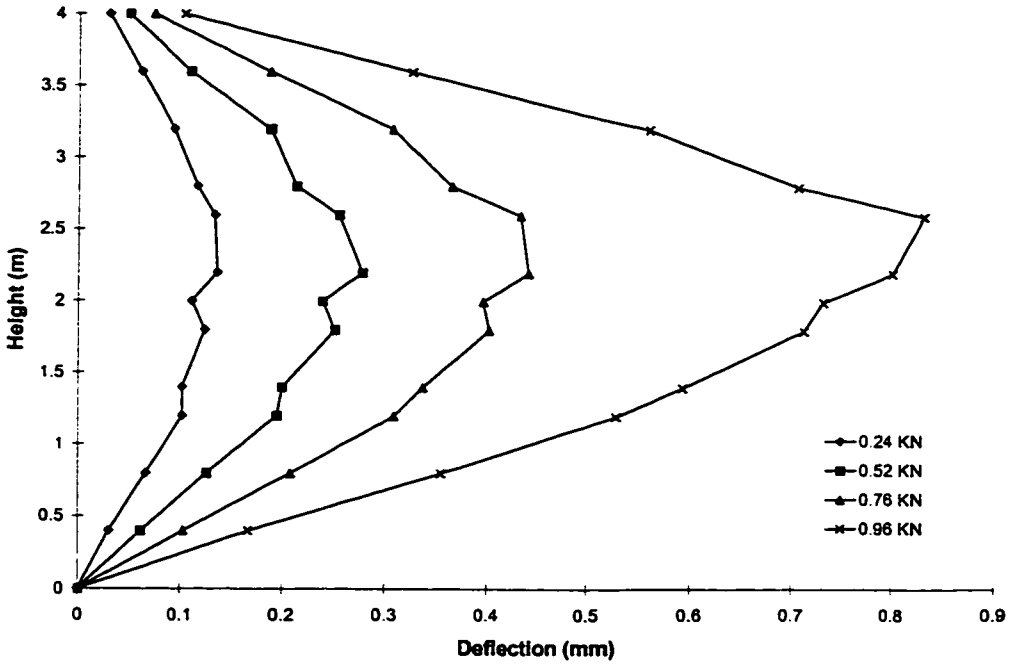

Figure 4.28 Deflection of the Wall Along the Height - Unreinforced Wall

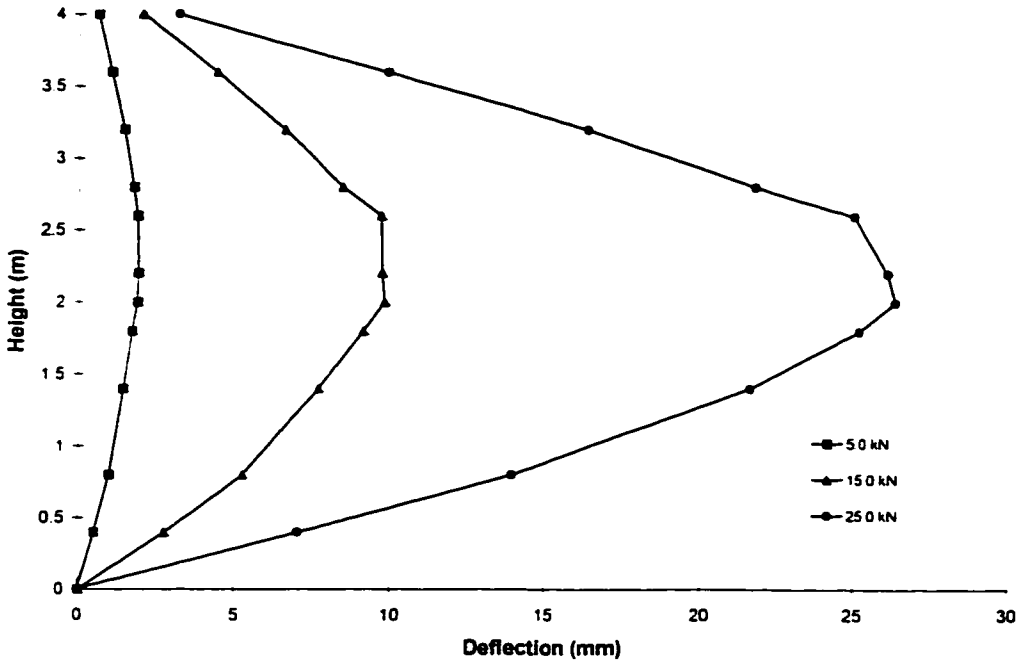

Figure 4.29 Typical Fiber Reinforced Wall Deflection Along the Height

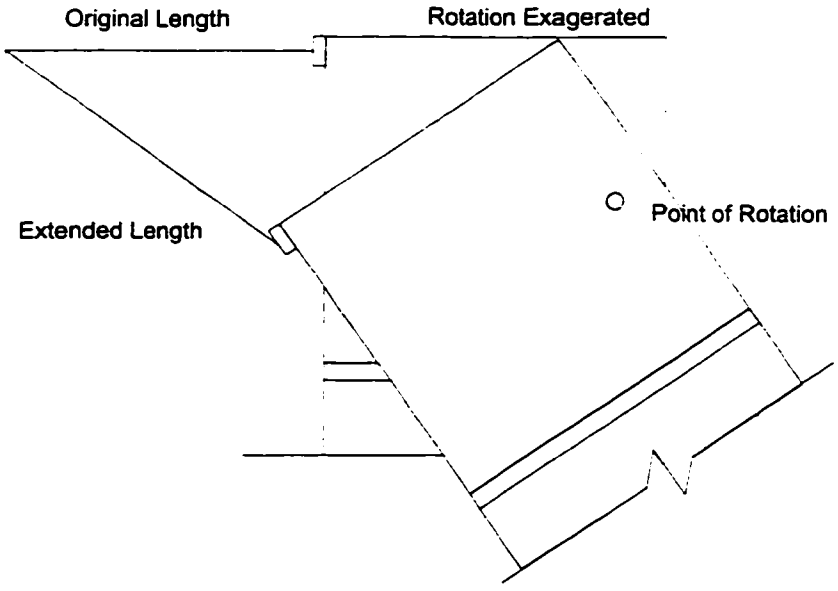

Figure 4.30 Error in Deflection Measurements

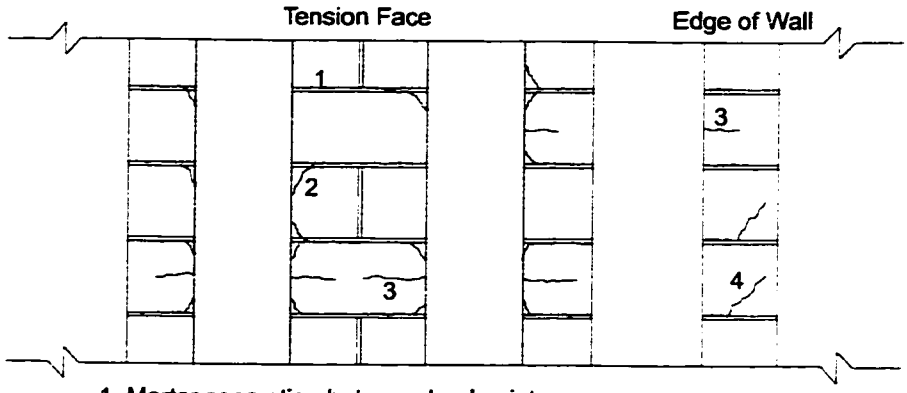

1 Mortar separation between load points

2 Diagonal cracks from fiber reinforcement to mortar joint

3 Horizontal cracks within the block

4 Flexure-shear cracks in the edge blocks

Figure 4.31 Progression of Cracks During a Typical Test

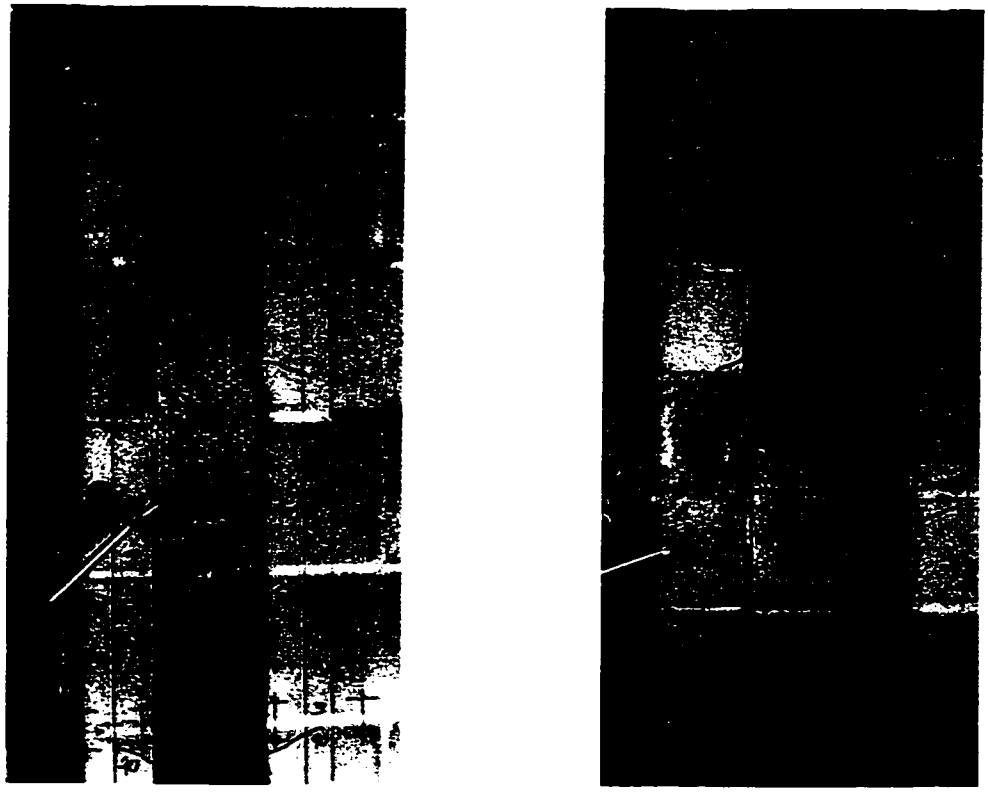

a. Specimen ICST 10 b. Specimen ICST 11

Figure 4.32 Crack Patterns for Typical Specimens

5 DISCUSSION OF TEST RESULTS AND ANALYTICAL MODEL

5.1 Introduction

This chapter explains the effect of the variables investigated: type, amount, and layout of reinforcement, axial load effects, and cyclic loading, primarily with respect to their influence on the load - deflection behaviour of the specimens. In all sections average values of modulus of elasticity and reinforcement thickness were used in the various calculations. It should be noted that the actual reinforcement thickness on each specimen will vary. Despite this source of error, comparisons and general conclusions can still be made.

5.2 Discussion of Test Results

5.2.1 Material Type

Figure 5.1 compares the load - deflection response for specimens reinforced with one of each of the three different types of fiber used. The three specimens shown are all from Series One and have the same masonry material properties. The only significant difference is the slope of the second portion of the response. This slope is determined by the stiffness of the reinforcement used. Table 5.1 lists the tensile load carrying capacity per unit width of each type of reinforcement based on results obtained from the coupon tests. The values for carbon fiber sheet and glass fiber sheet are similar. Figure 5.1 shows MCST 4, reinforced with carbon sheets, and MGST 5, reinforced with glass sheets, having approximately the same response. Both specimens were reinforced with two strips, each 250 mm wide. MCS 6, reinforced with four carbon straps, is obviously stiffer. While carbon strap and carbon sheet both contain carbon fibers, the higher density of fibers in the strap gives it greater stiffness.

5.2.2 Amount of Reinforcement

The easiest way to see the effect of the amount of reinforcement on the load - deflection response is to compare adjusted stiffness'. The last column of Table 5.2 summarizes the reinforcement ratios for each specimen expressed as a percentage. The width of reinforcement used in the calculation of the reinforcement ratios is based on the width perpendicular to the direction of the fibers. The thickness of the reinforcement for specimen ICST 8 is the actual measured thickness of the tensile test coupons for carbon sheets with two layers. This thickness is slightly more than twice the thickness of one carbon sheet from the tension tests. The difference is accounted for by using the measured modulus of elasticity for two carbon sheets, shown in Table 5.3, which is slightly lower than the value of E_R for one carbon sheet.

Because of the different stiffness' of each fiber type, the calculated reinforcement ratios must be adjusted before any comparison between different fiber types can be made. The reinforcement ratios are adjusted by multiplying them by the modulus of elasticity of the fiber type used. The resulting number reflects a combination of the stiffness and amount of fiber used. The new "adjusted" stiffness is then normalized with the specimen which has the lowest adjusted stiffness. Table 5.3 summarizes these calculations. The angled fiber specimen, ICST 12, needs a further adjustment before a comparison can be made. The modulus of elasticity for one carbon sheet represents the stiffness in the direction of the fibers. Composite theory states the off-axis modulus of elasticity can be calculated by multiplying the modulus in the primary direction by $\cos^2\theta$, where θ is the angle from the primary direction to the direction desired (Tsai and Hahn, 1980). Therefore, the modulus of elasticity in Table 5.3 for specimen ICST 12 was determined by multiplying 47375 MPa, the E_R for one carbon sheet, by $\cos^2 37°$. The normalized values allow for easy comparison between the specimens. For instance, MCST 4 has twice the amount of carbon fiber reinforcement as ICST 10 and this ratio is confirmed in the normalized values of the table.

The measured difference in stiffness is determined by comparing the slope of the second portion of the load - deflection response of each specimen. The second section refers to the linear portion of the load - deflection response. It is assumed that the masonry does not contribute to the stiffness for these comparisons; however, as explained in Section 5.2.5, cyclic behaviour, it is shown that the level of damage of the masonry does have a slight effect. The exact effect on the stiffness could not be quantified based on the one test performed. Table 5.3 shows the reduction in stiffness for the cyclic test, specimen MCST 7-4, compared to the original test using specimen MCST 4.

The slope was determined by plotting a regression line through the second section data points from the load - deflection response. The regression lines are calculated by the method of least squares. Figures 5.2 and 5.3 show the regression lines and their respective slopes and R^2 values. Data points from the initial portion of the load - deflection response were removed until the regression line obtained the maximum R^2 value possible. Any sharp reduction in load was manually removed from the response in an attempt to obtain a more accurate representation of the slope. Reductions in load occur when the test was halted and the specimen experienced creep. The slope of the second section was normalized the same way as the adjusted stiffness'. Not enough data was available for specimen MCS 2-1 to plot a regression line. The test was stopped shortly after the non-linear portion of the load - deflection response. The last column in Table 5.3 shows the percent difference in the normalized adjusted stiffness and the normalized slope of the second section. The specimens reinforced with one layer of carbon fiber sheet or strap have the least amount of variability. The specimens which contain other variables such as different fiber type, orientation, axial load, and cyclic loading, add an unknown effect to the stiffness and slope relationship. From the carbon fiber specimens with the same variables it is reasonable to conclude that the relationship between the amount of reinforcement and the slope of the second section of the load - deflection response is one to one. Therefore, as an example, using twice as much carbon fiber sheet will result in twice as much stiffness.

5.2.3 Layout of Reinforcement

It is difficult to determine the exact effect of the layout on the load - deflection response of the curves. The layout does affect the width of the cracks caused by mortar joint debonding. This is most clearly observed with specimen ICST 12, reinforced with angled carbon sheets. The pattern that the intersecting sheets develop results in three different cross sections over the masonry joints. Figure 5.4 illustrates the different cases labeled as joint A, B, and C. At any given joint the same amount of reinforcement is present. During the test, at an applied lateral load of 18 kN, recorded strains for joints within the constant moment region were 18000 microstrain for position 1, 12000 for position 2, 26000 for position 3, and 35000 for position 4. This difference in strain is a result of the way the reinforcement is distributed across the joint. For the other tests where the reinforcement is oriented vertically, the strains within the constant moment region are approximately equal. While the layout of the fibers does not noticeably affect the overall load - deflection response, the difference in masonry joint strains will have an effect on the localized behaviour of the specimen. For instance, specimen ICST 12 failed across the joint which experienced the largest level of mortar debonding which occurred at a location within the constant moment region having the same fiber orientation as joint C in Fig. 5.4.

5.2.4 Axial Load

Two specimens were tested with applied axial load. Specimens ICST 9 and ICST 13 were tested with 10 kN and 30 kN axial load respectively. To further examine the effect, a control specimen, ICST 11, was tested with the same layout, masonry material, and reinforcement type but without any applied axial load. Figure 5.5 compares the load - deflection response of these three specimens. The figure shows the initial stiffness of a specimen increases with an increase in axial load. Because the axial load introduces compression across

the cross section of the specimen, debonding and cracking is delayed. Therefore, it takes a higher load to achieve the same value of centerline deflection as the control specimen. The second portion of the load - deflection response decreases in slope with an increase in axial load because the axial load introduces second order effects to the specimen. The figure shows regression lines and their corresponding equations calculated in the same manner as described in Section 5.2.2. Table 5.4 summarizes the second section slope for each test and compares them to the control test. The results show that a 10 kN axial load will reduce the stiffness of the second portion of the response by 10% while a 30 kN axial load reduces the stiffness by 21%. There is not enough data to accurately determine a relationship between the reduction in stiffness and the amount of axial load.

5.2.5 Cyclic Behaviour

Only one test, MCST 4, from the 13 tests investigated involved cyclic loading. This specimen is a re-test of specimen MCST 4. Additional carbon fiber reinforcement was applied to what was the compression face of MCST 4. The specimen was then reversed and loaded with the old compression face now acting in tension. This was done in an attempt to retain the initial stiffness of the masonry as the old compression face was still uncracked. Figure 5.6 illustrates this procedure.

The load - deflection response for MCST 7-4 is shown in Fig. 5.7 and is compared with the original test MCST 4. It can be clearly seen that after each cycle the load - deflection envelope common to all of the tests is maintained. The entire response can still be separated into two sections. If only the envelope is considered, the characteristic two section curve is observed. For each cycle, when the specimen is unloaded, any existing cracks or debonded joints "re-seal". These sections no longer have any ability to resist tensile loads and the characteristic "pre-cracked" portion of the curve is greatly reduced. Despite the loss in tensile capacity, the moment of inertia of the section still contributes to the

stiffness. Once the neutral axis of the section has returned to the location experienced before the reduction in load, the familiar envelope resumes. The second portion of the load - deflection response occurs when the moment of inertia of the masonry is very small compared to the stiffness contribution of the reinforcement. No visual degradation of the masonry or reinforcement, other than the standard crack patterns, was observed. The reduction in stiffness of the second portion of the load - deflection response is a result of the previous damage from test MCST 4 to the specimen. Because the tension contribution of the masonry is small the reduction in stiffness is small. The fiber reinforcement acting in compression did not effect the behaviour of the wall other than slightly increasing the shear resistance of the specimen. The compression reinforcement did not debond from the wall at any time during the test. The loading points were adjusted so they did not bear against the fibers or restrain them in any way.

5.3 Investigation of Test Results and Analytical Model

5.3.1 Introduction

To this point the two section behaviour of the load - deflection response has been well established. This section investigates this behaviour further using numerical methods to justify the initial observed response. Tables of test to predicted ratios and relevant charts are presented.

5.3.2 Section One Behaviour

For calculation purposes, the load - deflection response can be idealized by separating it into two linear sections. In order to define the transition point which separates the first and second sections of the load - deflection response, a common procedure was developed. The second section behaviour of the load - deflection response is more easily quantifiable than the initial non-linear section.

For this reason the reference points used in the analytical model are determined starting from the second section behaviour and working back along the load - deflection response. A regression line was fit to the data in the second portion of the curve as discussed in Section 5.2.2. This line was used as the basis for defining the location where the second section behaviour begins. The transition point is identified as the location where the load - deflection curve becomes tangent to the regression line or where the regression line intersects the curve, whichever occurs first. Figure 5.8 illustrates the determination of the transition point for both cases. The corresponding load and deflection at this point becomes the test values P_t and Δ_t.

A plane sections analysis was then conducted to determine the calculated values for the transition point. The following assumptions were made in determining the model:

a. Masonry is ineffective in tension
b. Only the face shell can carry compression
c. A triangular stress block is used for compressive stresses
d. Compression strains are within the elastic range
e. Tensile component of epoxy neglected
f. Axial load effects neglected

These assumptions form the basis for calculation of all predicted values. Figure 5.9 shows the assumed strain and force distributions.

5.3.2.1 Calculation of Predicted Transition Load (P_{tp})

To begin the calculation of the transition load an initial strain in the reinforcement is required. From test results, the average of the strain readings within the constant moment region at P_t were used as the strain at which transition occurs. Using this strain, ε_r, as a constant, the following steps were followed.

First, an initial assumption on masonry compression strain, ε_m, is made. From test results, the masonry compressive strain is approximately 1/3 of the fiber reinforcement strain at the transition point. This value varies from test to test but $1/3\varepsilon_r$ is a good starting value. The depth to the neutral axis from the extreme compression fiber is then calculated as:

$$c = \left(\frac{\varepsilon_m}{\varepsilon_m + \varepsilon_r}\right) \cdot d \qquad [1]$$

Strain compatibility was performed on several specimens using recorded fiber reinforcement joint tension strains and the corresponding masonry joint compression strains at various levels of lateral load. The position of the neutral axis was calculated using Eq. 1. Based on the position of the neutral axis, and assuming the reinforcement strains are accurate, the compressive force required to balance the tensile force was calculated assuming a parabolic masonry stress - strain response and using the recorded f'_m values from the prism tests. The recorded f'_m values greatly overestimated the concrete compressive force. Therefore, a reduced modulus of elasticity for the masonry in compression was used and the stress in the masonry was calculated as:

$$\sigma_m = \frac{\varepsilon_m \cdot f'_m}{0.0025} \qquad [2]$$

Equation 2 assumes the masonry responds linearly up to a value of 2500 microstrain. The masonry code suggests that this value be 2000 microstrain but the test results suggest this limiting value can be increased. The modulus of elasticity calculated by the $f'_m/0.0025$ portion of Eq. 2 is lower than the value reported from the compression tests of the masonry prisms. Figure 5.10 illustrates the reason for this difference. The modulus of elasticity reported from the prism tests was calculated using a maximum strain of 1000 microstrain. No data was recorded past this point, beyond the elastic region. It is recognized

that this simplification will consistently underestimate the strength of the masonry; however, results will be conservative and still agree well with test values.

The compressive force is calculated assuming a triangular stress block in the face shell. If the position of the neutral axis is outside of the face shell then the stress block actually has the shape of a trapezoid. For simplicity, the difference in areas between a triangle and trapezoid are small due to the relatively small strains experienced, and a triangular distribution can still be used. With this in mind, the following equation is used for calculating the compressive force in the masonry:

$$C_M = 0.5 \cdot \sigma_m \cdot b \cdot x \qquad [3]$$

In which if $c > a$, $x = a$

And if $c < a$, $x = c$

Because the stress - strain relationship for the fiber reinforcement is linear until failure, the force in the fibers can be calculated as:

$$T_R = \varepsilon_r \cdot A_r \cdot E_r \qquad [4]$$

In which ε_r is the strain in the reinforcement at the transition point or the assumed value of strain which corresponds to the transition point.

Next, ε_m is changed and the procedure repeated until C_M is equal to T_R. Once the forces have converged the moment and total applied load can be calculated.

$$M = T_R \cdot \left(d - \frac{x}{3}\right) \qquad [5]$$

$$P = \frac{2 \cdot M}{L_1} \qquad [6]$$

The solver function in Microsoft Excel was used to perform the iterations. Excel used the following conditions during the calculations:

Max. iteration time:	100 seconds
Max. iterations:	100
Precision:	0.000001
Tolerance:	5%
Convergence:	0.001 kN

If calculating by hand, convergence is reached when C_M differs from T_R by less than $\pm$ 0.2 kN. The position of the neutral axis does not chance significantly within this range.

This iterative procedure is only required to obtain the location of the neutral axis from which the deflection is calculated. The prediction of the transition load is based on the assumed initial fiber reinforcement strain and, since the resultant compressive force is assumed to lie within the face shell at approximately 1/3a, the internal moment arm is relatively constant and does not greatly affect the calculation of P_{tp}. Thus, a quick estimate of the transition load can be calculated without iterations by using:

$$P_{tp} = \frac{2 \cdot \varepsilon_r \cdot A_r \cdot E_r \cdot \left(d - \frac{a}{3}\right)}{L_1} \qquad [7]$$

5.3.2.2 Calculation of Predicted Transition Deflection (Δ_{tp})

Because the specimens were loaded with simple supports as boundary conditions, the maximum centerline deflection can be calculated using an equation from any beam diagram table. The deflection equation requires the

applied load, geometry of the loading and reaction points, modulus of elasticity of masonry, and a global moment of inertia. The first step in determining the transition deflection is to calculate the transformed moment of inertia of the section within the constant moment region.

$$I_o = \left[\frac{b \cdot a^3}{12} + b \cdot a \cdot \left(\frac{D}{2} - \frac{a}{2}\right)^2\right] \cdot 2 + A_r \cdot n \cdot \left(d - \frac{D}{2}\right)^2 \qquad [8]$$

Equation 8 takes into consideration the masonry face shell and ignores the contribution of the remainder of the section. This is because at any given joint where the forces are being calculated only the face shell is mortared leaving the remainder of the block unbonded. The $bh^3/12$ component for the reinforcement will always be insignificant because of the small thickness and has not been included in the calculation. The moment of inertia is taken about the centroid of the masonry section instead of the transformed section. The centroid of the transformed section does not differ more than a few millimeters from the masonry centroid, again because of the small thickness of the fibers, and the extra effort involved in calculating the transformed centroid is not necessary.

Next, the cracked moment of inertia in the constant moment region is calculated about the location of the neutral axis obtained from Eq. 1. The cracked moment of inertia is based on the contribution from the remaining effective compression zone after mortar debonding and is calculated as:

$$I_{cr} = \frac{b \cdot x^3}{12} + Q + A_r \cdot n \cdot (d - c)^2 \qquad [9]$$

In which if $c > a$, $\quad Q = b \cdot a \cdot \left(c - \frac{a}{2}\right)^2$

And if $c < a$, $\quad Q = b \cdot c \cdot \left(\frac{c}{2}\right)^2$

Before a simple beam deflection equation can be used, a constant value for the moment of inertia of the section is required. Figure 5.11 shows how an approximate value for the total moment of inertia is calculated using I_o and I_{cr}. It is assumed that I_{cr} occurs throughout the constant moment region. Near the end supports, at the location of zero moment, the uncracked moment of inertia, I_o, occurs. A 6th degree spandrel was assumed to approximate the transition of the moment of inertia from I_{cr} to I_o. Table 5.5 shows the deflections obtained using the different degree spandrels that were investigated, along with the deflection obtained from simply assuming I_{cr} over the whole section. Deflections were calculated using Eq. 11 which is explained later in this section. The global moment of inertia, I_{approx}, was calculated using Eq. 10 in which the coefficients 2/7, 2/5, and 2/3 are used for a 6th degree, 4th degree, and 2nd degree spandrel respectively. I_{approx} is equal to I_{cr} when only the I_{cr} value is considered. It was found that a 6th degree spandrel most closely approximated the moment of inertia near the ends of the span length. This "curve fitting" was done because the exact behaviour is much more complicated and beyond the scope of this research. Higher degree spandrels did not result in any marked improvement in the deflection predictions. The approximate moment of inertia is calculated by summing the areas under the curves and dividing by the total span.

$$I_{approx} = \frac{I_{cr}\ L + \frac{2}{7}\cdot(I_o - I_{cr})\cdot L_1}{L} \qquad [10]$$

Using this global moment of inertia and the modulus of elasticity from the linear stress - strain range of the masonry prisms, the transition deflection can be calculated as:

$$\Delta_{tp} = \frac{0.5\cdot P\cdot L_1\cdot\left[3\cdot L^2 - 4\cdot L_1^{\,2}\right]}{24\cdot E_m\cdot I_{approx}} \qquad [11]$$

The recorded E_m value is used because the transition point typically occurs when the compression ε_m is less than the limit of the E_m readings from the prism tests.

5.3.2.3 Section One Results

The above calculations were performed for all of the fiber reinforced tests except MCS 2-1. As mentioned earlier, there was not enough data available from specimen MCS 2-1 to accurately define the location of the transition point. Table 5.6 summarizes the results and compares test to predicted data. The table lists the strain in the reinforcing fiber that was used in the calculations and separates the results into three categories, load, deflection, and slope. For the angled fiber specimen, ICST 12, the reinforcement strain in the direction of the fibers was used and the force in the fibers multiplied by cos 37° to represent the equivalent vertical force. For the deflection calculation, the transformed moment of inertia was multiplied by $\cos^2 37°$ to account for the equivalent vertical moment of inertia. The slope is calculated simply by dividing the load by the deflection. Table 5.6 is represented graphically by Fig. 5.12 through 5.14. Figure 5.12 shows the relationship between the test and predicted values of applied lateral transition load. The axes have been kept to the same scale for better comparison. A diagonal line represents the point where the test value is identical to the predicted value. With the exception of two specimens, the predicted values are on or above this line, giving conservative results.

The two most outlying tests, specimen MGST 5 and ICST 8, may be explained by an inaccurate strain reading. With specimen ICST 8, reinforced with two layers of carbon sheets, there may be shear forces between the layers of sheet which will affect the strain in the outer fibers. The strains recorded on the outer fibers may be higher than the strains on the sheet just below. Figure 5.15 illustrates the reasoning for this concept.

For MGST 5 the average strain is based on only two readings taken at the vertical centerline of each strip of reinforcement. These two readings may not give an accurate representation of the average strain within the constant moment region.

One last issue common to all of the tests is the pattern of strains along the width of the reinforcement as illustrated in Chapter 3. The strain recorded in the center of the fiber sheets is the maximum strain experienced across the width and does not represent the average strain across the width of the reinforcement. All of these factors make it difficult to assess the feasibility of the analytical model.

Despite the sources of error the results are fairly consistent because the calculations depend mostly on the strain in the reinforcement and do not fluctuate much with different positions of the neutral axis. This means that the internal moment arm is relatively insensitive to the type and amount of reinforcement.

The deflections are a little more difficult to calculate effectively. This is because of the high variation of EI. The analytical model assumes a global moment of inertia for the entire specimen when in actuality, the masonry blocks represent a constant moment of inertia while the masonry joints represent discrete reductions in the moment of inertia.

Figure 5.13 shows more scatter in the results than Fig. 5.12. This is because the calculated position of the neutral axis is not always the same as the test position thus affecting the moment of inertia. Also, outlying points are for tests whose exact properties are not known as well as the other tests. For instance, specimens MCS 3-2 and MCST 7-4 are both tests of previously damaged specimens and the reduction in the stiffness is not accounted for in the model, thus the deflection is underpredicted. For specimen ICST 12 the exact effectiveness of the carbon fibers in the vertical direction is not known. Overall, the deflection calculations use the transition load as a starting point so any errors in the load will translate into errors in the deflection.

Figure 5.14 compares the test to predicted stiffness of the first section slopes. This is just a convenient way to compare the load and deflection on the same plot. Again, there is some scatter but overall the results stay close to the diagonal one to one ratio reference line.

5.3.3 Section Two Behaviour

Now that the first portion of the load - deflection response has been quantified and the transition point identified, the second section behaviour can be developed. The behaviour of the second section can be separated into two variables needed to define the behaviour. The first variable is the slope which is directly related to the stiffness of the fiber reinforcement. The second variable is the ultimate failure values of load and deflection which identify the end of the second section. The next two sub-sections describe how each variable was quantified.

5.3.3.1 Calculation of the Slope (S_{2p})

Earlier, in Section 5.2.2, the relationship between the amount of reinforcement and the slope of the second section of the load - deflection response was identified. Looking again at Table 5.3, the relationship is best identified by the single layer carbon fiber specimens with the reinforcement aligned in the vertical direction and no other variables considered. These specimens are MCS 6, MCST 4, ICST 10, and ICST 11. Based on these four tests the relationship between the amount of fibers and the slope or stiffness of the second section of the load - deflection response can be quantified by plotting the slope against the adjusted stiffness. Figure 5.16 shows the resulting relationship and its corresponding regression analysis. The slope of the linear regression line was used to predict the slope based on the reinforcement ratio and modulus of elasticity of the reinforcement.

$$S_{2p} = 4.552 \cdot \rho \cdot E_R \qquad [12]$$

The resulting slope is in N/mm and begins at the location of the transition point calculated in the previous section. In order to determine the end of the second section behaviour, the ultimate failure load must be identified.

5.3.3.2 Calculation of Failure Load (P_{up})

The predicted failure load is the lowest calculated value from the three different modes of failure; sliding shear, flexure - shear, and flexure. Each mode of failure has its own set of calculations.

One test failed due to sliding shear of the mortar joint. This occurred because there was not enough reinforcement overlapping the lower mortar joint. To calculate the sliding shear resistance of masonry, CSA Standard S304.1 (1994) uses the following equation:

$$V_r = \phi_m \cdot \mu \cdot C \qquad [13]$$

in which: ϕ_m = 1.0 for analysis purposes

μ = 1.0 for masonry to masonry slide plane

C = compressive force in the masonry acting normal to the sliding plane plus the factored yield strength of standard steel vertical reinforcement

For the specimen in question, MCS 3-2, it is assumed that there is no effective vertical reinforcement crossing the mortar joint, so the sliding shear force becomes equal to the compressive force in the wall. The approximate self weight of the wall is 10 kN. This is based on a wall weight of 2.11 kN/m^2 taken from CSA Standard S304.1 (1994) for 200 mm block and normal weight masonry materials. Specimen MCS 3-2 failed at the lower mortar joint so the full weight of the wall can be used. In this case, the total applied load required to fail at this

location would be twice the shear resistance or 20 kN. While the upper mortar joint should have failed at a much earlier load because only one course of masonry rests above it, it is known that more vertical reinforcement overlapped the upper joint and restrained the failure from occurring.

The flexure - shear failure mode requires a little more effort. Figure 5.17 shows the position of the forces in relation to the shear and bending moment diagrams. Pure shear through the block is not likely to occur because of the high shear span to depth ratio. This almost guarantees that flexure failure will occur before shear; however, when the deflections become excessive, a flexure - shear crack begins to form and propagates until the flexural reinforcement de-bonds from the specimen and shearing occurs. This mode of failure should occur near the loading points where the moment and shear are at a maximum. Keeping this in mind, the following method for calculating the ultimate load for flexure - shear is suggested.

CSA S304.1 (1994) provides the following equation for calculating the factored out-of-plane shear resistance for unreinforced walls.

$$V_r = \phi_m \cdot (v_m \cdot A_e + 0.25 \cdot P) \qquad [14]$$

In which: P = axial compressive load at the section in question

ϕ_m = resistance factor for masonry

A_e = effective area = $b \cdot a$ for this research

v_m = masonry shear strength

$$= 0.16 \cdot \left(2 - \frac{M_f}{V_f \cdot d}\right) \cdot \sqrt{f'_m}$$

For the tests investigated $\frac{M_f}{V_f \cdot d} = 6$ and S304.1 states this value need not be greater than one. This reduces v_m to $0.16 \cdot \sqrt{f'_m}$. Axial load effects will be ignored because the large deflections experienced during loading reduces the

ability of the axial load to resist other forces. Eliminating the ϕ_m factor, Eq. 14 is reduces to:

$$V_r = 0.16 \cdot \sqrt{f'_m} \cdot b \cdot a \qquad [15]$$

From which the applied lateral load equals:

$$P_{up} = 2 \cdot V_r = 0.32 \cdot \sqrt{f'_m} \cdot b \cdot a \qquad [16]$$

Equation 16 is limited to specimens with a shear span to depth ratio greater than one. The equation assumes the full width of the compression face shell resists the shear forces. This does not account for the reduction in the effective width when a crack intrudes into the compression zone. The equation also does not consider any resistance provided by the fiber reinforcement.

For the flexure mode of failure, two values were calculated. One value is based on the rupture of the reinforcement fiber and uses the ultimate strains from the tension coupon tests. For the glass fiber specimen, since no ultimate strain was obtained, an approximate value of 20000 microstrain was used based on an assumed maximum elongation of approximately 2%. For simplification the internal moment arm of the masonry section is taken as d - 1/3a. The compression resultant force is assumed to act at the centroid of the previously assumed triangular compressive stress block. Using this assumption, the maximum moment caused by the ultimate reinforcement strains can be calculated using:

$$M = \varepsilon_r \cdot A_r \cdot E_r \cdot \left(d - \frac{1}{3} \cdot a \right) \qquad [17]$$

In which ε_r equals the ultimate reinforcement strains from Table 3.4.

The ultimate failure load due to rupture of the reinforcement can then be calculated:

$$P_{up} = 2 \cdot \frac{M}{1200} = \frac{1}{600} \cdot \left[\varepsilon_r \cdot A_r \cdot E_r \cdot \left(d - \frac{1}{3} \cdot a \right) \right] \qquad [18]$$

The other value is based on the crushing of the masonry. Crushing was assumed to occur over the whole width of the face shell when the stresses reached f'_m. Using the same assumptions for the moment arm and compressive stress block as the fiber rupture mode of failure, the moment caused by crushing is equal to:

$$M = f'_m \cdot \frac{1}{2} \cdot b \cdot a \cdot \left(d - \frac{1}{3} \cdot a \right) \qquad [19]$$

And the ultimate failure load is:

$$P_{up} = 2 \cdot \frac{M}{1200} = \frac{M}{600} \cdot \left[0.5 \cdot f'_m \cdot b \cdot a \cdot \left(d - \frac{1}{3} \cdot a \right) \right] \qquad [20]$$

5.3.3.3 Section Two Results

Table 5.7 summarizes the results of the second section behaviour. In the mode of failure column SS stands for sliding shear, FS stands for flexure - shear, and R stands for rupture of the reinforcement. The values in bold are the lowest calculated failure load applicable to that specimen. While there is significant variation in the test to predicted results, the mode of failure is correctly identified for the specimens. Figure 5.18 compares the test to predicted slopes. The figure shows that the slope is overestimated for some of the tests. Figure 5.19

compares the test to predicted ultimate failure loads. Again there is a tendency to overestimate the value.

The high variation in test to predicted results for the ultimate failure loads can be explained a number of ways. The flexure shear failure mode uses the prism strength determined in Chapter 3 in the calculation. As explained earlier, the prism test results were flawed and the f'_m values reported are not representative of the actual strengths of the test specimens. For future tests, every effort should be made to ensure the construction of the masonry prisms is as close as possible to the construction of the full scale specimens. Also, the prisms should be tested under an eccentric compressive load to obtain the flexural compressive strength which is more representative of the behaviour of the walls. For the specimens which failed due to rupture of the fiber reinforcement, the actual failure load is much smaller than the predicted. This is because the predicted failure loads are based on direct tension of the fiber reinforcement. The fibers on the test specimens are subjected to bending stresses and are influenced by stress concentrations at a mortar joint crack, both of which will reduce the ultimate strength of the fibers.

Using the calculated ultimate load and the transition load calculated earlier the final deflection can be determined as:

$$\Delta_{up} = \Delta_{tp} + \left(\frac{P_{up} - P_{tp}}{S_{2p}} \right) \qquad [21]$$

Table 5.8 summarizes the final ultimate loads and corresponding ultimate deflections. The test to predicted results generally do not agree well for the ultimate deflections. This is mainly due to the predicted value of P_{up}. Because the deflection is dependent on the assumed change in load, any difference in the test to predicted values for ultimate load will lead to a significant difference in the calculated ultimate deflection. What is important to observe is that regardless of the value of the deflection, the slope still agrees quite well with the slope obtained from the regression analysis.

5.3.4 Overall Behaviour

The overall behaviour of the specimen compared with the results from the analytical model is shown in Fig. 5.20. The figure shows the original behaviour of ICST 10, the approximated two section response, and the response from the analytical model. The ultimate deflection was over predicted in this case and a second chart has been added with a reduced scale to better show the comparison of the slopes. The general trend of the specimen is predicted accurately by the model.

The results for the remainder of the tests is shown in Fig. 5.21 and 5.22. Only the idealized linear load - deflection response is compared to the analytical model results. As noted earlier in this chapter, the model does not account for some of the test variables and this results in very poor accuracy for some of the tests.

5.3.5 Conclusions

Recognizing that masonry is a material with a certain amount of "built in" variability, the model agrees fairly well with the tests performed. Without upgrading to a more accurate finite element model, the proposed model gives a quick estimate of the behaviour of the specimens. For design purposes, the reinforcement strains needed to calculate the transition point can be taken as the average of the exact strains for the tests investigated. For the types of reinforcement investigated these strains are approximately 1100, 1900, and 2500 microstrain for carbon strap, glass sheet, and carbon sheet respectively. These strains, while not exact, will give an estimate of the location of the transition point. Overall, the model is a simple way to evaluate the effectiveness of externally applied fiber reinforcement on unreinforced, ungrouted masonry walls.

Table 5.1
Comparison of Composite Fiber Strengths

		Glass Sheet	Carbon Sheet	Carbon Strap
E	(MPa)	17770	47375	185181
$t_{avg.}$	(mm)	1.805	0.729	1.286
$E^*t_{avg.}$	(kN/mm)	32.1	34.5	238.1

Table 5.2
Determination of Reinforcement Ratios

Fiber Type	Specimen	Fiber thickness $t_{avg.}$ (mm)	width (mm)	# of strips	A_R (mm^2)	b (mm)	d (mm)	$\rho = A_R/bd$ %
	MCS 2-1	1.286	50	2	129	1190	190.6	0.057
Carbon Strap	MCS 3-2	1.286	50	2	129	1190	190.6	0.057
	MCS 6	1.286	50	4	257	1190	190.6	0.113
Glass Sheet	MGST 5	1.805	250	2	903	1190	190.9	0.397
	MCST 4	0.729	250	2	365	1190	190.4	0.161
	MCST 7-4	0.729	250	2	365	1190	190.4	0.161
	ICST 8	1.51	250	2	755	1205	193.8	0.323
Carbon Sheet	ICST 9	0.729	250	2	365	1205	193.4	0.156
	ICST 10	0.729	125	2	182	1205	193.4	0.078
	ICST 11	0.729	250	2	365	1205	193.4	0.156
	ICST 12	0.729	125	4	365	1205	193.4	0.156
	ICST 13	0.729	250	2	365	1205	193.4	0.156

Table 5.3
Comparison of Reinforcement Ratio and Slope of Load - Deflection Response

Descripton of Variability	Specimen	ρ (%)	E_R (MPa)	ρ * E_R (MPa)	normalized	slope (kN/mm)	normalized	Difference %
Carbon Strap	MCS 2-1	0.057	185181	105.0	2.8	Not enough available data		
Previously Damaged	MCS 3-2	0.057	185181	105.0	2.8	0.5589	3.2	-13
Glass Sheet	MGST 5	0.397	17770	70.6	1.9	0.3985	2.3	-20
Previously Damaged	MCST 7-4	0.161	47375	76.2	2.1	0.3277	1.9	9
10 kN Axial Load	ICST 9	0.156	47375	74.1	2.0	0.3123	1.8	11
30 kN Axial Load	ICST 13	0.156	47375	74.1	2.0	0.2733	1.6	22
Angled Fibers	ICST 12	0.156	30217	47.3	1.3	0.1841	1.1	17
Two Layers	ICST 8	0.323	43850	141.8	3.8	0.5699	3.3	15
	MCS 6	0.113	185181	209.9	5.7	0.952	5.4	4
Carbon Fibers	MCST 4	0.161	47375	76.2	2.1	0.3643	2.1	-1
One Layer	ICST 10	0.078	47375	37.1	1.0	0.1749	1.0	0
	ICST 11	0.156	47375	74.1	2.0	0.3452	2.0	1

Table 5.4
Reduction in Stiffness From Applied Axial Load

Specimen	Slope (kN/mm)	Normalized	Axial Load (kN)	Reduction in Stiffness (%)
ICST 11	0.3452	1.00	0	0
ICST 9	0.3123	0.90	10	10
ICST 13	0.2733	0.79	30	21

Table 5.5

Approximation of Centerline Deflection

		Calculated Transition Deflections							
				Spandrel Degree					
	Actual	Icr		n^2		n^4		n^6	
Specimen	Deflection (mm)	(mm)	% diff	(mm)	% diff	(mm)	% diff	(mm)	% diff
MSC 2-1				Not enough data					
MCS 3-2	19.6	12.2	37.8	6.6	66.3	8.1	58.7	9.0	54.1
MCS 6	12.9	6.9	46.5	5.4	58.1	5.9	54.3	6.2	51.9
MGST 5	13.0	14.0	7.7	5.6	56.9	7.4	43.1	8.5	34.6
MCST 4	9.0	14.3	58.9	6.1	32.2	7.9	12.2	9.0	0.0
MCST 7-4	26.1	27.1	3.8	11.5	55.9	15.0	42.5	17.2	34.1
ICST 10	9.2	23.5	155.4	4.7	48.9	6.9	25.0	8.7	5.4
ICST 11	9.5	19.5	105.3	6.5	31.6	8.9	6.3	10.5	10.5
ICST 9	10.0	24.4	144.0	8.1	19.0	11.1	11.0	13.1	31.0
ICST 13	13.0	21.7	66.9	7.2	44.6	9.9	23.8	11.7	10.0
ICST 8	14.0	26.6	90.0	13.2	5.7	16.5	17.9	18.5	32.1
ICST 12	25.7	32.5	26.5	7.6	70.4	10.9	57.6	13.5	47.5
Average Difference (%)			68		45		32		28

Table 5.6

Section One Behaviour Results

Specimen	Transition Strain ($\mu\varepsilon$)	Transition Load			Transition Deflection			Slope of First Section		
		Test	Predicted		Test	Predicted		Test	Predicted	
		P_t (kN)	P_{tp} (kN)	P_t/P_{tp}	Δ_t (mm)	Δ_{tp} (mm)	Δ_t/Δ_{tp}	S_1 (kN/mm)	S_{1p} (kN/mm)	S_1/S_{1p}
MCS 2-1					Not enough data					
MCS 3-2	1795	15.0	12.6	1.19	19.6	9.0	2.19	0.77	1.41	0.54
MCS 6	1164	18.6	16.5	1.13	12.9	6.2	2.09	1.44	2.67	0.54
MGST 5	1852	13.9	8.9	1.56	13.0	8.5	1.52	1.07	1.04	1.03
MCST 4	1918	10.9	9.2	1.18	9.0	9.0	1.00	1.21	1.02	1.19
MCST 7-4	3643	16.6	18.7	0.89	26.1	17.2	1.52	0.64	1.09	0.58
ICST 10	2768	7.6	6.9	1.10	9.2	8.7	1.06	0.83	0.79	1.04
ICST 11	2246	12.4	11.1	1.12	9.5	10.5	0.90	1.31	1.06	1.24
ICST 9	2803	13.8	13.8	1.00	10.0	13.1	0.76	1.38	1.05	1.31
ICST 13	2495	14.7	12.3	1.20	13.0	11.7	1.11	1.13	1.05	1.07
ICST 8	2984	18.0	29.0	0.62	14.0	18.5	0.76	1.29	1.57	0.82
ICST 12	3136	15.9	13.3	1.20	25.7	14.5	1.77	0.62	0.92	0.68

Table 5.7

Section Two Behaviour Results

Specimen	Slope of Second Section: Test S_2 (kN/mm)	Slope of Second Section: Predicted S_{2p} (kN/mm)	S_2/S_{2p}	Failure Load P_u (kN)	Predicted Failure Loads, P_{up} (kN): Sliding Shear	Flexure-Shear	Flexure: Rupture	Flexure: Crush	P_u/P_{up}	Mode of Failure: Test	Mode of Failure: Pred.
MCS 2-1	Not enough data					36.0	105.4	45.3		N/A	
MCS 3-2	0.5589	0.4778	1.17	21.75	**19.2**	36.0	105.4	45.3	1.13	SS	SS
MCS 6	0.952	0.9557	1.00	46.38		**36.0**	210.9	45.3	1.29	FS	
MGST 5	0.3985	0.3214	1.24	35.96		**36.0**	95.8	45.3	1.00	FS	
MCST 4	0.3643	0.3470	1.05			**36.0**	67.0	45.3		N/A	
MCST 7-4	0.3277	0.3470	0.94	32.7		**36.0**	59.5	45.3	0.91	FS	
ICST 10	0.1749	0.1687	1.04	20.89		55.0	**33.8**	94.9	0.62		R
ICST 11	0.3452	0.3374	1.02	41.65		**55.0**	67.6	94.9	0.76	FS	
ICST 9	0.3123	0.3374	0.93			**55.0**	67.6	94.9		N/A	
ICST 13	0.2733	0.3374	0.81	37.72		**55.0**	67.6	94.9	0.69	FS	
ICST 8	0.5699	0.6974	0.82	50.19		**55.0**	111.1	94.9	0.91	FS	
ICST 12	0.1841	0.3374	0.55	22.72		55.0	**43.1**	94.9	0.53		R

Table 5.8

Ultimite Predicted Faillure Load and Deflections

Specimen	Transition Values Load P_{tp} (kN)	Transition Values Deflection Δ_{tp} (mm)	Predicted Failure Load P_{up} (kN)	Failure Deflection Predicted Δ_{uc} (mm)	Failure Deflection Actual Δ_u (mm)
MCS 2-1	Information Not Available				
MCS 3-2	12.6	9.0	19.2	22.8	31.3
MCS 6	16.5	6.2	36.0	26.6	42.4
MGST 5	8.9	8.5	36.0	92.9	69.6
MCST 4	9.2	9.0	36.0	67.0	N/A
MCST 7-4	18.7	17.2	36.0	67.0	77.5
ICST 10	6.9	8.7	33.8	168.1	82.1
ICST 11	11.1	10.5	55.0	140.6	91.2
ICST 9	13.8	13.1	55.0	135.2	N/A
ICST 13	12.3	11.7	55.0	138.2	88.3
ICST 8	29.0	18.5	55.0	55.8	63.1
ICST 12	13.3	14.5	43.1	152.6	61.5

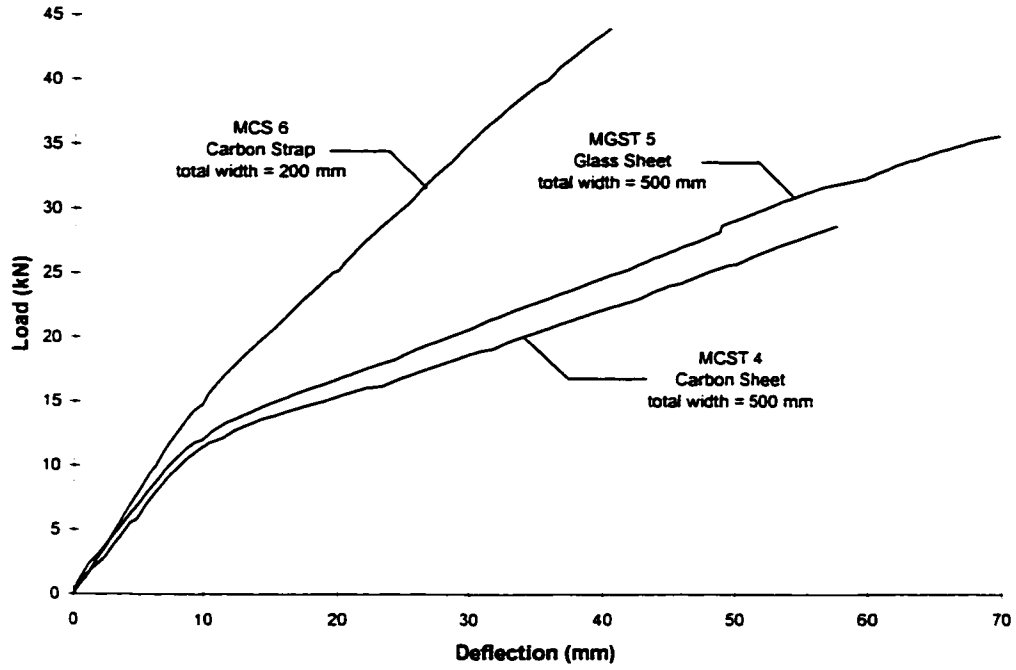

Figure 5.1 Effect of Fiber Type on Specimen Load - Deflection Behaviour

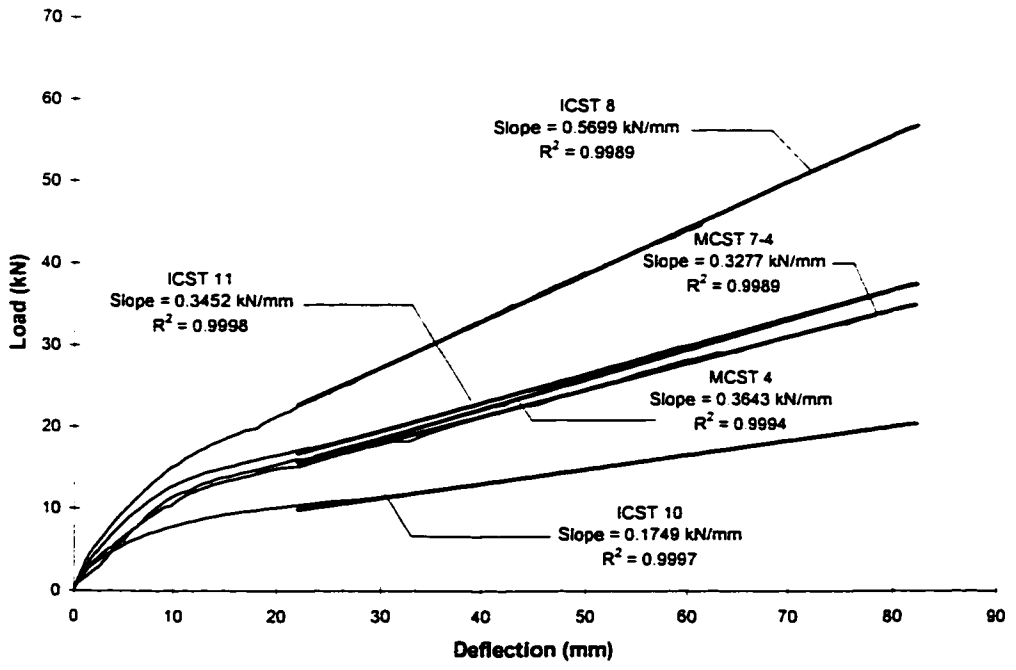

Figure 5.2 Regression Lines for Carbon Fiber Sheet Specimens

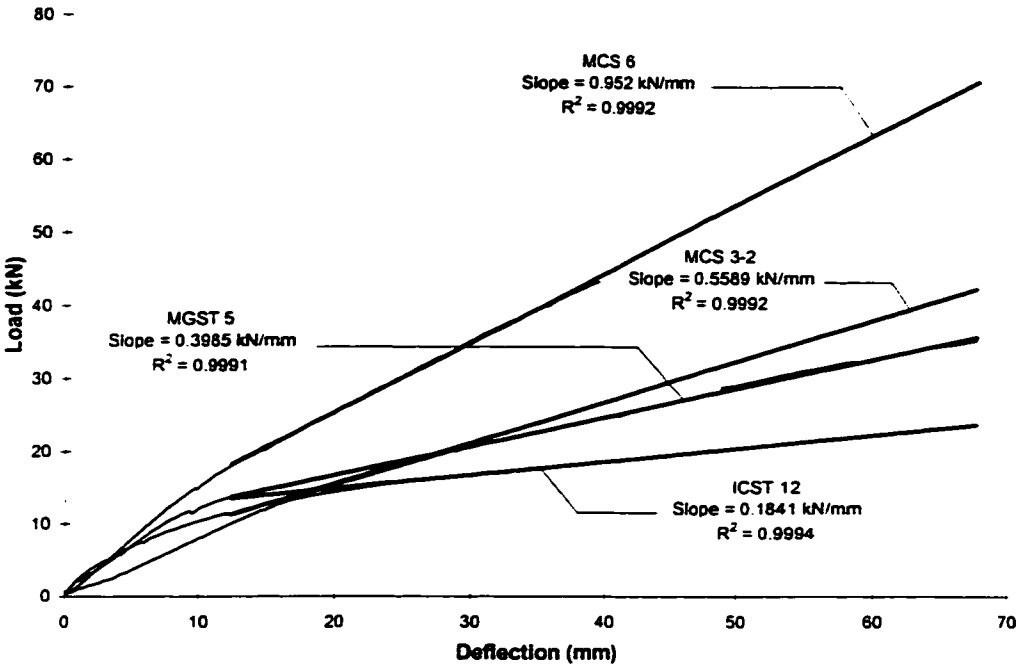

Figure 5.3 Regression Lines for Remaining Specimens

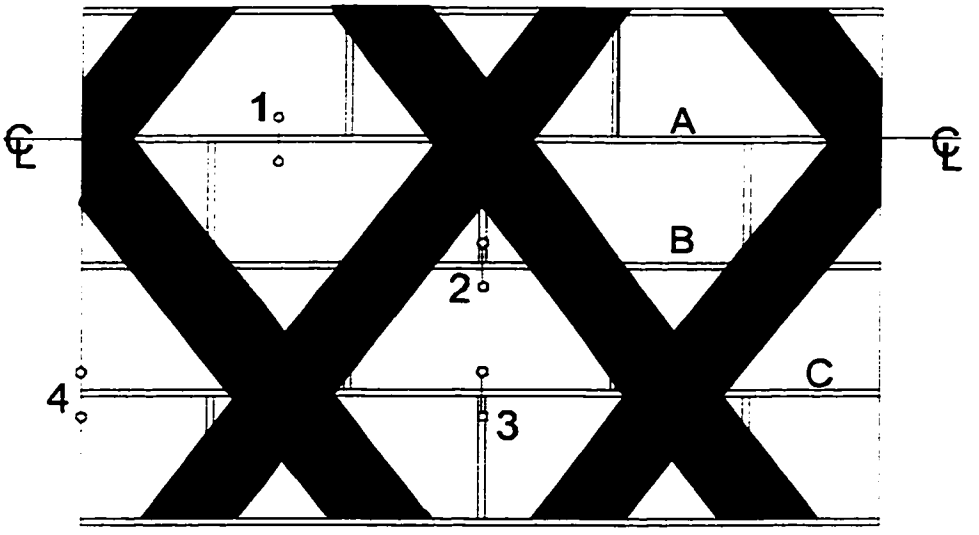

1. 18000 με = 0.9 mm
2. 12000 με = 0.6 mm
3. 26000 με = 1.3 mm
4. 35000 με = 1.8 mm

Figure 5.4 Effect of Reinforcement Layout - ICST 12

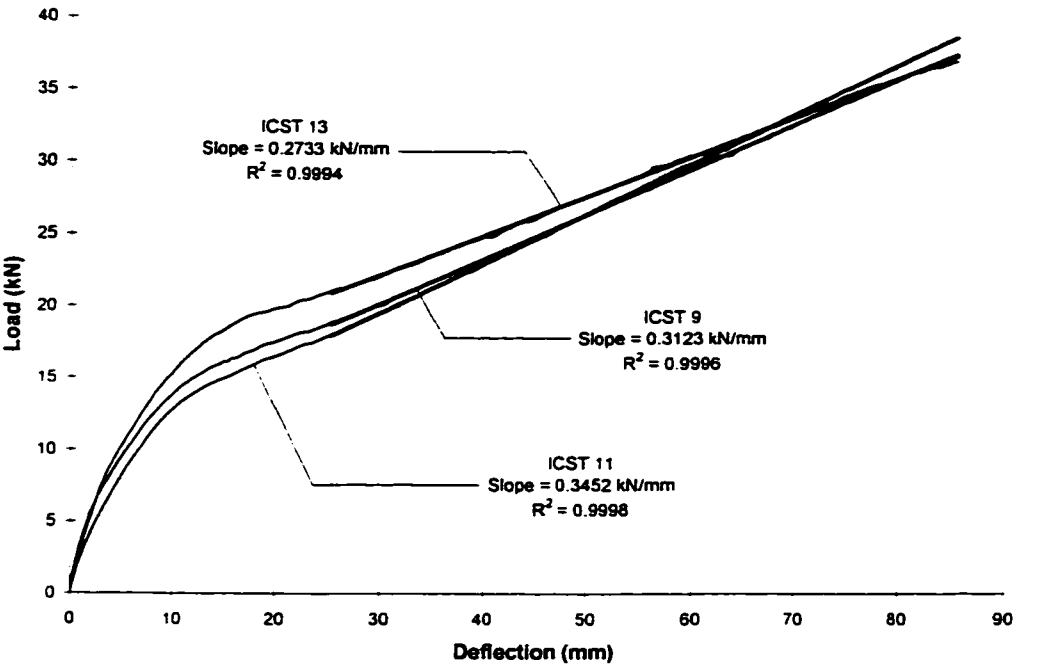

Figure 5.5 Effect of Axial Load

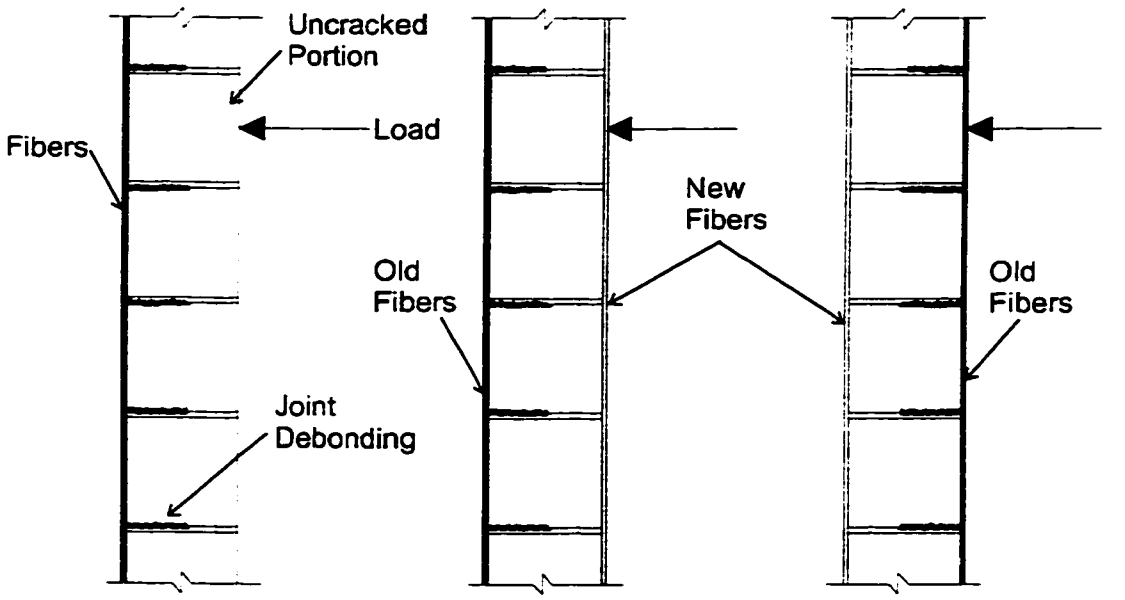

Original specimen cracks on tension face. (MCST 4)

Carbon fibers applied to compression face.

Specimen is rotated and tested with the uncracked section now in tension.

Figure 5.6 Preparation of Specimen MCST 7-4

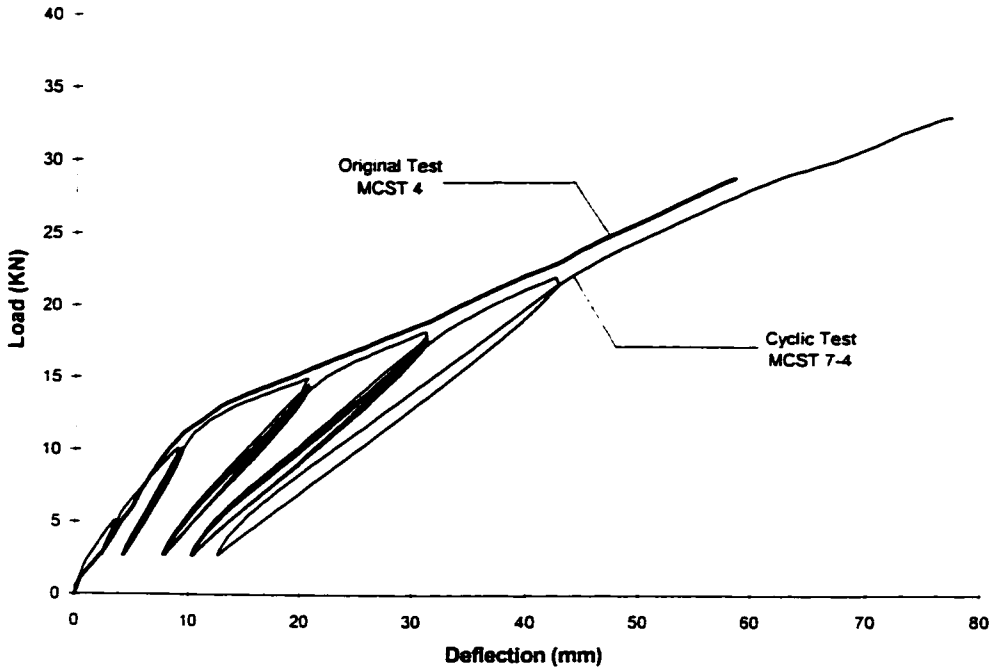

Figure 5.7 Effect of Cylcic Loading

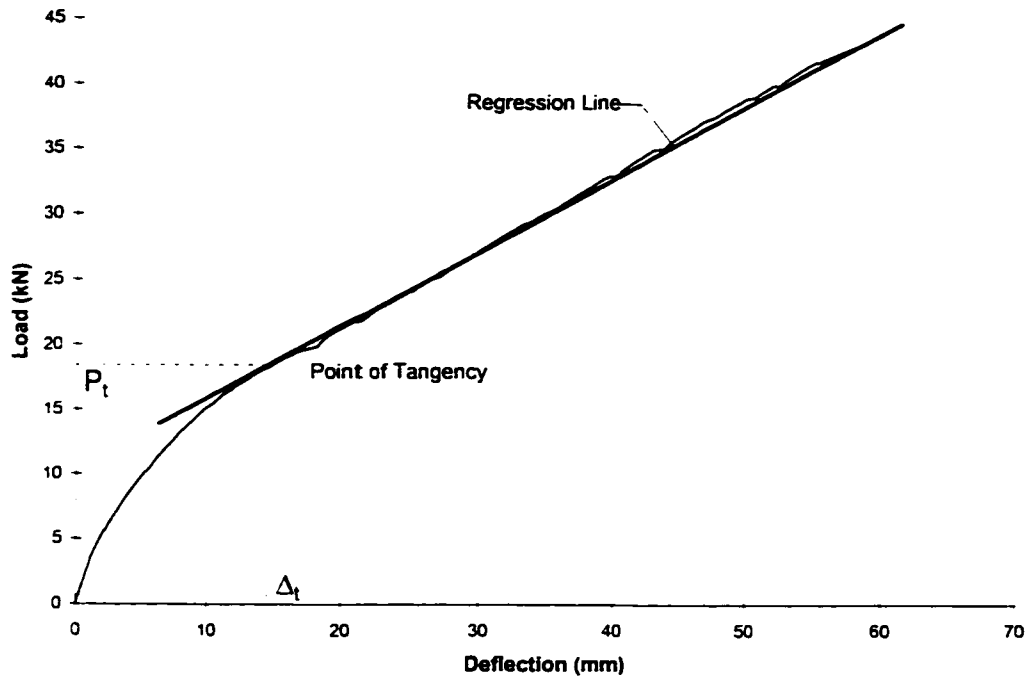

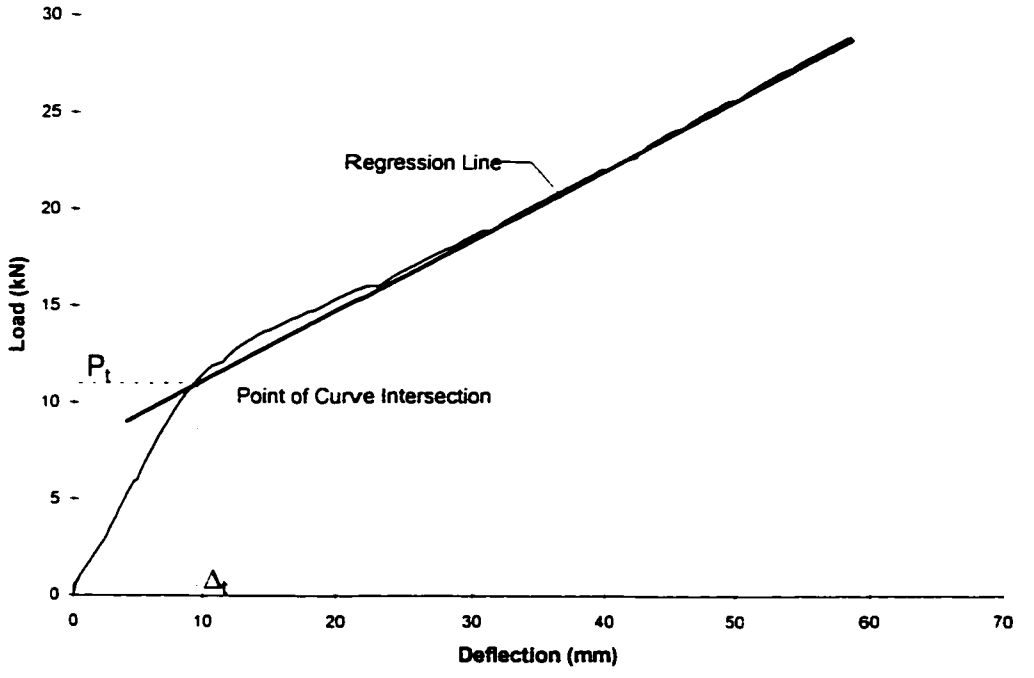

Figure 5.8 Determination of the Transition Point

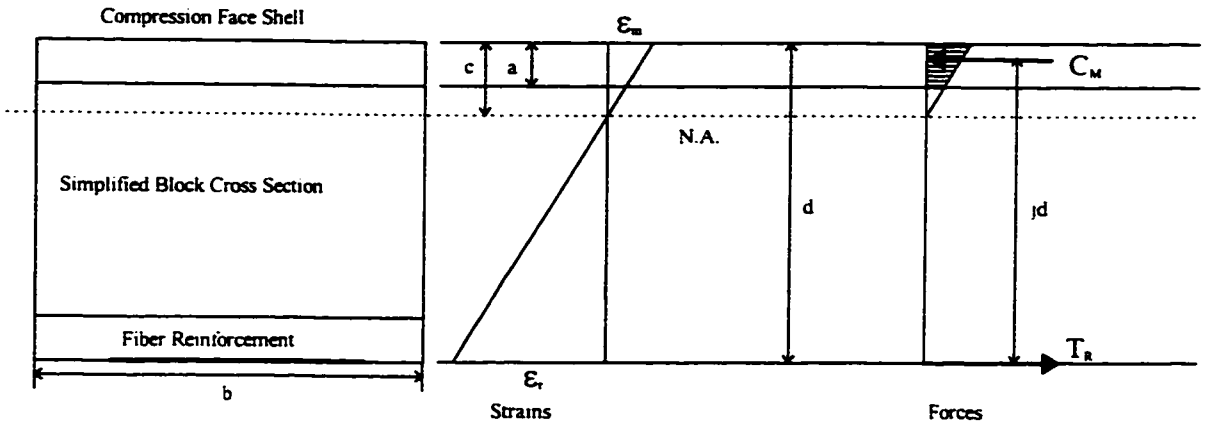

Figure 5.9 Internal Mechanics of Simplified Cross Section

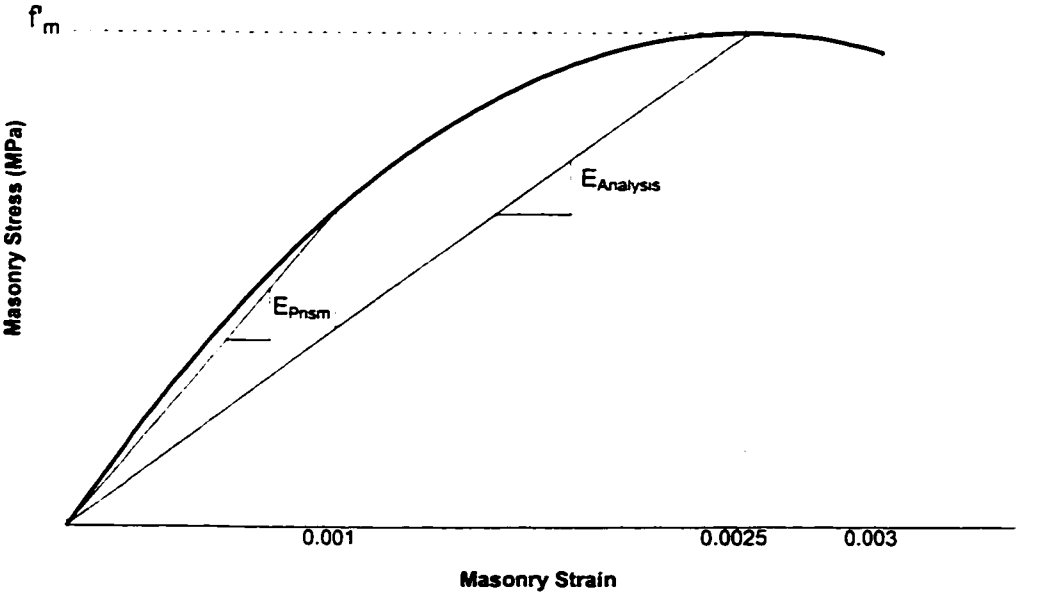

Figure 5.10 Difference in Masonry Prism Modulus of Elasticity

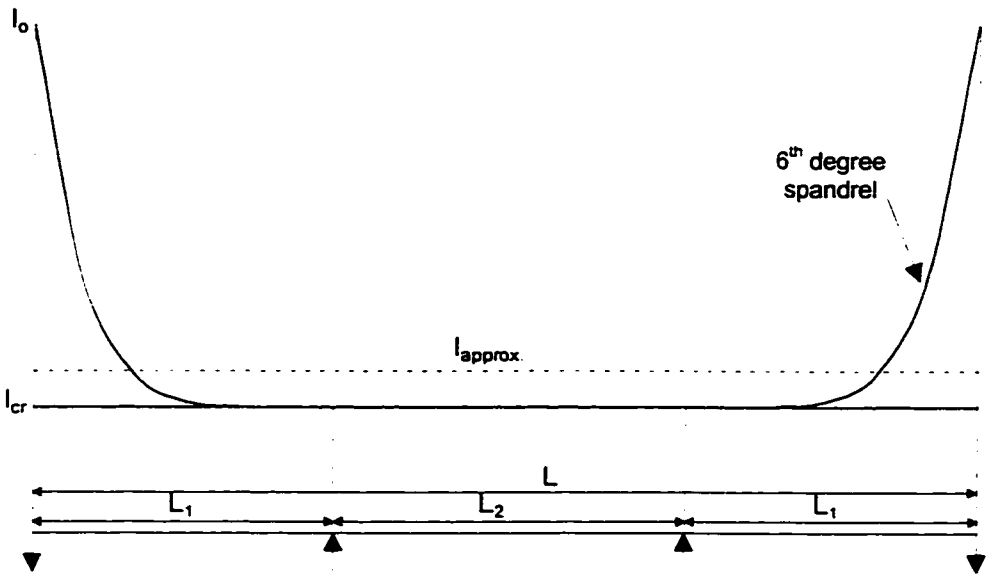

Figure 5.11 Determination of a Global Moment of Inertia

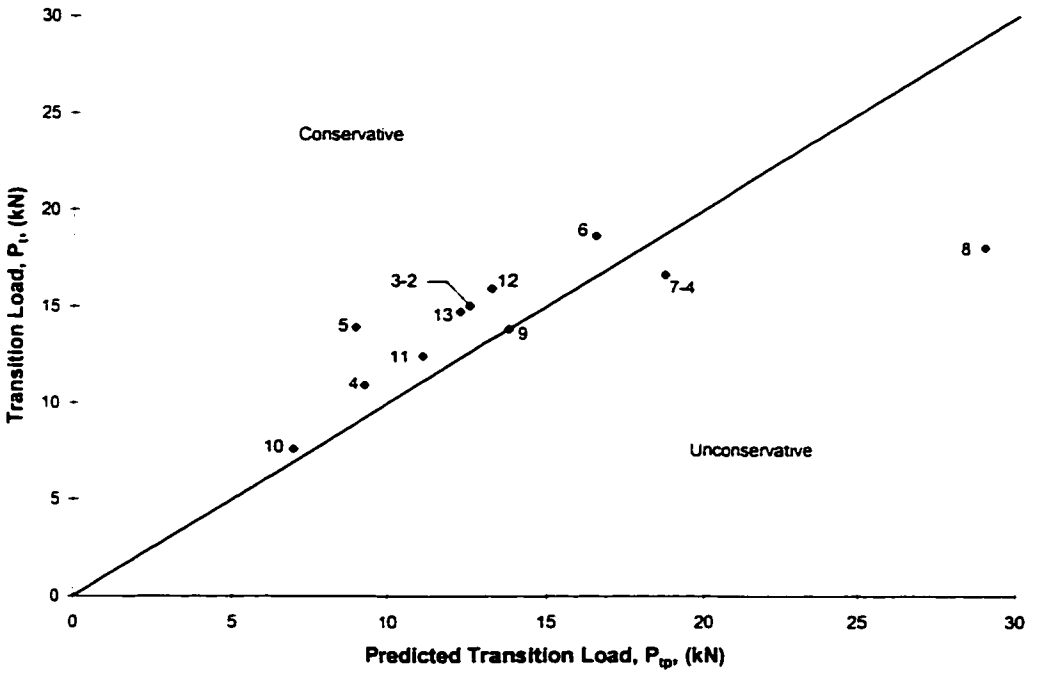

Figure 5.12 Transition Load Test to Predicted Results

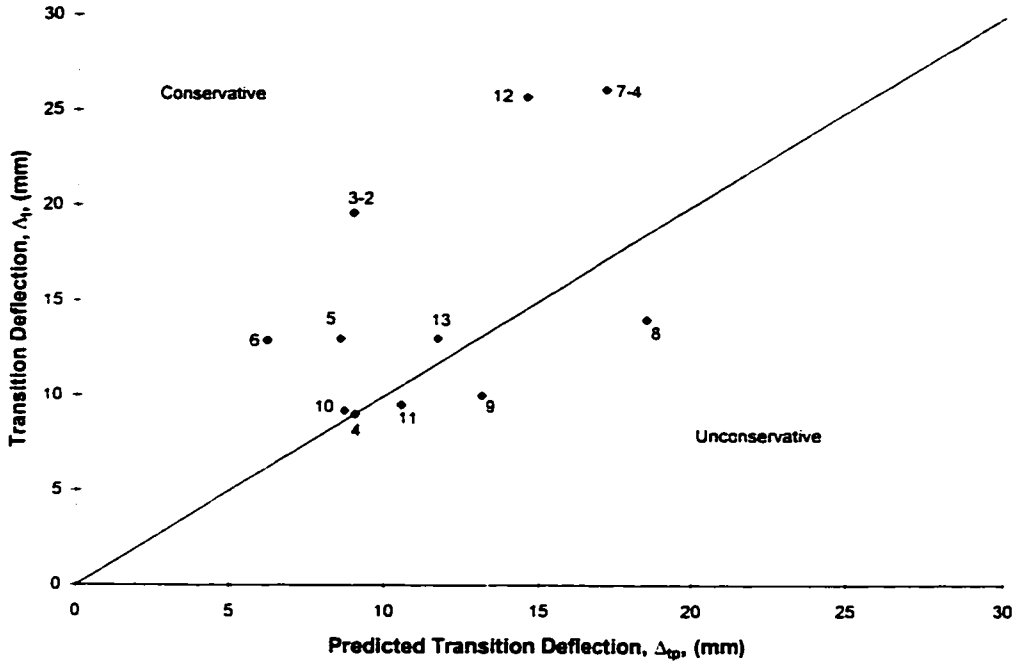

Figure 5.13 Transition Deflection Test to Predicted Results

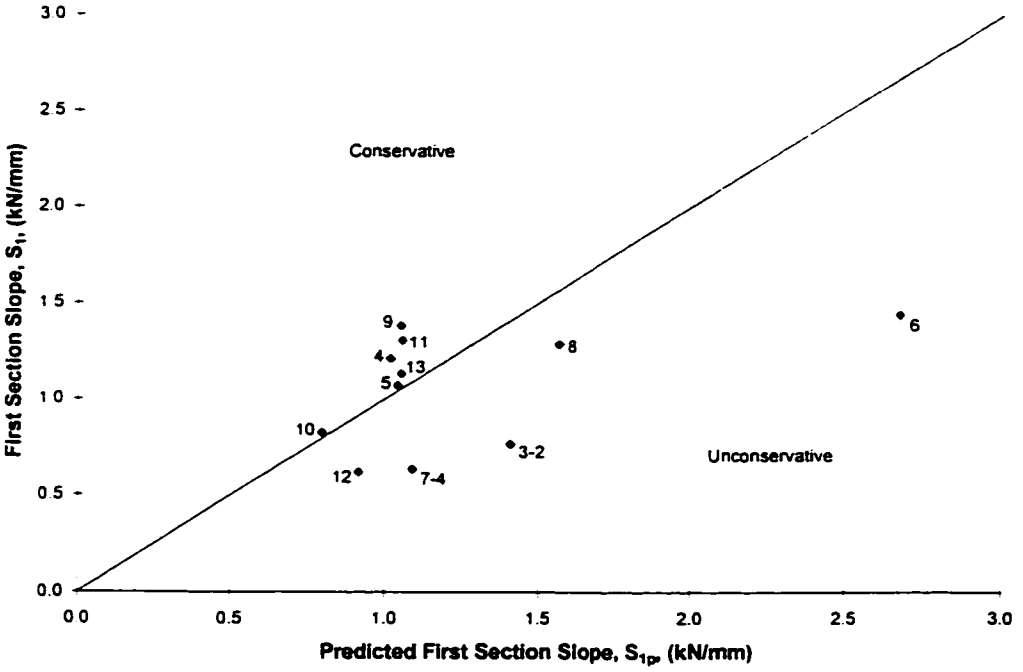

Figure 5.14 Section One Slope Test to Predicted Results

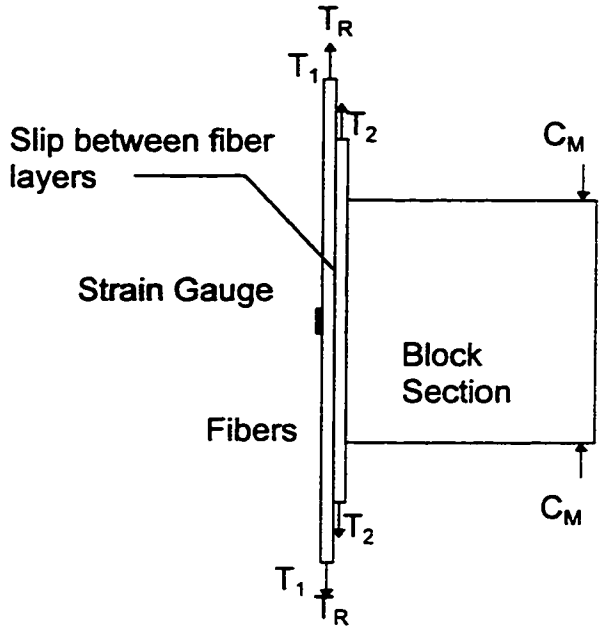

Figure 5.15 Possible Source of Error in Strain Gauge Reading

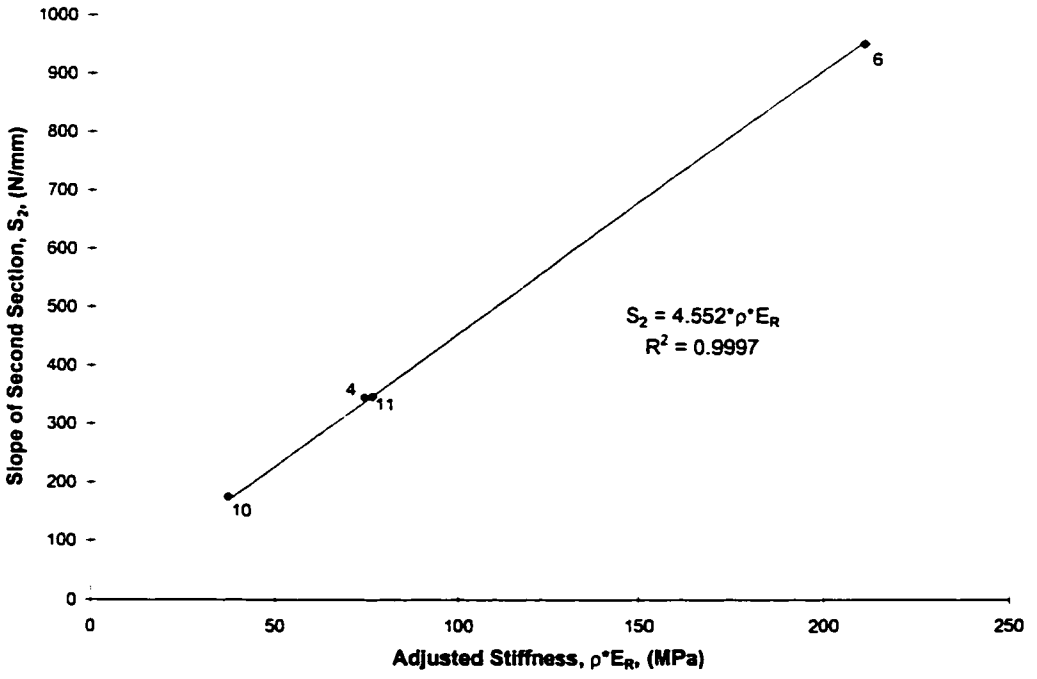

Figure 5.16 Relationship Between Slope and Stiffness

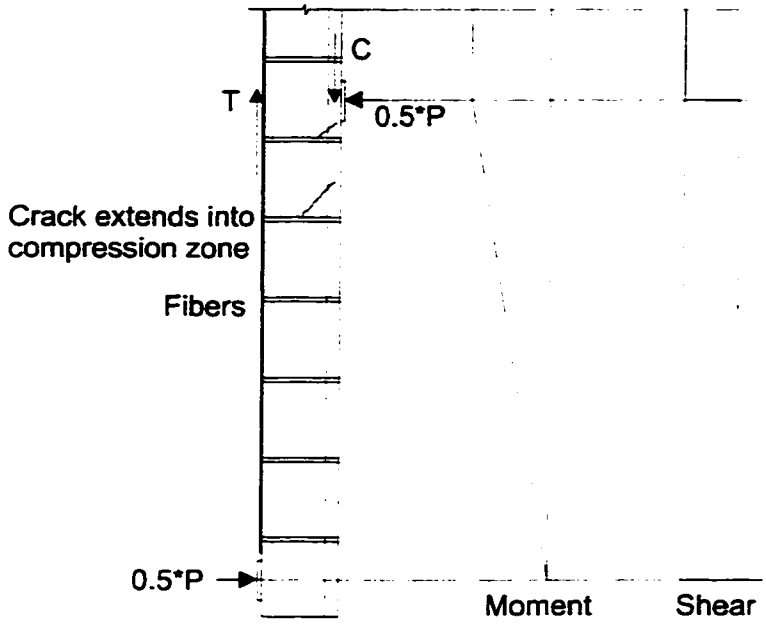

Figure 5.17 Conditions at Point of Typical Flexure Shear Failure

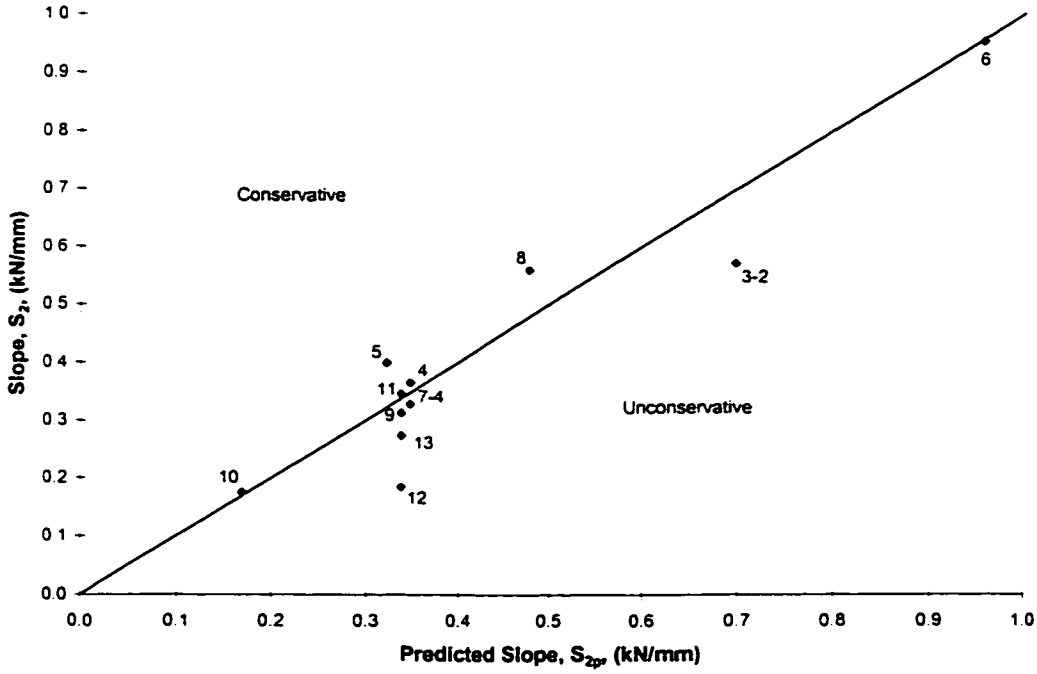

Figure 5.18 Second Section Slope Test to Predicted Results

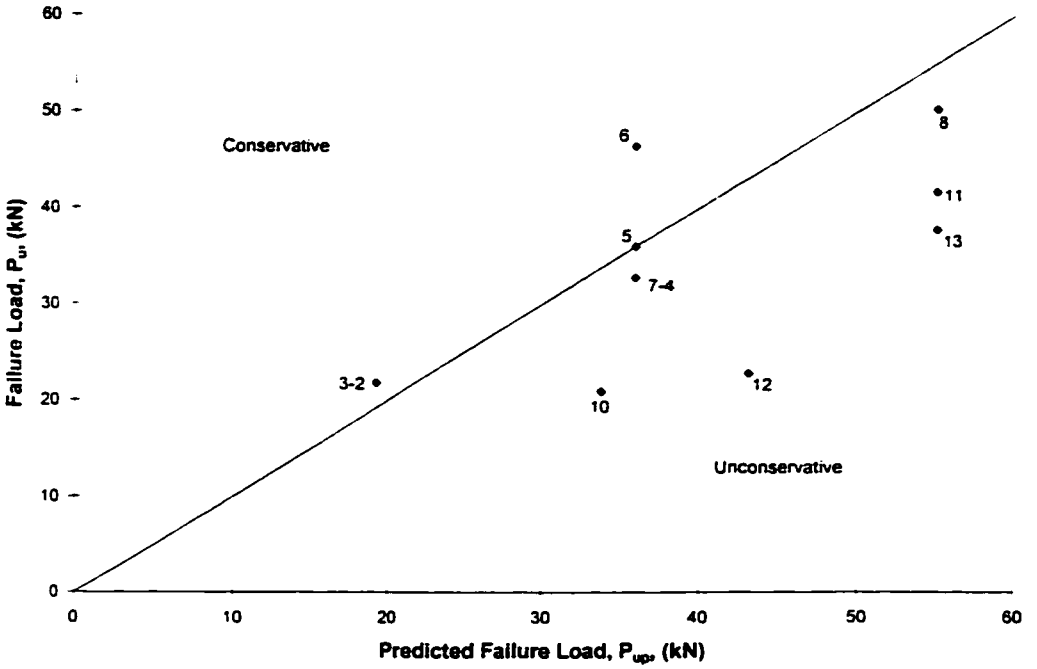

Figure 5.19 Ultimate Failure Load Test to Predicted Results

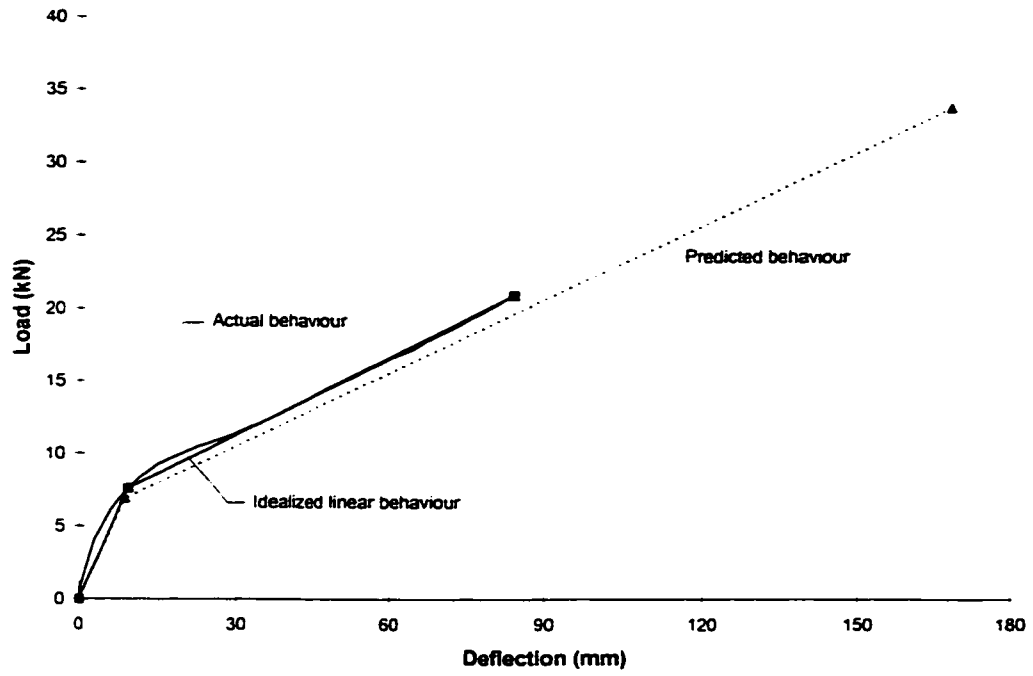

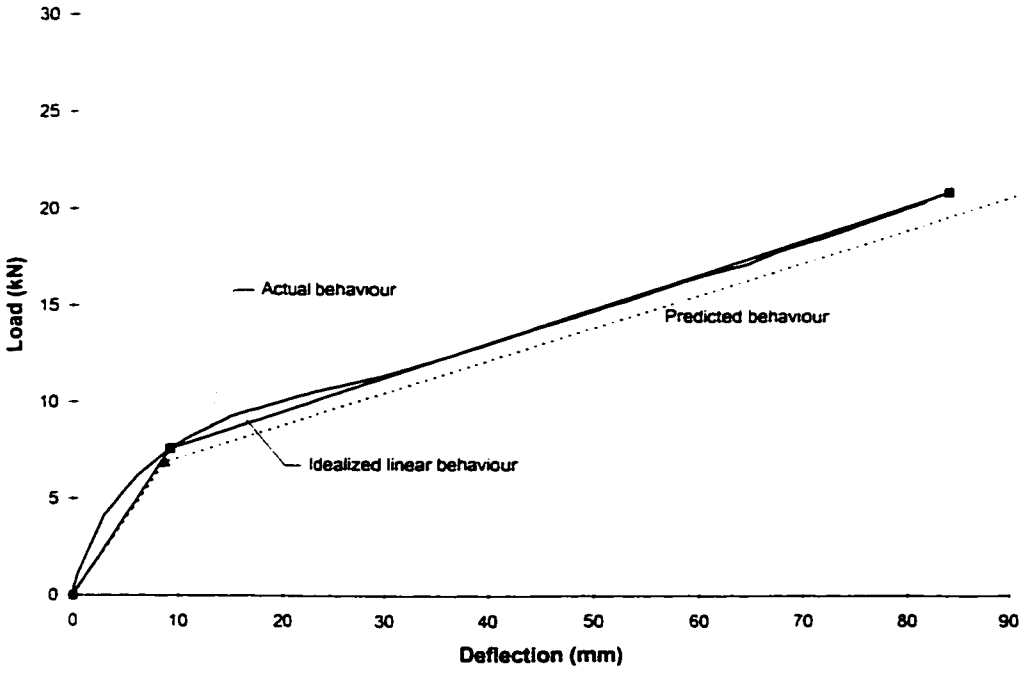

Figure 5.20 Overall Analytical Model Results

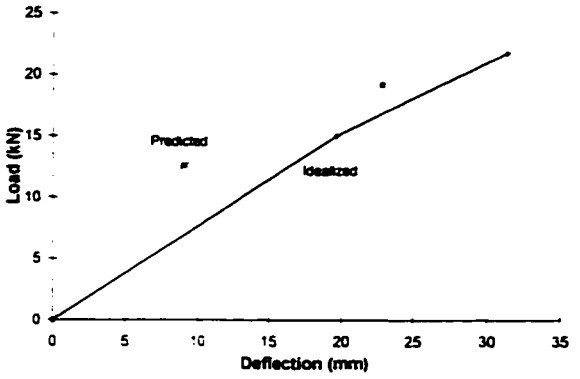

MCS 3-2
Two, 50 mm wide carbon straps

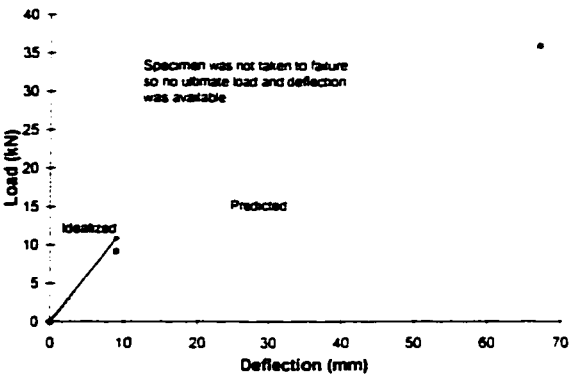

MCST 4
Two, 250 mm wide carbon sheets

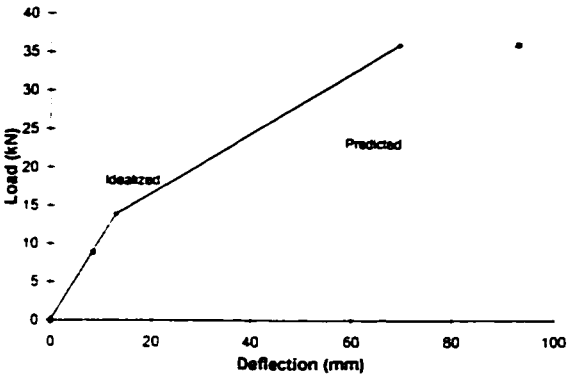

MGST 5
Two, 250 mm wide glass sheets

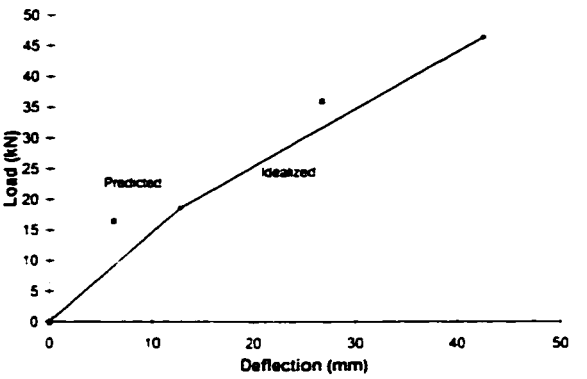

MCS 6
Four, 50 mm wide carbon straps

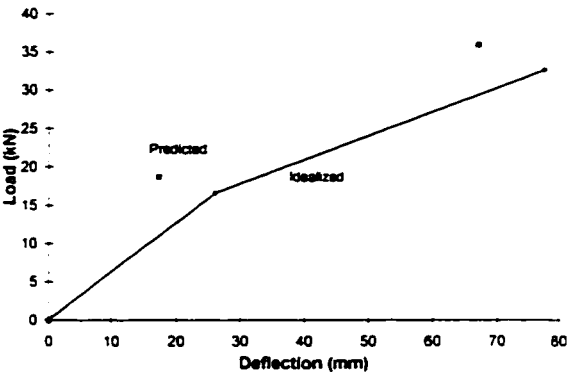

MCST 7-4
Two, 250 mm wide carbon sheets
cyclic loading

Figure 5.21 Series One Individual Analytical Model Results

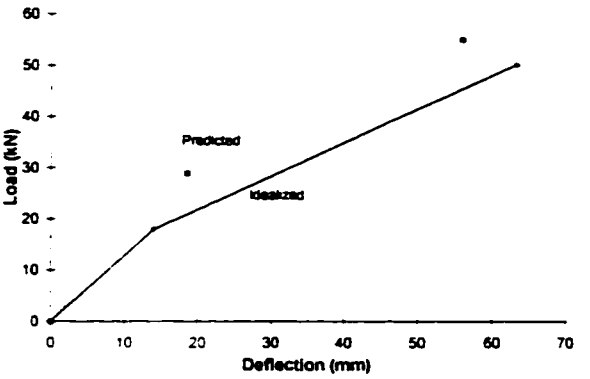

ICST 8
Two, 250 mm wide carbon sheets
two layers per sheet

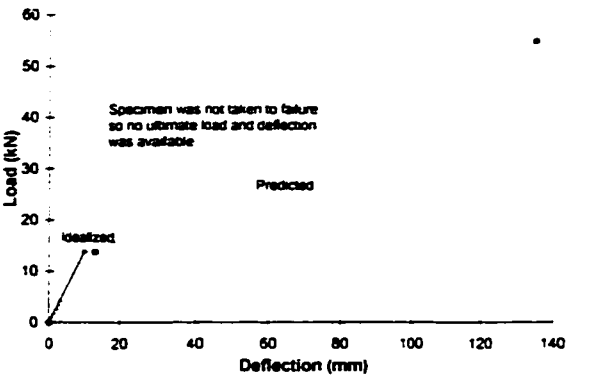

ICST 9
Two, 250 mm wide carbon sheets
10 kN applied axial load

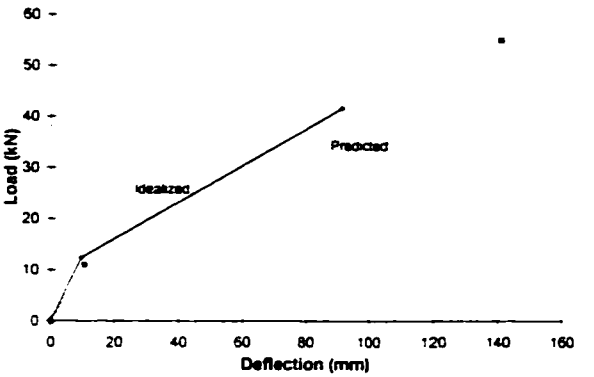

ICST 11
Two, 250 mm wide carbon sheets

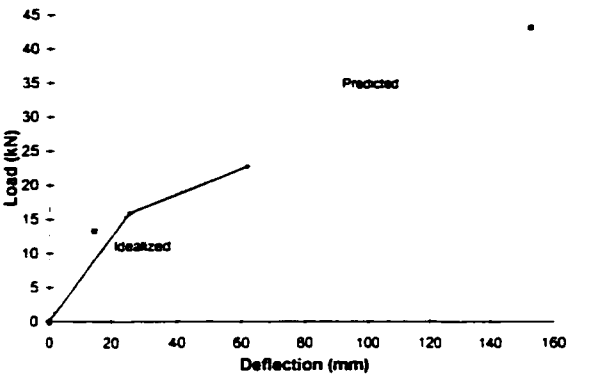

ICST 12
Ten, 125 mm wide carbon sheets
angled at 37° from vertical

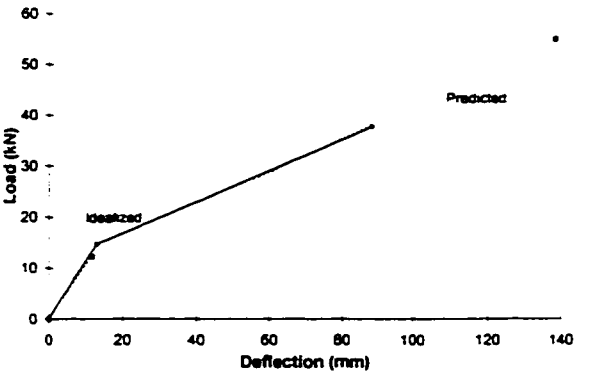

ICST 13
Two, 250 mm wide carbon sheets
30 kN applied axial load

Figure 5.22 Series Two Individual Analytical Model Results

6. SUMMARY, CONCLUSIONS, AND RECOMMENDATIONS

6.1 Summary

A large percentage of the existing infrastructure around the world consists of buildings constructed with unreinforced masonry. Many of these buildings do not meet current code standards for seismic zones. A literature review showed that conventional methods of rehabilitation have several undesirable qualities. Fiber reinforced polymers are beginning to be employed in the rehabilitation of masonry structures in an effort to provide a more convenient solution. Little information exists about the out-of-plane resistance of unreinforced masonry wall strengthened with FRP. This lack of information led to the development of an experimental program presented in this thesis.

A total of thirteen tests were performed on ten full scale masonry wall specimens constructed in two series. Each specimen was tested in the out-of-plane direction using two line loads placed at one third the length of the span from the reaction supports. Seven tests were performed on four specimens constructed with metric dimension block in Series One. Six tests were performed on six specimens constructed with imperial dimension block in Series Two. The specified dimensions of the specimens was 4 m high by 1.2 m long by 0.2 m wide. Five parameters were investigated: type, amount, and layout of the fiber reinforcement, axial load effects, and the effects of cyclic loading.

The total applied load and deflections along the height of the specimen was recorded for each test. Also, masonry and fiber reinforcement strains were measured at various locations. Individual material tests were performed on the masonry mortar, masonry blocks, and each type of fiber reinforcement used.

A simple analytical model based on strain compatibility in the constant moment region of the specimen was developed to predict the load - deflection response of a specimen. The model simplifies the overall behaviour of a specimen into two linear sections. The transition of the first section to the second section is identified and the final failure mode and values are calculated.

6.2 Conclusions

The overall behaviour of the specimens was similar. The load - mid-span deflection response for all the specimens can be characterized by separating it into two sections. The first section is non-linear and represents the stiffness contribution of the masonry materials. The second section is linear and represents the stiffness contribution from the fiber reinforcement.

The type of fiber reinforcement used affects the overall stiffness of a specimen. Similarly, the amount of fiber used affects the stiffness. It was determined that the relationship between the slope of the linear second section of the load - deflection response and the adjusted stiffness, $\rho \cdot E_R$, is one to one. The layout of the fiber reinforcement has more of a direct effect on the local joint strain behaviour than the overall behaviour. The introduction of axial load increases the first section stiffness and reduces the second section stiffness. Finally, the specimen subjected to cyclic loading experienced a reduction in the first section stiffness after each cycle but maintained the original load - deflection envelope previously obtained.

The analytical model presented provides a good estimate of the load - deflection response of a specimen despite several sources of error.

Overall results show that the strength and ductility of the specimens is increased significantly when strengthened with FRP. The fiber reinforcement is easy to handle and apply. The use of FRP for strengthening unreinforced masonry walls appears to be a promising alternative to conventional rehabilitation methods.

6.3 Recommendations

While this research satisfies the objective of identifying the general behaviour of unreinforced masonry walls strengthened with FRP and subjected to out-of-plane loads, some aspects were not studied enough to develop a full understanding of their effect.

One possible source of error in the calculations for the analytical model is tensile contribution of the various epoxy glues used. There were some inconsistencies in the calculations that suggested there may be some tensile forces being resisted by the epoxy. Further tests need to be performed to determine the tensile resistance of the epoxy glue and the effect it has on the stiffness of the masonry materials it is applied to.

The strain distribution pattern across the width of the fiber reinforcement identified in Chapter 3 needs to be further investigated. A more complete understanding of this distribution will allow for a more accurate estimate of the strain across the width of the fibers and any given level of lateral load. This in turn will lead to more accurate predictions from the analytical model.

A finite element study should be performed to better predict the behaviour of the specimens. This should only be done when enough information about each material is obtained, especially the effect of the epoxy as mentioned earlier.

An issue which needs to be addressed if fiber reinforced polymers is to be seriously considered as a rehabilitation alternative in buildings is the fire rating of the fibers and epoxy. Tests need to be performed to determine the combustibility of these materials during and after curing. The fibers may need additional fire protection in order to satisfy the code requirements for fire safety.

Finally, because the cyclic load test performed was only in one direction, a full cyclic testing program should be performed. This will provide a more accurate representation of the behaviour of these various types of fiber reinforcement when subjected to a seismic event.

References

Abboud, Bechara E., Hamid, Ahmad A., and Harris, Harry G. 1996. "Flexural Behavior of Reinforced Concrete Masonry Walls Under Out-of-Plane Monotonic Loads". ACI Structural Journal, May-June, V. 93, No. 3, pp. 327-335.

Abboud, B. E., Hamid, A. A., and Harris, H. G. 1990. "Small-Scale Modeling of Concrete Block Masonry Structures". ACI Structural Journal, V. 87, No. 2, Mar.-Apr., pp. 145-155.

Abrams, D. P. 1992. "Strength and Behavior of Unreinforced Masonry Elements". Tenth World Conference on Earthquake Engineering, Balkema, Rotterdam, pp. 3475-3480.

Abrams, D. P., Angel, R., and Uzarski, J. 1996. "Out-of-Plane Strength of Masonry Infill Panels". Earthquake Spectra, V. 12, No. 4, Nov., pp. 825 - 844.

Abu-Tair, A. I., Rigden, S. R., and Burley, E. 1996. "Testing the Bond Between Repair Materials and Concrete Substrate". ACI Materials Journal, V. 93, No. 6, Nov. - Dec., pp. 553 - 558.

Alexander, J. G. S., and Cheng, J. J. R. 1996 "Field Application and Studies of Using CFRP Sheets to Strengthen Concrete Bridge Girders". 2nd Advanced Composite Material in Bridges and Structures Conference, Montreal, Quebec, Aug. 11-14.

Alexander, J. G. S., and Cheng, J. J. R. 1997. "Shear Rehabilitation of G Girder Bridges Using CFRP Sheets". Structural Engineering Report No. 218, Department of Civil and Environmental Engineering, University of Alberta, Oct., 181 pages.

Angel, R., Uzarski, J. 1996 "Estimating Transverse Strength of Masonry Infills". Worldwide Advances in Structural Concrete and Masonry: Proceedings of the CCMS Symposium, Session 403, Chicago, Illinois, Apr. 15-18, pp. 101-111.

Arduini, Marco, Di Tommaso, Angelo, and Nanni, Antonio. 1997. "Brittle Failure in FRP Plate and Sheet Bonded Beams". ACI Structural Journal, July-Aug., pp. 363-370.

ASTM Standard C109/C 109M-95, 1995. "Standard Test Method for Compressive Strength of Hydraulic Cement Mortars (Using 2-in. or [50mm] Cube Specimens)". American Standard for Testing of Materials.

ASTM Standard D3039/D 3039M-95a, 1995. "Standard Test Method for Tensile Properties of Polymer Matrix Composite Materials". American Standard for Testing of Materials.

ASTM Standard E178-94, 1994. "Standard Practice for Dealing with Outlying Observations". American Standard for Testing of Materials.

Bhende, D., Ovadia, D. 1994. "Out-of-Plane Strengthening Scheme for Reinforced Masonry Walls". Concrete International, V. 16, Apr., pp. 30-34.

Boettcher, R. 1991. "New Applications of High Strength Aramid Fiber Composites in Concrete Structures". Brittle Matrix Composites, Elsevier Applied Science, Amsterdam, The Netherlands, V. 3, pp. 308-317.

Bruneau, M. 1994 "State-of-the-Art Report on Seismic Performance of Unreinforced Masonry Buildings". Journal of Structural Engineering, V. 120, No. 1, Jan., pp. 230 - 251.

Chajes, M. J., et. al. 1996. "Bond and Force Transfer of Composite Material Plates Bonded to Concrete". ACI Structural Journal, V. 93, No. 2, Mar. - Apr., pp. 208 - 217.

CSA Standard CAN3 - A165.1-M94, 1994. "Concrete Masonry Units"

CSA Standard CAN3 - A369.1-M90, 1990. "Method of Test for Compressive Strength of Masonry Prisms"

CSA Standard S304.1. 1994. "Masonry Design for Buildings (Limit States Design)".

Deniaud, C., and Cheng, J. J. R. 1998 "Shear Rehabilitation of Type G Girders Using ACM : Experimental Study". 5th International Conference on short and Medium Span Bridges, Calgary, Alberta, July 13-16.

Droumoussis, E. H., and Cheng, J. J. R. 1994 "Shear Strengthening of Concrete Girders Using Carbon Fiber Reinforced Plastic Sheets". Structural Engineering Report No. 205, Department of Civil Engineering, University of Alberta, Oct., 177 pages.

Ehsani, M. R. 1995. "Seismic Retrofitting of Concrete and Masonry Structures with Composite Materials: Research and Field Applications". Proceedings of the Third National Concrete and Masonry Engineering Conference, San Francisco, California, June 15-17, pp. 19-31.

Ehsani, M. R., Saadatmanesh, H., and Al-Saidy, A. 1997. "Shear Behavior of URM Retrofitted with FRP Overlays". Journal of Composites for Construction, V. 1, No. 1, Feb., pp. 17-25.

Erki, M. A., Rizkalla, S. H. 1993. "FRP Reinforcement for Concrete Structures". Concrete International, V. 15, June, pp. 48-53.

Ghanem, G., Zied, M. A., and Salama, A. E. 1994. "Repair and Strengthening of Masonry Assemblages Using Fiber Glass". Proceedings of the Tenth International Brick and Block Masonry Conference, Calgary, Canada, V. 2, pp. 499-508.

Glanville, J., Hatzinikolas, M., and Ben-Omran, H. 1996 "Engineered Masonry Design - Limit States Design". Winston House, Winnipeg, Manitoba.

Hatzinikolas, M. A., Longworth, J., and Warwaruk, J. 1978. "Concrete Masonry Walls" Structural Engineering Report No. 70, Department of Civil and Environmental Engineering, University of Alberta, Sep.

Hamid, A. A., Mahmoud, A. D. S., and El Magd, S. A. 1994. "Strengthening and Repair of Unreinforced Masonry Structures: State-of-the-Art". Proceedings of the Tenth International Brick and Block Masonry Conference, Calgary, Canada, V. 2, pp. 485-497.

Heintz, Jon A., Wosser, Thomas D. 1995. "Strengthening of an Unreinforced Masonry Building". IABSE Symposium, San Francisco, California, V. 73, No. 1, pp. 163-168.

Hutchinson, D. L., Yong, P. M. F., and McKenzie, G. H. F. 1984. "Laboratory Testing of a Variety of Strengthening Solutions for Brick Masonry Wall Panels". Proceedings, Eighth World Conference on Earthquake Engineering, San Francisco, Vol. 1, pp. 575-582.

Kingsley, G. R. 1995. "Evaluation and Retrofit of Unreinforced Masonry Buildings". Proceedings of the Third National Concrete and Masonry Engineering Conference, San Francisco, California, June 15-17, pp. 709-727.

La Mendola, L., Papia, M., and O'Conner, E. 1995. "Strengthening of Unreinforced Masonry Buildings". Journal of Structural Engineering, V. 121, Nov., pp. 1581-1587.

Lissel, S., Tilleman, D., Sayed-Ahmed, E. Y., and Shrive, N. G. 1998. " Carbon Fibre Reinforced Plastic (CFRP) Prestressed Masonry". 8th Canadian Masonry Sypmosium, Jasper, Alberta, May 31 - June 3, pp. 610-621.

Manfredi, G., Mazzolani, S., and Masi, A. 1992. "Review of Existing in Experimental Testing of Masonry Structures Subjected to Horizontal Loads". Tenth World Conference on Earthquake Engineering, Balkema, Rotterdam, pp. 3557-3562.

Manzouri, T., et al. 1996. "Repair and Retrofit of Unreinforced Masonry Structures". Earthquake Spectra, V. 12, No. 4, Nov., pp. 903-922.

Mazzolani, S., Masi, A. 1992. "Review of Existing in Experimental Testing of Masonry Structures Subjected to Horizontal Loads". Tenth World Conference on Earthquake Engineering, Balkema, Rotterdam, pp. 3557-3562.

Meier, U. 1996. "Composites for Structural Repair and Retrofitting". Proceedings of the First International Conference on Composites in Infrastructure, Tuscon, Arizona, U.S.A., pp. 1202-1216.

Meier, U., et al. 1992. "Strengthening of Structures with CFRP Laminates: Research and Applications in Switzerland". Proceedings of the Fifth International Conference on Advanced Composite Materials in Bridges and Structures, Sherbrooke, Canada, pp. 243-251.

Meier, Urs, Kaiser, Hanspeter. 1991. "Strengthening of Structures with CFRP Laminates". Proceedings, Advanced Composite Materials for Civil Engineering Structures, MT Div./ASCE, Las Vegas, Jan. 31, pp. 224-232.

Modena, Claudio. 1994. "Repair and Upgrading Techniques of Unreinforced Masonry Structures Utilized after the Friuli and Campania / Basilicata Earthquakes". Earthquake Spectra, V. 10, No. 1, pp. 171-185.

Plecnik, J., Cousins, T., and O'Conner, E. 1986. "Strengthening of Unreinforced Masonry Buildings". Journal of Structural Engineering, V. 112, May, pp. 1070-1087.

Pomonis, A., et. al. 1992. "Shaking Table Tests on Strong Motion Damagingness Upon Unreinforced Masonry". Tenth World Conference on Earthquake Engineering, Balkema, Rotterdam, pp. 3533-3538.

Prawel, S. P., Reinhorn, A. M., and Kunnath, S. K. 1986. "Seismic Strengthening of Structural Masonry Walls with External Coatings". Proceedings, Third U.S. Conference on Earthquake Engineering, V. 2, Earthquake Engineering Res. Inst. (EERI), El Cerrito, California, pp. 1323-1334.

Qamaruddin, M., Chandra, B. 1991. "Behaviour of Unreinforced Masonry Buildings Subjected to Earthquakes". Masonry Society Journal, V. 9, No. 2., pp. 47-55.

Schwegler, G. 1994. "Masonry Construction Strengthened with Fiber Composites in Seismically Endangered Zones". Tenth European Conference on Earthquake Engineering, Vienna, Austria, V. 3, pp. 2299-2303.

Schwegler, G., Kelterborn, P. 1996. "Earthquake Resistance of Masonry Structures Strengthened with Fiber Composites". Proceedings, Eleventh World Conference on Earthquake Engineering, Acapulco, Mexico.

Seible, F., et. al. 1994. "The US-TCCMAR Full-Scale Five-Story Masonry Research Building Test: Part I - Executive Summary". Report No. SSRP - 94/01, University of California, San Diego, Structural Systems Research Project, Jan.

Seible, F. 1995. "Structural Rehabilitation with Advanced Composites". Proceedings of the IABSE Symposium Extending the Lifespan of Structures, San Francisco, U.S.A., pp. 391-398.

Seible, F., Karbhari, V. 1996. "Advanced Composites for Civil Engineering Applications in the United States". Proceedings of the First International Conference on Composites in Infrastructure, Tuscon, Arizona, U.S.A., pp. 21-37.

Sheppard, P., Tercelj, S. "The Effect of Repair and Strengthening Methods for Masonry Walls". Proceedings, Seventh World Conference on Earthquake Engineering, V. 6, Turkish Nat. Committee on Earthquake Engineering, Ankara, Turkey, pp. 255-262.

Stetson, M. B., Goodspeed, C. H. 1992. "Fundamental Considerations in the Design of Flexural Concrete Members With Non-Prestressed FRP Reinforcement". Advanced Composite Materials in Bridges and Structures, pp. 141-149.

Tomazevic, M., and Weiss, P. 1994. "Seismic Behavior of Plain and Unreinforced Masonry Buildings". Journal of Structural Engineering, V. 120, No. 2, Feb., pp. 323 - 338.

Triantafillou, T. C. 1998, "Strengthening of Masonry Structures Using Epoxy-Bonded FRP Laminates". Journal of Composites for Construction, V. 2, No. 2, May, pp. 96-104.

Tsai, S., and Hahn, H. 1980 "Introduction to Composite Materials", Technomic Publishing Company Inc., Lancaster, Pennsylvania,

Weeks, J., et al. 1994. "The US-TCCMAR Full-Scale Five-Story Masonry Research Building Test: Part V - Repair and Retest". Report No. SSRP - 94/05, University of California, San Diego, Structural Systems Research Project, Jan.

IMAGE EVALUATION
TEST TARGET (QA-3)

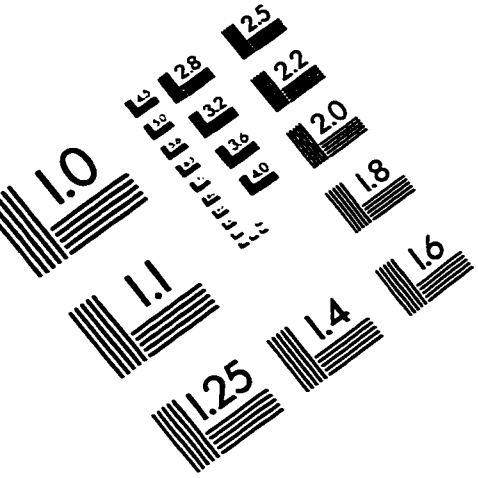

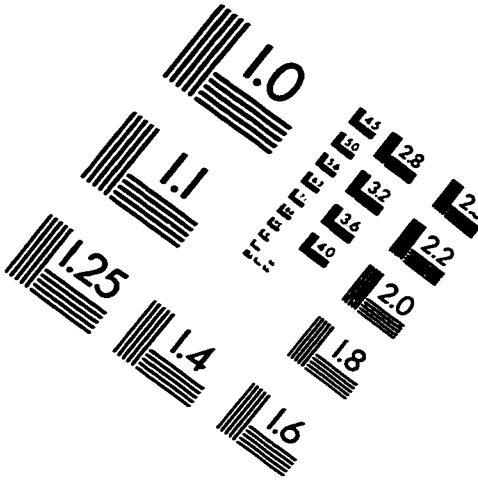

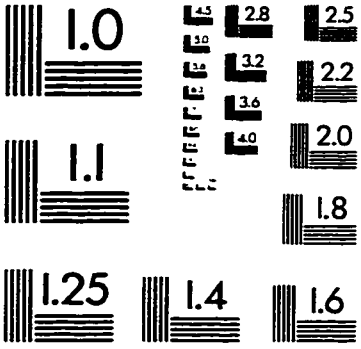

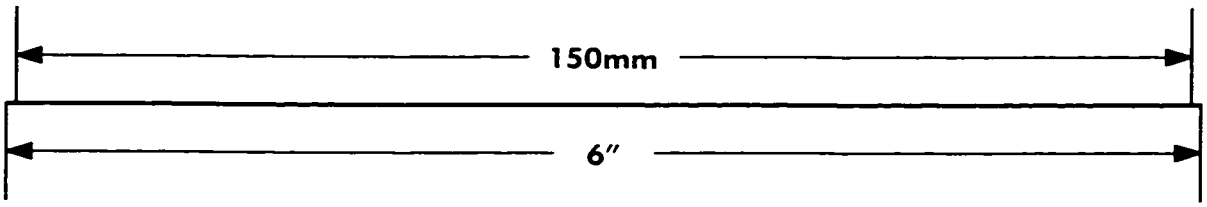

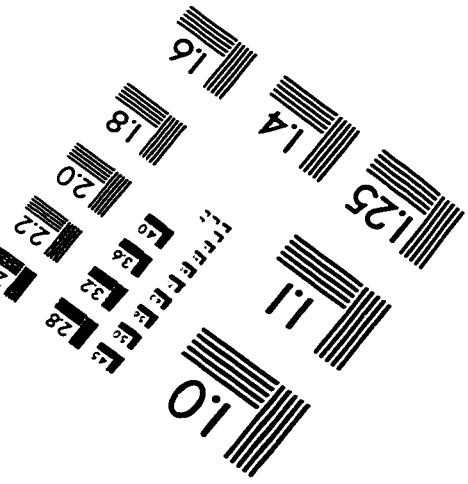

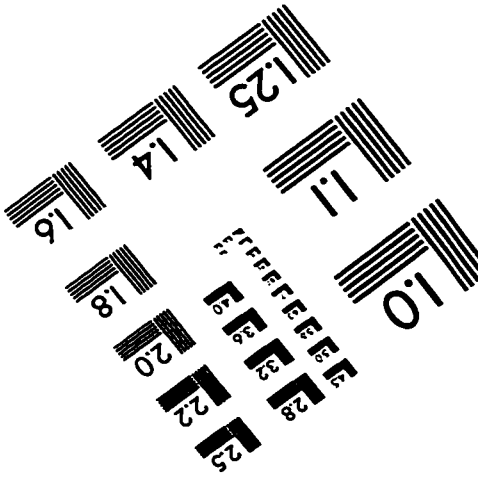

APPLIED IMAGE, Inc
1653 East Main Street
Rochester, NY 14609 USA
Phone: 716/482-0300
Fax: 716/288-5989